



**Characterization of Coastal Aquifers in Bo Yang District, Songkhla Province,
Using Shallow Seismic and Vertical Electrical Sounding Methods**

Jiraporn Srattakal

**A Thesis Submitted in Partial Fulfillment of the Requirements for the Degree of
Master of Science in Geophysics
Prince of Songkla University
2012
Copyright of Prince of Songkla University**

Thesis Title Characterization of Coastal Aquifers in Bo Yang District,
Songkhla Province, Using Shallow Seismic and Vertical
Electrical Sounding Methods
Author Miss Jiraporn Srattakal
Major Program Geophysics

Major Advisor :

.....
(Dr. Helmut Dürrast)

Examining Committee :

.....Chairperson
(Dr. Passakorn Pananont)

Co-advisor :

.....
(Dr. Sawasdee Yordkayhun)

.....
(Dr. Suttida Rakkapao)

.....
(Dr. Sawasdee Yordkayhun)

.....
(Dr. Helmut Dürrast)

The Graduate School, Prince of Songkla University, has approved this
thesis as partial fulfillment of the requirements for the Master of Science Degree in
Geophysics

.....
(Prof. Dr. Amornrat Phongdara)
Dean of Graduate School

ชื่อวิทยานิพนธ์	การกำหนดลักษณะชั้นหินอุ้มน้ำบริเวณชายฝั่งของตำบลบ่อทรายจังหวัดสงขลาโดยการใช้วิธีการคลื่นสั้นสะเทือนระดับตื้นและการวัดค่าสภาพต้านทานไฟฟ้าแบบหยั่งลึก
ผู้เขียน	นางสาวจิราภรณ์ ศรีธาทากาล
สาขาวิชา	ธรณีฟิสิกส์
ปีการศึกษา	2554

บทคัดย่อ

ในภาคใต้ของประเทศไทยมีชุมชนและหมู่บ้านมากมายที่ตั้งอยู่ในบริเวณใกล้ชายทะเล มีหลายพื้นที่ที่มีความสามารถในการใช้น้ำบาดาลจำกัด เนื่องจากการรุกคืบของน้ำเค็มเข้าสู่ชั้นหินอุ้มน้ำ ตำบลบ่อทรายตั้งอยู่ในเทศบาลสงขลา เป็นศูนย์กลางการเมืองและการปกครองของจังหวัด ซึ่งมีหลายหน่วยงานตั้งอยู่ บริเวณชายฝั่งของตำบลบ่อทรายมีประชากรอยู่อย่างหนาแน่น น้ำจืดมีความจำเป็นสำหรับพื้นที่นี้ การศึกษาในครั้งนี้มีวัตถุประสงค์เพื่อกำหนดลักษณะของชั้นหินอุ้มน้ำบริเวณชายฝั่งของตำบลบ่อทรายจังหวัดสงขลาโดยการสำรวจทางธรณีฟิสิกส์ซึ่งประกอบไปด้วยการสำรวจด้วยวิธีคลื่นไหวสะเทือนแบบสะท้อนและหักเห และการวัดค่าสภาพต้านทานไฟฟ้าแบบหยั่งลึก การใช้วิธีคลื่นสั้นสะเทือนสามารถกำหนดโครงสร้างของชั้นดินและการใช้วิธีการหยั่งลึกในแนวตั้งเพื่อระบุการรุกตัวของน้ำเค็มเข้าสู่ระบบน้ำบาดาล ซึ่งผลจากการสำรวจแสดงให้เห็นถึงโครงสร้างของชั้นหินอุ้มน้ำ แบ่งออกเป็น 3 ชั้น คือ ชั้นหินอุ้มน้ำชั้นแรก อยู่ใกล้ผิวดิน เป็นชั้นน้ำบาดาลระดับตื้น อยู่ที่ความลึก 2-10 เมตรจากผิวดิน ชั้นหินอุ้มน้ำชั้นที่สอง อยู่ที่ระดับความลึก 30-40 เมตรจากผิวดิน มีค่าสภาพต้านทานไฟฟ้าต่ำแสดงให้เห็นว่ามีการรุกคืบของน้ำเค็มเข้ามามากในชั้นนี้ ชั้นหินอุ้มน้ำชั้นที่สาม อยู่ที่ระดับความลึก 50-70 เมตร บางพื้นที่ได้มีการแทรกตัวของน้ำเค็มเข้ามาในชั้นนี้

Thesis Title Characterization of Coastal Aquifers in Bo Yang District, Songkhla Province, Using Shallow Seismic and Vertical Electrical Sounding Methods

Author Miss Jiraporn Srattakal

Major Program Geophysics

Academic Year 2011

ABSTRACT

Southern Thailand has an extensive coastline, with villages and cities often located near the shoreline. In many areas, the availability of fresh groundwater resource is limited due to the intrusion of saline (marine) water into coastal aquifers. Bo Yang District, the study area of this work, is located in Songkhla Municipality, and it is the political and administrative center of the province, with various offices, departments, and military units. The coastal area of Bo Yang District is densely populated. Freshwater consumption is necessary and vital for the population in the study area. The objective of this study is to characterize the coastal aquifers by using shallow seismic reflection and refraction methods to delineate subsurface structures and using vertical electrical sounding method to characterize the aquifers and identify saline water intrusion into the groundwater system. The results show that the subsurface can be divided into three aquifers. The first aquifer has a depth between 2-10 m; groundwater within the first aquifer is fresh water. The second aquifer is located at depth between 30-40 m; groundwater within the second aquifer is brackish water. The third aquifer has a depth between 50-70 m, groundwater within the third aquifer is freshwater, brackish, and also saline water.

ACKNOWLEDGEMENTS

The work in this thesis has been an inspiring, often exciting, sometimes challenging, but always interesting experience. I would like to express my gratitude to my advisor, Dr. Helmut Dürrast for the continuous support, advice, encouragement and patience during the study.

I would like to express my sincere thanks to my co-advisor Dr. Sawasdee Yordkayhun for his suggestions and invaluable discussions during the seismic reflection data acquisition.

My thanks go to the Graduate School, Prince of Songkla University for the research grant in carry out this study, and thanks to the Department of Physics, Faculty of Science, Prince of Songkla University, including the faculty members, administrative staffs, and all students in geophysics for their support.

Finally, I am deeply grateful to my family for their moral support and their encouragement during a challenging time.

Jiraporn Srattakal

TABLE OF CONTENTS

CONTENT	PAGE
ABSTRACT (IN THAI)	iii
ABSTRACT (IN ENGLISH)	iv
ACKNOWLEDGEMENTS	v
TABLE OF CONTENTS	vi
LIST OF TABLES	ix
LIST OF FIGURES	x
CHAPTER 1 INTRODUCTION	1
1.1 Groundwater	2
1.2 Coastal aquifers	3
1.3 Geophysical investigations of coastal aquifers in previous studies	6
1.4 Objective	15
CHAPTER 2 RESEARCH METHODOLOGY	16
2.1 Study area	16
2.2 Theory of seismic methods	19
2.2.1 Elastic constants and waves	21
2.2.2 Seismic data acquisition	24
2.3 Seismic refraction method	27
2.3.1 Seismic refraction data acquisition	35
2.3.2 Seismic refraction data processing	37
2.4 Seismic reflection method	41
2.4.1 Seismic reflection data acquisition	47
2.4.2 Seismic reflection data processing	50
2.4.2.1 Header correction	52
2.4.2.2 Geometry input	52
2.4.2.3 Trace editing	52
2.4.2.3.1 Bad trace killing	53
2.4.2.3.2 First arrival muting	54
	vi

TABLE OF CONTENTS (CONTINUED)

CONTENT	PAGE
2.4.2.3.3 Surgical muting	55
2.4.2.4 CDP sorting	56
2.4.2.5 Velocity analysis	56
2.4.2.6 Frequency filtering	56
2.4.2.6.1 Fourier transformation	57
2.4.2.6.2 Band-pass filter	58
2.4.2.7 Scaling	59
2.4.2.8 NMO correction	61
2.4.2.9 Stacking	63
2.5 Vertical electrical sounding method	64
2.5.1 Vertical electrical sounding data acquisition	68
2.5.2 Vertical electrical sounding data processing	69
CHAPTER 3 RESULTS	71
3.1 Geology and hydrogeology	71
3.2 Results of SK01 site	75
3.3 Results of SK02 site	77
3.4 Results of SK03 site	81
3.5 Results of SK04 site	86
3.6 Results of SK05 site	87
3.7 Results of SK06 site	90
3.8 Results of SK07 site	93
3.9 Borehole information	95
CHAPTER 4 DISCUSSION AND CONCLUSION	104
4.1 Geophysical investigations in a city	104
4.2 Data integration for specific sites	104
4.3 Hydrogeological model of Bo Yang	111
4.4 Conclusions	115

TABLE OF CONTENTS (CONTINUED)

CONTENT	PAGE
BIBLIOGRAPHY	117
APPENDIX	120
A RESISTIVITY FIELD DATA	121
PUBLICATION	133
VITAE	140

LIST OF TABLES

TABLE		PAGE
2.1	P wave velocities in materials.	21
2.2	Seismic refraction data acquisition in the Bo Yang district.	35
2.3	Seismic reflection data acquisition in the Bo Yang district.	50
2.4	Best band-pass filters with truncation frequency that contains dominant signal frequency bandwidth of the Bo Yang survey.	58
2.5	Resistivity values of water and sediments (modified from Zohdy et al, 1993).	65
3.1	Classification of water base on the total dissolved solids (TDS) (modified from Wendell, 2007).	74
3.2	Borehole data show the location and screen interval.	102

LIST OF FIGURES

FIGURE		PAGE
1.1	Ground water occurs in the pore spaces of geologic formations (modified from Heath, 1998).	2
1.2	Features Affecting the Coastal Aquifers (Kumar, 1987).	4
1.3	Schematic illustrations of some of the modes of saltwater intrusion (Reilly and Goodman, 1987).	6
1.4	Optimum offset section (~1 km long) from line 200, with two borehole logs for reference (note that these boreholes are both ~2 km offline). These data were acquired with the source and geophones planted in the bottom of a water-filled klong (canal), and the water-saturated surface conditions have contributed to the high frequency of the recorded data (Nutalaya et al., 1985).	8
2.1	Map of Thailand with the location of study area (modified from http://geology.com/world/thailand-satellite-image.shtml [8 August, 2011]).	17
2.2	Map of study area showing geophysical measurement locations on Bo Yang District, Songkhla Province (modified from Royal Thai Survey Department, 1997).	18
2.3	Snell's law (modified from Parasnis, 1997).	22
2.4	Huygens's principle (Sheriff and Geldart, 1995)	23
2.5	Diffracted wavefront (Sheriff and Geldart, 1995).	24
2.6	Geometrics SmartSeis.	25
2.7	Stacking chart of multifold coverage showing common offset gather, common shot gather and CMP gather (Stone, 1994).	27
2.8	Theoretical raypath diagram seismic refraction and reflection (modified from Telford et al, 1990).	28
2.9	Travel time-distance graph of seismic reflection and refraction (modified from Sheriff and Geldart, 1995).	30

LIST OF FIGURES (CONTINUED)

FIGURE		PAGE
2.10	Raypath diagram of three layers case (modified from Boyd, 2003).	31
2.11	Raypaths and travel time curves for a dipping refractor (modified from Burger, 1992).	34
2.12	The seismic refraction survey stations (a) line SKR01, (b) line SKR02, (c) line SKR03 and (d) line SKR04.	36
2.13	Shot record raw data of survey line SKR03.	38
2.14	Example of picking the first break of shot record raw data of survey line SKR03.	39
2.15	Time-distance graphs used as a layer assignment for each layer of survey line SKR03.	39
2.16	Depth and elevation of layers beneath shot points and geophones of survey line SKR03.	40
2.17	2D velocity–depth model of survey line SKR03.	40
2.18	Geometry travel time curve for a horizontal reflector (modified from Sheriff and Geldart, 1995).	43
2.19	Reflected seismic waves that travel through multiple horizontal layers show an increase in travel time with increasing offset distance (Sheriff and Geldart, 1995).	45
2.20	Geometry travel time curve for a dipping reflector (modified from Sheriff and Geldart, 1995).	47
2.21	Seismic reflection survey stations (a) line SKL01, (b) line SKL02, (c) line SKL03, (d) line SKL04, (e) SKL05 and (f) SKL06	48
2.22	Time-distance graph show main phases that need to be considered for choosing the optimum offset in a field survey (from Pullan and Hunter, 1990)	49

LIST OF FIGURES (CONTINUED)

FIGURE		PAGE
2.23	Series of test records recorded or the determination of the optimum offset (a) offset of 5 m (b) offset of 10 m and (c) offset of 15 m. An optimum offset of 15 m was chosen for the final records.	50
2.24	Processing flow for seismic reflection data.	51
2.25	Shot record raw data of survey line SKL05.	52
2.26	Shot record raw data (a) before and (b) after applying the trace edit process of survey line SK06.	54
2.27	Shot record raw data (a) before and (b) after applying the first arrival mute process of survey line SKL05.	55
2.28	Shot record raw data, (a) without filtering, (b) after applying band-pass filtering with a filter function of 10-20-200-300 Hz, (c) band-pass filtering with a filter function of 20-50-150-250 Hz and (d) band-pass filtering with a filter function of 20-100-150-250 Hz of survey line SKL05.	59
2.29	Shot record raw data and series of AGC gained section with window lengths 0.05, 0.1, 0.2 s of survey line SKL05.	60
2.30	Principle of NMO correction, the reflections are aligned using the correct velocity, such that the events are horizontally, then all the separate traces are stacked (summed).	62
2.31	NMO correction of a reflection, (a) reflection is not corrected, (b) corrected with proper velocity, (c) correction velocity is too low and (d) correction velocity is too high (Yilmaz, 1987).	63
2.32	Stacked section of survey line SKL05.	64
2.33	Electrode arrays in common use. (a) Wenner, (b) Schlumberger, (c) Pole-dipole and (d) Dipole-dipole (modified from Telford et al, 1990).	67
2.34	Schlumberger electrodes array.	68

LIST OF FIGURES (CONTINUED)

FIGURE		PAGE
2.35	Resistivity meter, ABEM Terrameter SAS 1000.	69
2.36	VES model of survey line SKV09.	70
3.1	Geological map of Songkhla province (from Department of Mineral Resources, 2007)	72
3.2	Total dissolved solids and groundwater expected yield map of Songkhla Province (Bureau of groundwater Resource 12 Songkhla, 2005).	73
3.3	Location of seismic refraction (SKR01), seismic reflection (SKL01) and VES (SKV01) profiles at SK01 site.	75
3.4	2D velocity–depth model of survey line SKR01.	76
3.5	Seismic section of survey line SKL01.	77
3.6	VES model of survey point SKV01.	77
3.7	Location of seismic refraction (SKR02), seismic reflection (SKL02) and VES (SKV02, SKV03) profiles at SK02 site.	78
3.8	2D velocity–depth model of survey line SKR02.	79
3.9	Seismic section of survey line SKL02.	79
3.10	VES model of survey point SKV02.	80
3.11	VES model of survey point SKV03.	81
3.12	Location of seismic refraction (SKR03), seismic reflection (SKL03) and VES (SKV04, SKV05, SKV06, SKV07) profiles at SK03 site.	82
3.13	2D velocity–depth model of survey line SKR03.	83
3.14	Seismic section of survey line SKL03.	83
3.15	VES model of survey point SKV04.	84
3.16	VES model of survey point SKV05.	85
3.17	VES model of survey point SKV06.	85
3.18	VES model of survey point SKV07.	86
3.19	Location of seismic reflection (SKL04) profiles at SL04 site.	86

LIST OF FIGURES (CONTINUED)

FIGURE		PAGE
3.20	Seismic section of survey line SKL04.	87
3.21	Location of seismic reflection (SKL05) and VES (SKV09, SKV10) profiles at SK05 site.	88
3.22	Seismic section of survey line SKL05.	89
3.23	VES model of survey point SKV07.	89
3.24	VES model of survey point SKV10.	90
3.25	Location of seismic refraction (SKR04), seismic reflection (SKL06) and VES (SKV08) profiles at SK06 site.	91
3.26	2D velocity–depth model of survey line SKR04.	91
3.27	Seismic section of survey line SKL06.	92
3.28	VES model of survey point SKV08.	93
3.29	Location of VES (SKV11, SKV12) profiles at SK07 site.	93
3.30	VES model of survey point SKV11.	94
3.31	VES model of survey point SKV12.	95
3.32	Borehole data of log of boring number TH405.	97
3.33	Borehole data of log of boring number H230.	98
3.34	Borehole data of log of boring number H1383.	98
3.35	Borehole data of log of boring number H49.	99
3.36	Borehole data of log of boring number H237.	100
3.37	Borehole data of log of boring number H186.	101
3.38	Borehole data of log of boring number H0043.	101
3.39	Location and chloride distribution of borehole in the study area (red points) shows the location of borehole have a lithology log (yellow points) shows the location of borehole not have lithology log (base map from GoogleEarth).	103

LIST OF FIGURES (CONTINUED)

FIGURE		PAGE
4.1	Comparison the correlation between (a) seismic refraction data (b) VES data and (c) integrated interpretation of seismic reflection and seismic refraction of SK01 site	105
4.2	Comparison the correlation between (a) seismic refraction data (b) VES data and (c) integrated interpretation of seismic reflection and seismic refraction of SK02 site.	106
4.3	Comparison the correlation between (a) seismic refraction data (b) VES data and (c) integrated interpretation of seismic reflection and seismic refraction of SK03 site.	108
4.4	Seismic section of survey line SKL04.	109
4.5	Comparison the correlation between (a) seismic reflection data (b) VES data and (c) borehole data of log of boring number TH405 of SK05 site.	110
4.6	Comparison the correlation between (a) seismic refraction data (b) seismic reflection data of SK06 site.	111
4.7	Resistivity cross section of the study area placed perpendicular to the coast along a southwest-northeast.	112
4.8	Resistivity cross section of the study area placed perpendicular to the coast along a southwest-northeast.	114
4.9	Resistivity cross section of the study area placed parallel to the coast along a southeast-northwest.	115

CHAPTER 1

INTRODUCTION

Groundwater is one of the most important natural resources that sustain life on the earth. The global demand for freshwater will increase in the coming years. The high demand for freshwater, suggests clearly that, surface water can no longer meet the projected demand. This growing demand is putting enormous pressure on water resources. Since many of the surface water sources have been degraded or depleted, due to exposure to pollution, increase in population, changes in climate and over-exploitation, much pressure is being exerted on the groundwater sources.

Of all the water on earth, it is estimated that 99.4% is surface water. Groundwater occurs only as 0.6% of the total. However, of the vast amount of surface water, most of it is in the form of saltwater in the oceans and inland seas (97%). Fresh surface water accounts for only 2% of the total volume of water.

Historically, surface water has accounted for most of the human consumption, because it is easily accessible (with the exception of arid regions, where groundwater may be the only reliable source of water). Modern development and population growth, however, has greatly increased water demands. Surface water resources are being depleted, and furthermore, contaminated. Alternative water resources have to be sought. In the last half century, the demand for groundwater has been rising steadily. Nowadays, groundwater use amount to about one-third of total freshwater consumption in the world. Groundwater resources can be divided into two more or less equal groups: shallow (less than 800 m deep) and deep (more than 800 m) groundwater (Bear et al., 1999).

The situation of the groundwater shortage near the coastline is often severe where a larger number of people live and the groundwater aquifers are threatened and/or contaminated by seawater intrusion. The groundwater contamination due to saltwater intrusion is usually caused by a violation of a sensitive hydrogeological balance that exists between freshwater and saltwater in coastal aquifers. This dynamic balance is often subverted by groundwater over-pumping and

other human activities (e.g. land drainage) that lower groundwater levels and cause seawater movement into the coastal aquifers. This problem is important for all coastal aquifers.

1.1 Groundwater

Groundwater occurs in pores, fractures, solution cavities and other openings in geologic formations. Figure 1.3 shows the groundwater occurs in the pore spaces of geologic formations. There are two types of porosity: primary porosity, which refers to openings that formed at the same time as the rock, such as the pores in well-sorted unconsolidated sand, and secondary porosity, which refers to openings that formed, such as fractures in granites and solution cavities in limestone. The nature of the water-bearing openings within a specific geologic formation depends to a large extent on the mineral composition and structure of the formation and the geologic processes that initially formed and then further modified it.

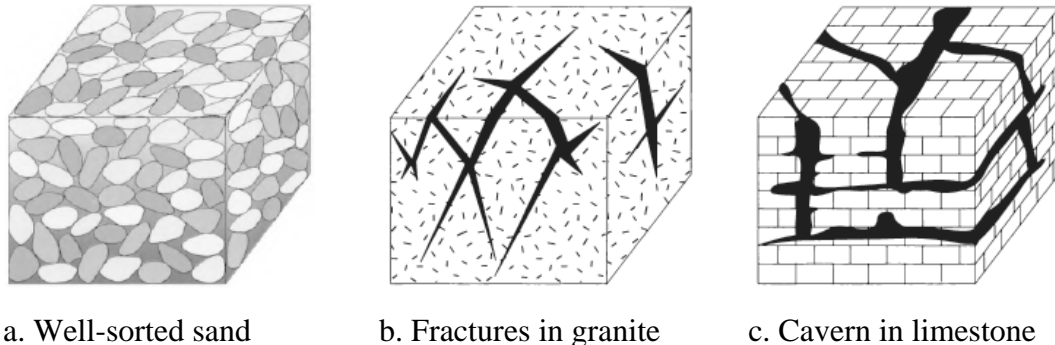


Figure 1.1 Groundwater occurs in the pore spaces of geologic formations (modified from Heath, 1998).

There are two types of aquifers; confined and unconfined (with semi-confined being in between). Unconfined aquifers are sometimes also called water table or phreatic aquifers, because their upper boundary is the water table or phreatic surface. Typically (but not always) the shallowest aquifer at a given location is unconfined, meaning it does not have a confining layer (aquitard or aquiclude) between it and the surface. The term "perched" refers to groundwater accumulating

above a low-permeability unit or strata, such as a clay layer. This term is generally used to refer to a small local area of groundwater that occurs at an elevation higher than a regionally-extensive aquifer. The difference between perched and unconfined aquifers is their size (perched is smaller).

If the distinction between confined and unconfined is not clear geologically (i.e. if it is not known if a clear confining layer exists, or if the geology is more complex, e.g., a fractured bedrock aquifer), the value of storativity returned from an aquifer test can be used to determine it (although aquifer tests in unconfined aquifers should be interpreted differently than confined ones). Confined aquifers have very low storativity values (much less than 0.01, which means that the aquifer is storing water using the mechanisms of aquifer matrix expansion and the compressibility of water, which typically are both quite small quantities. Unconfined aquifers have storativities (typically then called specific yield) greater than 0.01 (1 % of bulk volume); they release water from storage by the mechanism of actually draining the pores of the aquifer, releasing relatively large amounts of water (up to the drainable porosity of the aquifer material, or the minimum volumetric water content).

1.2 Coastal aquifers

Coastal zones contain some of the most densely populated areas in the world as they generally present the best conditions for productivity. However, these regions face many hydrological problems like, flooding due to cyclones and wave surge, and drinking freshwater scarcity due to problems of salt water intrusion. Features which affect coastal aquifers are summarized in Figure 1.2.

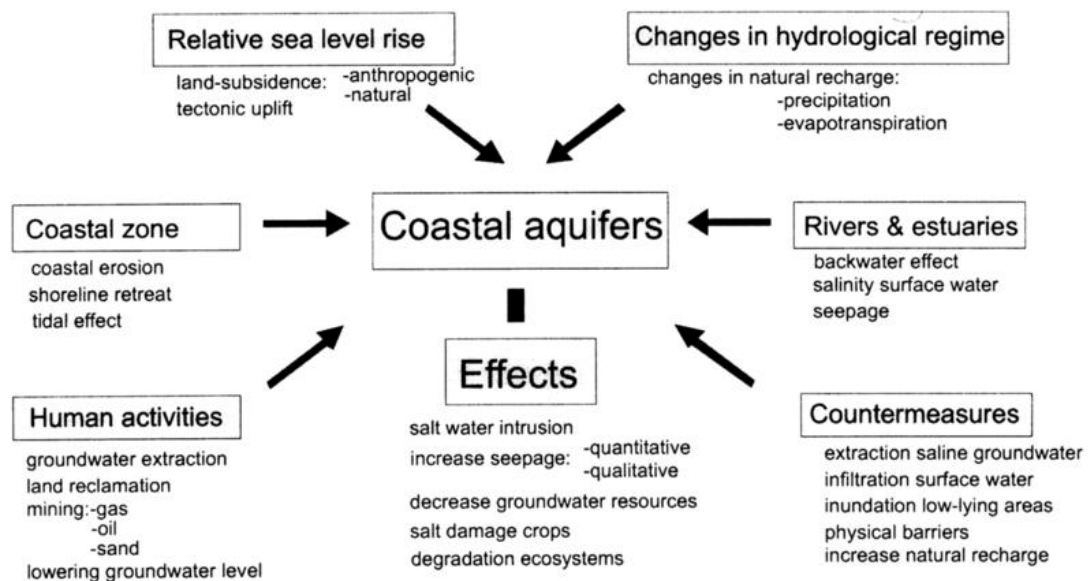


Figure 1.2 Features Affecting the Coastal Aquifers (Kumar, 1987).

When dealing with exploitation, restoration and management of fresh groundwater in coastal aquifers, the key issue is saltwater intrusion. The natural balance between freshwater and saltwater in coastal aquifers is disturbed by groundwater withdrawals and other human activities that lower groundwater levels, reduce fresh groundwater flow to coastal waters, and ultimately cause saltwater to intrude coastal aquifers. Although groundwater pumping is the primary cause of saltwater intrusion along the coasts, lowering of the water table by drainage canals also lead to saltwater intrusion. Other hydraulic stresses that reduce freshwater flow in coastal aquifers, such as lowered rates of groundwater recharge in seweraged or urbanized areas, also could lead to saltwater intrusion, but the impact of such stresses on saltwater intrusion, at least currently, likely is small in comparison to pumping and land drainage.

The variability of hydrogeologic settings, sources of saline water, and the history of groundwater withdrawals and freshwater drainage along the coasts have resulted in a variety of modes of saltwater intrusion. Saltwater can contaminate a freshwater aquifer through several pathways, including lateral intrusion from the ocean, by upward intrusion from deeper, more saline zones of a groundwater system,

and by downward intrusion from coastal waters. Figures 1.3 shows the schematic illustrations of some of the modes of saltwater intrusion in a multilayer, regional aquifer system caused by groundwater pumping at wells. Saltwater moves into the unconfined aquifer from the ocean and into the shallow part of the top confined aquifer from the major bay. The two freshwater-saltwater interfaces at the seaward boundary of each of the confined aquifers also move landward as saltwater is drawn inland from offshore areas.

Saltwater intrusion reduces freshwater storage in coastal aquifers and can result in the abandonment of freshwater supply wells when concentrations of dissolved ions exceed drinking-water standards. The degree of saltwater intrusion varies widely among localities and hydrogeologic settings. In many instances, the area contaminated by saltwater is limited to small parts of the aquifer and has little or no effect on wells pumped for groundwater supply. In other instances, contamination is of regional extent and has substantially affected groundwater supplies. The extent of saltwater intrusion into an aquifer depends on several factors, including the total rate of groundwater that is withdrawn compared to the total freshwater recharge to the aquifer, the distance of the stresses (wells and drainage canals) from the source (or sources) of saltwater, the geologic structure and distribution of hydraulic properties of the aquifer, and the presence of confining units that may prevent saltwater from moving vertically towards or within the aquifer. Moreover, the time required for saltwater to move through an aquifer and reach a pumping well can be quite long. Depending on the location and lateral width of the transition zone, many years may pass before a well that is unaffected by saltwater intrusion suddenly may become contaminated.

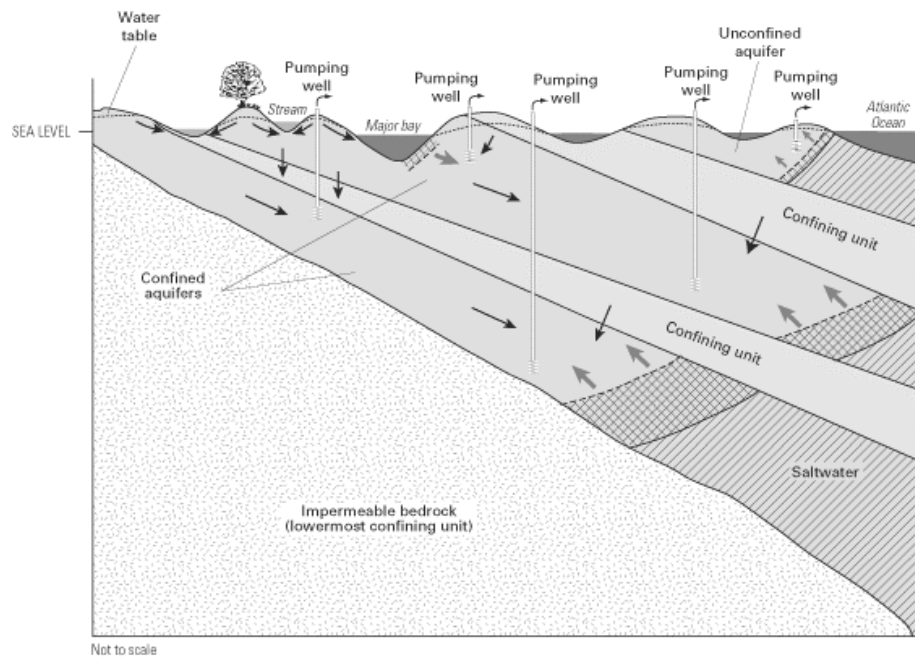


Figure 1.3 Schematic illustrations of some of the modes of saltwater intrusion (Reilly and Goodman, 1987).

1.3 Geophysical investigations of coastal aquifers in previous studies

Geophysical methods measure physical properties of the earth that can be related to hydrologic or geologic aspects of an aquifer, such as pore-water conductivity (Stewart, 1999). Although there are a variety of geophysical techniques that commonly are applied in groundwater investigations, two types of techniques electrical methods and seismic methods are particularly useful in coastal environments. Electrical methods have been widely applied in coastal and island environments because of their ability to detect increases in the conductivity of an aquifer that result from increases in pore-water conductivity (Stewart, 1999). The electrical conductivity of an aquifer is controlled primarily by the amount of pore space of the aquifer (or aquifer porosity) and by the salinity of the water in the pore space; increases in either the porosity or the concentration of dissolved ions result in increases in the conductivity of the groundwater. Because seawater has a high concentration of dissolved ions, its presence in a coastal aquifer can be inferred from measurements of the spatial distribution of electrical conductivity. Seismic methods, on the other hand, do not detect saltwater, but can be used to delineate the distribution

of geologic units within an aquifer that affect the distribution and movement of saltwater (Stewart, 1999).

Bangkok, the capital of Thailand, has a population of more than 6 million. It is located near the southern margin of the Lower Central Plain of Thailand, also known as the Lower Chao Phraya Basin. The Lower Central Plain is a complex block basin, filled with alluvial and deltaic sediments which may exceed 1,000 m in thickness (Nutalaya and Rau, 1981). The topmost unit of this sequence is thick of soft, Holocene marine clay 15–25 m. Beneath the Bangkok Clay, the Department of Mineral Resources, DMR, Thailand, has identified up to nine sand/gravel aquifers, separated by impermeable clays, within the upper 550 m of sediments (Nutalaya et al., 1985).

Whiteley et al. (1997) studied the shallow aquifers in Thailand by using seismic reflection method to map the shallow aquifer sequence beneath the Bangkok Clay. The survey was carried out in an area where reliable borehole information was available to aid in the interpretation of the seismic profiles.

The Bangkok Clay proved to be an excellent medium for high-resolution seismic surveying, and very little interference from ground roll was apparent, allowing reflections with up to 200 ms two-way travelttime (~150 m below surface) to be observed with a relatively small source receiver offset. It was established by trial shooting that a 5-m geophone interval with a single 100-Hz geophone per trace and an “optimum” or common offset of 30 m produced the desired combination of high quality shallow reflection data and reasonable line coverage. Information for velocity analyses was obtained by recording a 12-channel record with a 15-m source offset for each 12-channel geophone spread (i.e. every 60 m along the survey line). Record lengths were typically 200 ms, corresponding to a sample interval of 0.2 ms. One line (Bangkhan line) was acquired with a longer record length (500 ms; 0.5-ms sampling interval) and a source-receiver offset of 45 m, in order to image subsurface structure to depths of ~250 m.

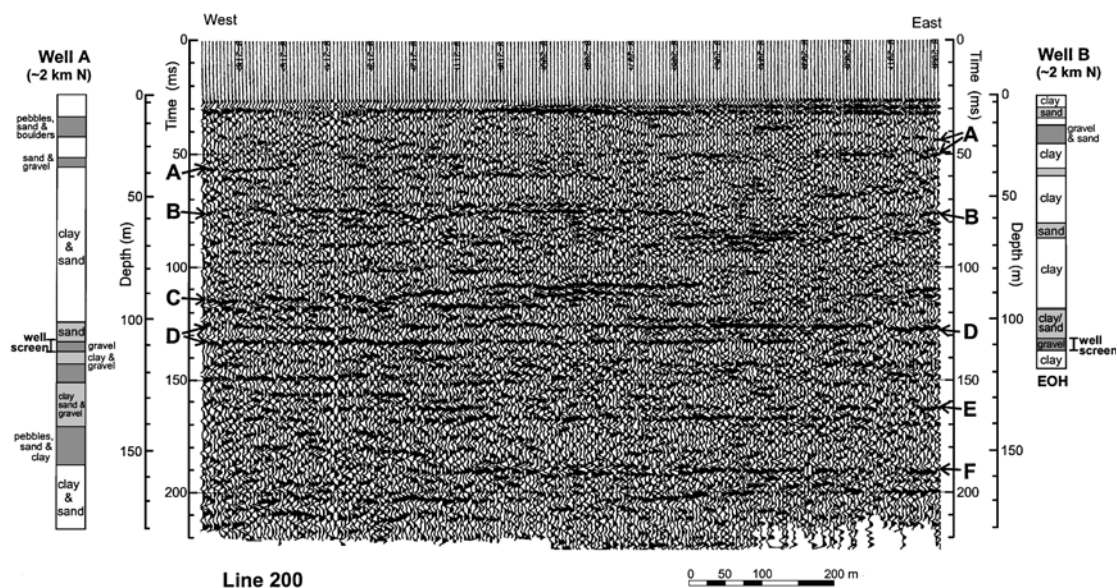


Figure 1.4 Optimum offset section (~1 km long) from line 200, with two borehole logs for reference (note that these boreholes are both ~2 km offline). These data were acquired with the source and geophones planted in the bottom of a water-filled klong (canal), and the water-saturated surface conditions have contributed to the high frequency of the recorded data (Natalaya et al., 1985).

Figure 1.4 shows the optimum offset section of line 200, along with two borehole logs from wells located approximately 2 km north of the line. The large distance between the boreholes and the survey line means that these logs can be used only as a very general guide in the interpretation of the seismic data. The data were acquired on line 200 by shooting the inhole shotgun source in the bottom of a Klong (water-filled canal). At about 60 m depth, a reflection (B), indicating a slightly irregular surface, is interpreted to be the top of coarse-grained layer (indicated as a sand unit in well B), which is likely the first aquifer in this area. Below this surface, larger amplitude reflections (C) at 80–90 m depth show some structure associated perhaps with a large channel cut. The borehole logs indicate that the sediments are becoming sandier at these depths. Coherent, flat-lying, continuous reflections at ~100 and 110 m depth (D) are interpreted to represent the sands and gravels associated with the second aquifer (indicated by the well screen positions in the two boreholes). This

is underlain by several other flat-lying, semi-continuous reflections in the 130–180 m zone (E and F), which are interpreted to represent deeper coarse-grained sequences. These layers do not appear to be as continuous in extent or character as the reflections associated with the second aquifer, but this may be partly caused by the decrease in signal strength with depth.

The seismic sections suggest that the first aquifer at about 30–60 m depth is not very continuous in the survey area. In contrast, the second aquifer at 90–130 m consistently produced coherent, continuous, relatively flat-lying reflections, and was an excellent marker horizon. This aquifer is probably hydraulically connected over much of the area surveyed. The deeper third aquifer in the 150–180 m depth range also appears to be relatively continuous over the survey area.

Samsudin et al. (2007) studied about coastal aquifers in the state of Kelantan, located in the northeastern corner of Peninsular Malaysia has an alluvial delta and coastal plain stretching about 40 km in length 10 km in width on its coast. The interpretation of geoelectrical resistivity sounding adjacent to an existing borehole showed good thickness correlation for subsurface layers. The first aquifer, at the surface, is about 4 m thick, with an apparent resistivity of more than 100 ohm-m. The second aquifer, which is separated by the clay layer, is about 18–33 m below the ground surface, with an apparent resistivity of less than 45 ohm-m. Since a resistivity value of 45 ohm-m was used to delineate brackish groundwater within the aquifer; the groundwater in the second aquifer is interpreted to be brackish. The seismic section shows the variation in thickness and depth of the second and third aquifers. The near-surface first aquifer could not be mapped by the reflection seismic technique. The second aquifer is located between 30 m and 40 m depth, and the deeper third aquifer is depicted between 50 m and 90 m in the seismic depth section.

An example of an application of seismic refraction is the study of Geke Island, Pingelap Atoll, Pohnpei (Ayers and Vacher, 1986). Deke is considered by Ayers and Vacher to be representative of many small atoll islands. Seismic refraction profiles reveal an essentially two-layer system, with unconsolidated sediments overlying more indurate units. The seismic refraction survey was able to map the boundary between the unindurated and indurated sediments. Vertical electrical

sounding and water quality data indicate that the freshwater lens is essentially contained within V_1 , with the top of the transition zone at or near the contact between units V_1 and V_2 . In this case, geologic boundary, which can be mapped on the basis of a contrast in seismic velocity, controls the position of the interface.

Seismic reflection is best applied in cases where the geometry of shallow geologic units with moderately complex geology influences the configuration of the interface. An example is the contact between younger, less permeable sediment and older, more permeable units in carbonate islands. This contact typically truncates the bottom of the freshwater lens (Ayers and Vacher, 1986), so that the position of the boundary controls the depth to the interface (Vacher et al., 1992). A similar boundary occurs where coarse, transgressive beach deposits overlie fine-grained sediments in barrier islands. The location and depth of the fine-grained units often control the thickness of the freshwater lens (Wait and Callahan, 1965; Harris, 1967). Electrical methods are less useful in these transgressive sequences because the fine-grained units are conductive, creating a geoelectric ambiguity between lithology and water quality. In this case, resolving the geologic boundary may be a more effective way of defining the freshwater lens than an ambiguous vertical profile of bulk conductivity.

Shallow, high resolution, seismic reflection methods are not well suited to reconnaissance surveys. Data acquisition rates are slow, elevations of all sources and detector locations must be determined, and considerable effort is expended in data processing. Reflection methods are best applied where detailed information is required and geologic conditions make electrical methods impractical. The ability of seismic methods to map significant changes in seismic velocity above or below the interface would make them an excellent choice for such an objective.

Miller et al. (1996) used high resolution seismic reflection method to study the stratigraphy and physic properties of coastal aquifers on the barrier islands of New Jersey. Five multichannel profiles, totaling 5.4 km in length, were collected from Island Beach State Park to Shipbottom, were careful selection of acquisition and processing parameters produced very high resolution profiles with penetration depths to 186 m. Synthetic seismograms were generated from geophysical logs from nearby wells for comparison with the seismic data and to confirm interpretations. This study

gave aquifers and confining units of interest are resolved in detail on the profiles. Typical aquifer responses include strong, continuous reflection peaks at the top of sand bodies and a less distinguishable seismic negative peak at the base of the units.

Shtivelman and Goldman (2000) using shallow reflection seismic and time domain electromagnetic (TDEM) were a detailed study of the coastal aquifer in the Mediterranean coast of Israel. The results of seismic survey show a sequence of reflected events which can be related to impermeable units located within and below the aquifer. The sea water intrusion was clearly detected as a geoelectric unit having resistivity less than 2 ohm-m approximately. In addition, the borehole information was used for correlation purposes.

Al-Amri (1996) used the vertical electrical sounding method for delineate the geometry of the water bearing layers and roughly estimate the salinity extent with respect to distance from the Red Sea coast. The VES results showed that it is possible to detect freshwater zones of medium resistivity (20 to 70 ohm-m) beneath strata with very low resistivity (<7 ohm-m) at depths of greater than 60 m. The highest groundwater potential is found mainly in the upstream of Wadi alluvium which contains lower clay content than found farther downstream.

Nowroozi et al. (1999) used electrical resistivity survey to study saltwater intrusion into the freshwater aquifer in the eastern shore of Virginia. Resistivity decreases with depth from the high value of the unsaturated zone near the surface to the low values of the saltwater saturates zone at depth of 30 to 130 m. Within the area covered by the cities of Onancock, Accomac and Wachapreague, low resistivity contours of less than 30 ohm-m are observed from 30 to 60 m depth. In 70 to 130 m depth range, a major part of Accomack County is covered by low resistivity contours of 10 to 30 ohm-m which connect the Chesapeake Bay to the Atlantic Ocean. Vertical profiles of the contour maps indicate the shape of the saltwater plumes. The interface appears to be as shallow as 30 m where intrusion has occurred and extends downward to a depth of 130 m.

Choudhury et al. (2001) used electrical resistivity and shallow refraction methods have been employed in the alluvial coastal belt of Digha, in the Eastern India for environmental study, to investigation the nature and status of

subsurface saline water contamination. Integrated of VES and shallow seismic refraction methods have delineated the various subsurface geological formations, the aquifer and the saline/brackish groundwater zones. Some zones of saline water intrusion have been delineated in the area in the depth ranges 0-5, 5-10, and 40-60 m.

Zouhri et al. (2008) used electrical resistivity and seismic methods for interpret the fresh/salt water interface and the structural and hydrodynamic conditions of the marine intrusion. Analyzed the water samples were collected from 28 wells for determined the hydrochemical characterization though a study of the spatial and temporal physico-chemical distribution. The results of this integrated study point unequivocally to a relationship between the physico-chemical properties of the groundwater and their physical and geological environment was found that the seawater encroachment into the groundwater aquifers rarely exceeds 500 m.

Samsudin et al. (2008) used a combination of hydrogeochemical and geophysical techniques to study the salinity of the groundwater aquifers in the coastal area of north Kelantan. The hydrogeochemical investigation analysis of major ion contents of the groundwater was conducted and other chemical parameters such as pH and total dissolved solids were also determined. For the geophysical study, both geoelectrical resistivity sounding and reflection seismic surveys were conducted to determine the characteristics of the subsurface and groundwater contained within the aquifers.

Because of its potential to detect changes in pore-water salinity, the surface electrical resistivity method can become a valuable aid in coastal groundwater exploration and investigations. With such concern Urish and Frohlich (1990) used electrical resistivity method to determine the freshwater layer. It was recognized that the lower boundary of the unsaturated zone corresponds to the top of the capillary zone, not to the water table, and that the lower boundary of the freshwater layer corresponds only approximately to the top of the freshwater-salt-water transition zone. The existence of freshwater layer can be ascertained qualitatively by visual inspection of electrical sounding curves, provided there is a freshwater/unsaturated layer thickness ratio of at least four.

Sikandar et al. (2010) used vertical electrical sounding (VES) was conducted at Chaj Doab and Rachna Doab with the objective of investigating

groundwater conditions. A total of 90 sites were selected with 43 sites in Chaj and 47 sites in Rachna Doabs. A total of 102 groundwater samples from nearby hydrowells at different depths were collected to develop a correlation between the aquifer resistivity of VES and the electrical conductivity (EC) of the groundwater and to confirm the resulted geophysical resistivity models. From the correlation developed, it was observed that the groundwater salinity in the aquifer may be considered low and so safe for irrigation if resistivity >45 ohm-m, and marginally for irrigation having resistivity between 25 and 45 ohm-m. The study area has resistivity values from 3.9 to 2,222 ohm-m at the top of the unsaturated layer, between 1.21 and 171 ohm-m, in the shallow aquifers, and 0.14-152 ohm-m in the deep aquifers of the study area. The results indicate that the quality of groundwater is better near the rivers and in the shallow layers compared to the deep layers

A shallow water seismic study was recently carried out as a part of a site investigation project in the Haifa Port Extension area near the Mediterranean coast of Israel (Shtivelman, 2001). The objectives of the study were estimating P- and S-wave velocity distribution below the seabed and detecting recent faulting at the site. The data acquisition was performed using bay cables and hydrophones placed at the seabed. The source of seismic energy was a single air gun for the reflection survey and explosives for the refraction survey.

Henley et al. (2007) tested “high-effort” method for high resolution surveys by using 2.5 m geophone spacing. The spread was 937.5 m in length, with 376 single geophone stations. For this survey, shots were spaced every 5 m along the line, which was shot from one end to the other without moving any portion of the spread. They created four other data sets by using all of the same original shot gathers, but decimating the receiver stations to simulate shot gathers with receiver intervals of 5 m, 10 m, 20 m and 40 m. The decimation was done by applying appropriate trace mixing to the input gathers before decimation, to simulate using the originals geophones in arrays.

Treadwey et al. (1988) study to using high-resolution seismic reflection data to investigate shallow subsurface structure associated with a segment of Lost River fault that was reactivated in the October 28, 1983, Borah Peak, Idaho,

earthquake, by using four different seismic lines using different sets of recording parameters produced reflections from different depth ranges and at different resolutions. All of the seismic lines were recorded using a 24-channel, fixed gain, 12-bit, digital seismograph. The receivers used were single 100 Hz geophones. Rifle sources, were used for all of the lines. Before the data were digitally sampled, they were filtered with a low-cut filter. The low-cut filters help attenuate low-frequency noise such as ground roll and increase the dominant frequency of the reflection signal. This paper demonstrates the advantages of using multiple shallow seismic surveys in defining complex geologic structure at various depths. The seismic data in this paper show that data collected using different recording parameters over the same line can produce radically different looking data and possibly even different interpretation.

Steeple and Miller (1990) studied possible pitfalls in data collection, processing, and interpretation in seismic reflection methods applied to engineering, environment, and groundwater problems. The applications shallower than 30 m by seismic reflection method measures different parameters than other geophysical methods, and requires careful attention to avoid pitfalls in data collection, processing, and interpretation. Path of the key to avoiding the pitfalls is to understand the resolution limits of the technique, and to plan carefully shallow reflection surveys around the geologic objective and the resolution limits.

Baker et al. (1999) used three distinct seismic reflections were obtained from within the upper 2.1 m of flood-plain alluvium in the Arkansas River valley near Great Bend, Kansas. Reflections were observed at depths of 0.63, 1.46, and 2.10 m. The wave field was densely sampled by placing geophone at 5 cm intervals, and near-source non-elastic deformation was minimized by using a very small seismic impulse source. They used a 96-channel Bison Model 24096 seismograph with 24-bit. Data were recorded with a $\frac{1}{4}$ ms sample interval, a 4 Hz low-cut filter. The seismic energy source was a single shot from a 0.22-caliber rifle using subsonic solid-point short ammunition. Interpreting the subsurface by comparing real and synthetic seismograms yielded reflecting boundaries at depths of 0.63, 1.46, and 2.1 m, with seismic P-wave velocities in each layer of 180, 255, and 205 m/s. Factors critical to obtaining seismic reflection information from depths

shallower than 2 m are low seismic P-wave velocities (<300 m/s) and high data frequency content (>400 Hz).

1.4 Objective

The Bo Yang District, the study area of this work, is located in Songkhla Municipality, and is the political and administrative center of the province, with various offices, departments, and military units. The coastal area of Bo Yang District is densely populated. Freshwater is necessary and vital for the population in the study area. The objective of this study is the characterization of the coastal aquifer in the Bo Yang district, Songkhla Province, by using shallow seismic methods to characterize subsurface structures and using VES method to characterize the aquifers and identify saline marine water intrusion into the groundwater system.

CHAPTER 2

RESEARCH METHODOLOGY

This chapter describes both the data acquisition and data processing employed in this study. In terms of data acquisition, this chapter describes what the primary data sources are, how data were collected, and how they were organized. In terms of data processing, this chapter explains the procedure of data processing. This chapter provides a contribution towards the main objective of this work, to describe how the formation subsurface can be determined and documentation of the coastal aquifers based on the geophysical data.

2.1 Study area

Thailand has more than 3,200 km coastline, mainly in the Southern part along the Andaman Sea in the West and the Gulf of Thailand in the East. Major provincial cities are located near the shorelines; Songkhla is one of these cities. Therefore, Songkhla serves as an example for cities with similar problems regarding saltwater intrusion of coastal aquifers.

The study area is located in a coastal area of the Bo Yang District of Songkhla Province (Figure 2.1) that has a population of more than 76,000 people. The city is bounded by the Gulf of Thailand to the east and the Songkhla Lake in the west, and the most of the area is coastal plain, an area of about 9.27 km². It is bounded by latitudes to 7° 56' N and longitude 100° 01'to 101° 06' E. The shape of the area is a long narrow peninsula along the south to north into the sea. Its elevation is approximately four meters above mean sea level, the municipality has a small hill on the north side are Khao Noi and Khao Tang Kuan , has a height from sea level about 60 and 80 meters respectively. Figure 2.2 shows the geophysical measurement locations in the Bo Yang district.

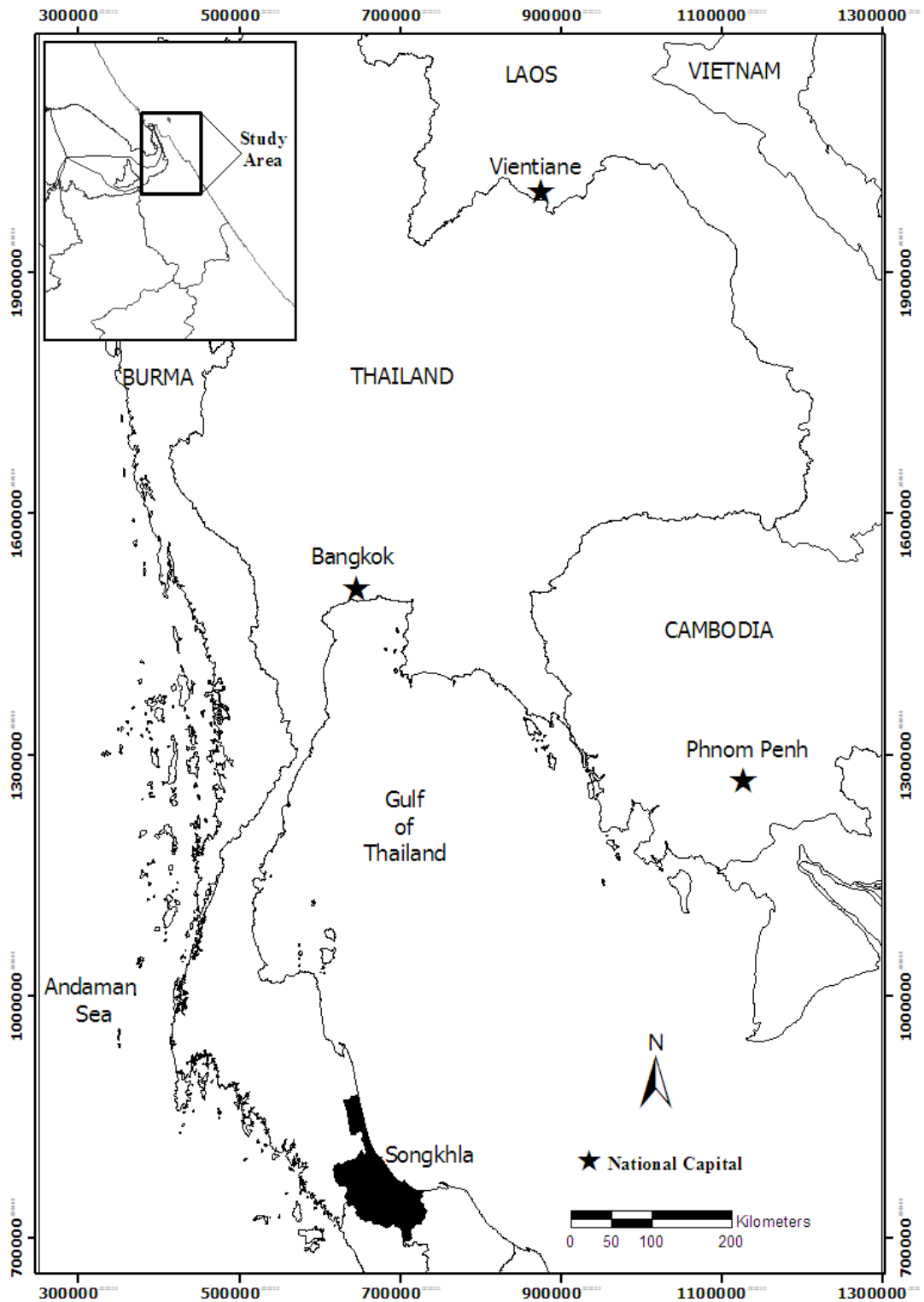


Figure 2.1 Map of Thailand with the location of study area (modified from <http://geology.com/world/thailand-satellite-image.shtml> [8 August, 2011]).

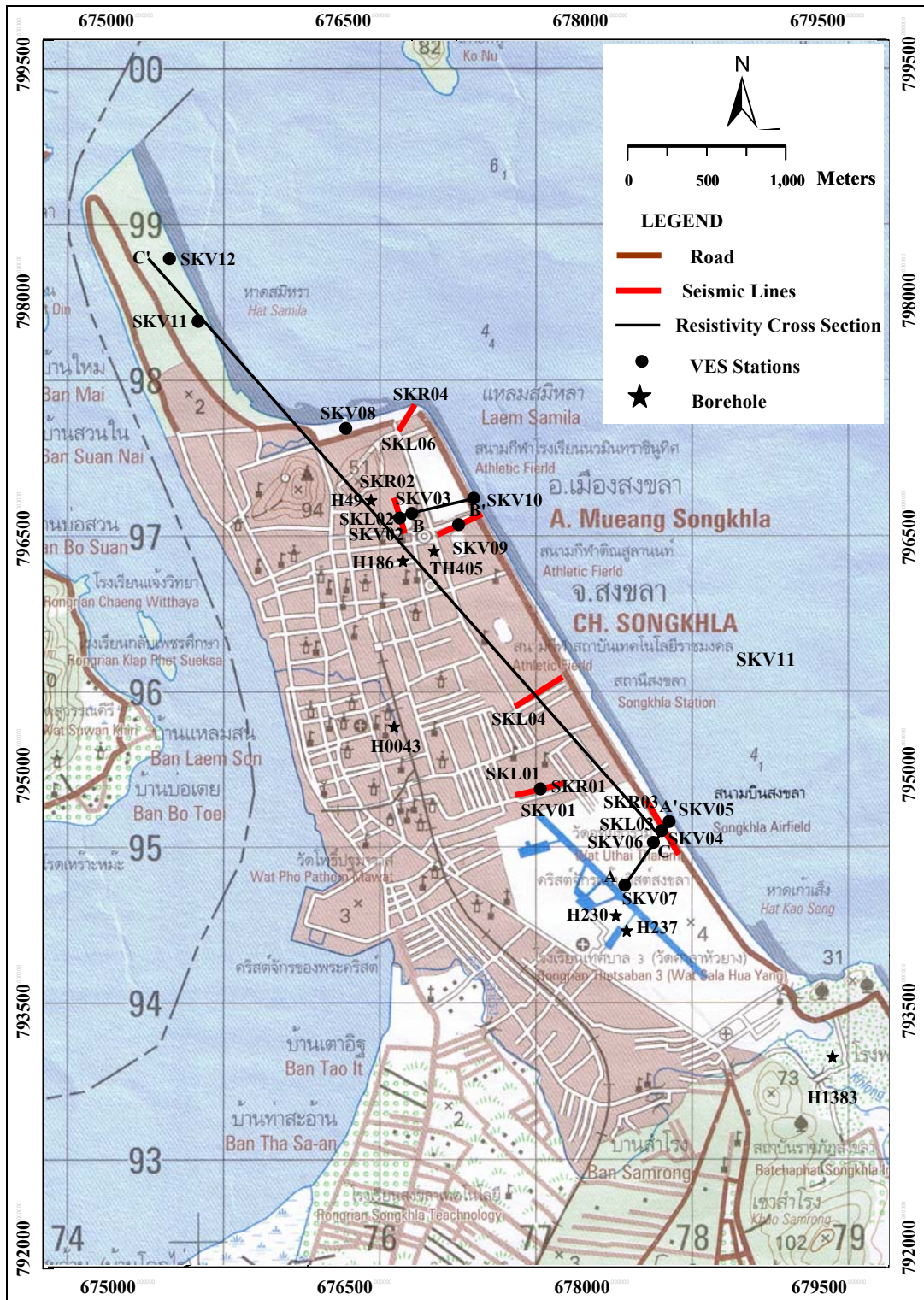


Figure 2.2 Map of study area showing geophysical measurement locations on Bo Yang District, Songkhla Province (modified from Royal Thai Survey Department, 1997).

2.2 Theory of seismic methods

Seismic surveys are the main tool for the examination of the subsurface, shallow seismic data is used for groundwater exploration. The seismic methods of geophysical exploration utilize the fact that elastic waves travel with different velocities in different rocks. The principle is to initiate such waves at a point and determine the time of arrival of the energy that is refracted and reflected by the discontinuities between different rock formations at a number of other points (Parasnis, 1997).

In seismic surveying, seismic waves are created by a controlled source and propagate through the subsurface. Some wave will return to the surface after refraction and reflection at geological boundaries within the subsurface. Instruments distributed along the surface detect the ground motion caused by these returning waves and hence measure the arrival time of the waves at different ranges from the source (Kearey and Brooks, 2002).

2.2.1 Elastic constants and waves

(a) Hooke's law

The basis of the seismic methods is the theory of elasticity. The elastic properties of substances are characterized by elastic modulus or constants which specify the relation between the stress and the strain. A stress is measured as force per unit area. It is a compressive stress if it acts perpendicular to the area and a shear stress if it acts parallel to it. A system of compressive stresses changes the volume but not the shape of a body; one of shear stresses changes the shape but not the volume.

The strains in a body are deformations which produce restoring forces opposes to the stresses. Tensile and compressive stresses give rise to longitudinal and volume strains which are measured as the change in length per unit length or change in volume per unit volume. Shear strains are measured as angle of deformation. It is usually assumed that the strains are small and reversible, that is, a body resumes its original shape and size when the stresses are relieved. Hooke's law states that the stress is proportional to the strain, the constant of proportionality being known as the elastic modulus or elastic constant.

(b) Seismic Waves and Velocity

If the stress applied to an elastic medium is released suddenly the condition of strain propagates within the medium as an elastic wave. There are several kinds of elastic waves:

In the longitudinal, compressional or P–waves, the motion of the medium is in the same direction as the direction of wave propagation. The P–wave velocity is given by

$$V_p = \sqrt{\frac{k + \frac{4}{3}\mu}{\rho}} \quad (2.1)$$

where V_p is the velocity of compressional wave [m/s], k is bulk modulus (incompressibility) [Pa], μ is the shear modulus [Pa] and ρ is the density of the medium [kg/m³].

In the transverse, shear or S–waves, the particles of the medium move at right angles to the direction of wave propagation and the velocity is given by

$$V_s = \sqrt{\frac{\mu}{\rho}} \quad (2.2)$$

where V_s is the velocity of shear wave [m/s].

Shear waves do not propagate through liquids and gases ($V_s = 0$). Shear waves can be polarized in such a way that the particles oscillate along a definite line perpendicular to the direction of wave propagation.

(c) Snell's law

The surfaces in a medium on which the wave motion has the same phase at all points are called wave fronts. The normal to a wave front at any point is the direction of a ray and is the instantaneous direction of wave propagation at that

point. In a medium of constant seismic velocity the rays are straight lines. In inhomogeneous media the rays are curved. It is often more convenient to describe wave propagation by means of rays rather than wave fronts (Parasnis, 1997).

Table 2.1 P wave velocities in materials.

Material	V_P (m/s)	References
Air	330 – 350	Loke, 1999
Water	1,450 – 1,530	Kohnen, 1974
Soil	100 – 500	Kohnen, 1974
Sand (loose)	200 – 2000	Loke, 1999
Sand (dry, loose)	200 – 1000	Loke, 1999
Sand (water saturated, loose)	1,500 – 2,000	Loke, 1999
Sandstone	1,400 – 4,500	Loke, 1999
Clay	1,000 – 2,500	Kohnen, 1974
Sand and gravel (wet)	500 – 1800	Loke, 1999
Sand and gravel (dry)	400 – 1500	Loke, 1999
Soil and Sand	250 – 600	Loke, 1999
Limestone	3,000 – 4,800	Loke, 1999
Granites	4,500 – 5,500	Loke, 1999

When seismic rays fall on the interface between two media may be reflected or refracted. In addition a mode conversion occurs, that is, an incident P wave, is reflected or refracted partly as a P wave and partly as an S wave (Figure 2.3). If θ is the angle made by any ray with the normal to the interface then Snell's law states that

$$\frac{\sin \theta}{V} = \text{const} \quad (2.3)$$

where V is the velocity of the wave in medium of any refracted or reflected wave travel trough [m/s], and θ is the incident angle [degree].

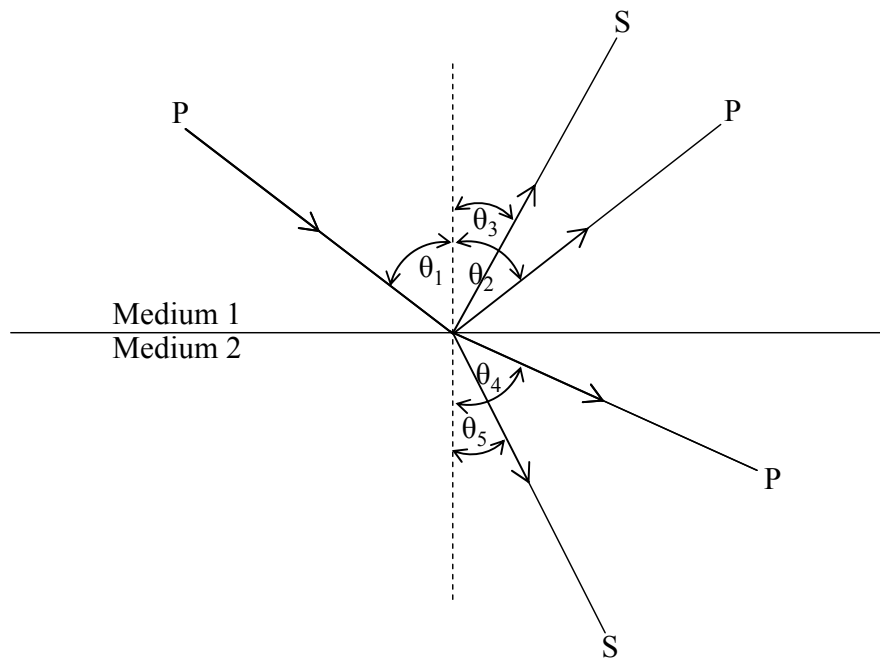


Figure 2.3 Snell's law (modified from Parasnis, 1997).

The general formula of Snell's law is given by

$$\frac{\sin \theta_1}{V_{P1}} = \frac{\sin \theta_2}{V_{P2}} = \frac{\sin \theta_3}{V_{S1}} = \frac{\sin \theta_4}{V_{P2}} = \frac{\sin \theta_5}{V_{S2}} \quad (2.4)$$

If θ_1 of the P wave is such as the ray will be refracted with angle $\theta_4=90^\circ$, it will travel along the interface with a velocity of the lower medium (V_{P2}) and then refracted back to the surface with the angle θ_1 . This incident angle is called the critical angle.

(d) Huygens's principle

The principle states that each point on a wave surface acts as a source for an expanding spherical wave and after a certain time lapse the envelope of all the wavelets defines the new wavefronts. The principle is used for the construction of wavefronts, provided that the location of a wavefront at a particular time and the velocity in the medium are known (Sjögren, 1984).

Every point on a wavefront can be considered a secondary source of spherical waves, and the position of the wavefront after a given time is the envelope of these secondary wavefronts (Figure 2.4). Huygens's construction can be used to explain reflection, refraction and diffraction of waves.

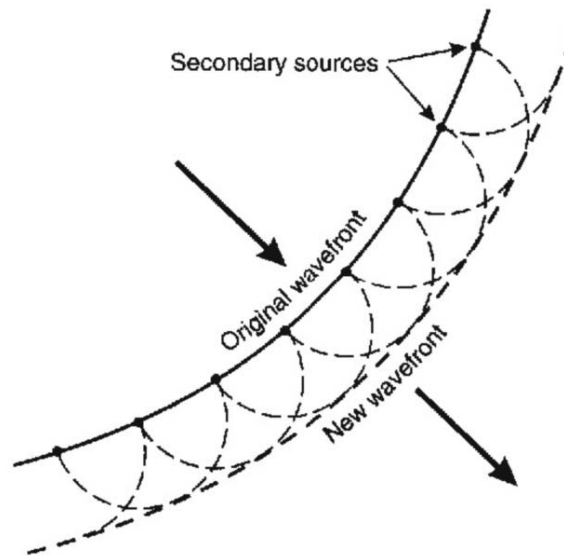


Figure 2.4 Huygens's principle (Sheriff and Geldart, 1995).

(e) Diffraction

Seismic waves can also be affected by objects that are smaller than their wavelength. Some examples are: the edge of a layer, a corner, and small objects such as boulders. When a seismic wave encounters these objects, seismic energy will be efficiently scattered in all directions. This is called diffraction. Huygens Principle can be used to understand this phenomenon. When a plane wavefront is incident on a plane boundary, each point of the boundary acts as a secondary source. The superposition of these secondary waves creates the reflection. If interface truncates abruptly, then secondary waves do not cancel at the edge, and diffraction is observed. Figure 2.5 shows diffracted wavefronts. Diffraction allows seismic energy to reach regions forbidden by ray theory, such as the shadow zone underneath the wedge (Telford et al., 1990). This explains how energy can propagate into shadow zones. A small scattering object in the subsurface such as a boulder will produce a single

diffraction. A finite-length interface will produce diffractions from each end, and the interior parts of the arrivals will be opposite polarity.

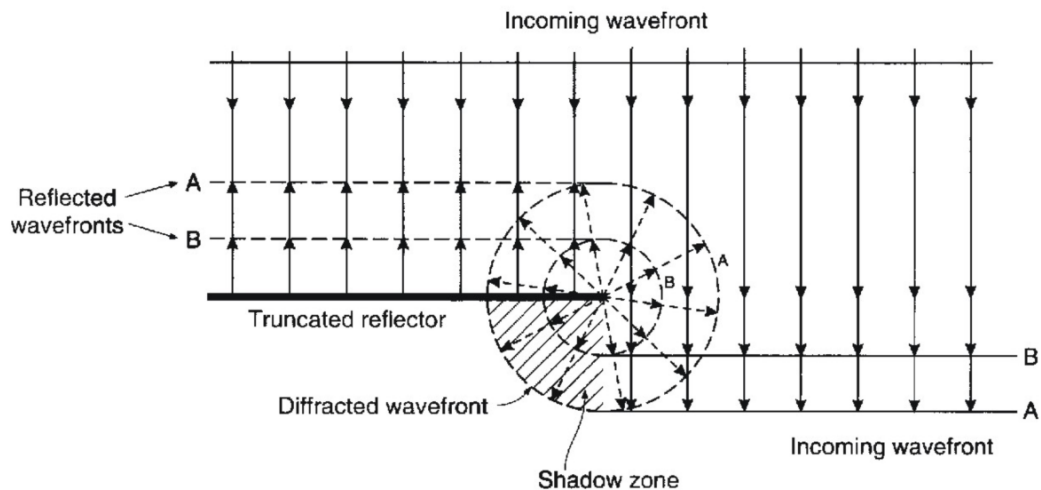


Figure 2.5 Diffracted wavefront (Sheriff and Geldart, 1995).

2.2.2 Seismic data acquisition

Seismic data acquisition is an important part of a seismic survey. There are many factors to consider in a site investigation. These factors depend on knowledge of the target area and include surface geology, well data, geophysical data, and expected depth of the target. There are the offset, geophone spacing, shot spacing, shot location, record length, and time sampling interval were determine. By establishing seismic data acquisition parameters prior to running a seismic survey, the survey can be done more efficiently in regard to time and equipment and will ensure better acquisition of subsurface geological information.

The Bo Yang data acquisition used the following survey equipment:

1. Geometrics SmartSeis (Figure 2.6).
2. Single geophones, 14-Hertz (vertical) geophones.
3. Roll-along switch.
4. Sledgehammer striking a steel plate was used as a seismic source.



Figure 2.6 Geometrics SmartSeis.

Geophone spacing

The geophone spacing is the distance on the surface between each geophone. The velocity, frequency and dip angle of the target horizon are used to calculate geophone interval, can be calculated using the following equation

$$G = \frac{V_a}{2f_{\max} \sin \theta} \quad (2.5)$$

where G is the geophone interval [m], V_a is the average velocity to target horizon [m/s], f_{\max} is the maximum expected frequency [Hz] and θ is the maximum dip angle of target horizon [degree].

Shot spacing

The shot spacing is the distance between source stations. The shot spacing is a function of the desired fold coverage and the number of recorder channels, can be calculated using the following equation

$$S = \frac{NG}{2F} \quad (2.6)$$

where S is the shot spacing [m], N is the number of recorder channels, G is the geophone spacing [m] and F is the fold coverage.

Sampling interval

A seismic survey is a sampling of the continuous medium of the earth. This sampling is possible when the signal sample is sufficient to resolve the layering. Most algorithms for designing seismic surveys relate to the basic rules for sampling continuous data. Sampling interval is the sample at a fixed rate in time of continuous seismic signal. These discrete samples should be reconstructed to the original continuous signal. In general, given the sampling interval, the highest frequency that can be restored is called the Nyquist frequency, can be calculated using the following equation

$$\text{Nyquist frequency} = \frac{1}{2\Delta t} \quad (2.7)$$

where Δt is the sampling interval [ms].

Fold coverage

Each source station yields a certain amount of subsurface coverage. For horizontal layers, the sampled point is half the distance from source to receiver. The subsurface sampling is half the interval of the surface coverage. Stacking of the signal in a common depth point survey improves the signal to noise ratio. This stacking cancels random noise. The signal to noise ratio can be computed from the square root of stacking components, which constitutes fold coverage. Therefore, fold coverage is an important parameter for improving signal to noise ratio. This parameter can be set before data acquisition by defining parameters of the survey line. The fold coverage can be calculated using the following equation (Stone, 1994),

$$F_{\max} = \frac{NG}{2S} \quad (2.8)$$

where F_{\max} is the maximum fold coverage, N is the number of recorder channels, G is the geophone interval [m] and S is the source interval [m]. The fold is a factor in computing the shot spacing. Fold also allows design of processing filters that discriminate against multiples and converts waves in the final seismogram. There are both good and bad aspects to high fold data. Figure 2.7 shows a stacking chart of multifold coverage. Seismic traces recorded from the same shot point are called a common shot gather. Seismic traces that have the same offset interval are called a common offset gather and seismic traces that have the same source to receiver midpoint are called a common mid point (CMP) gather.

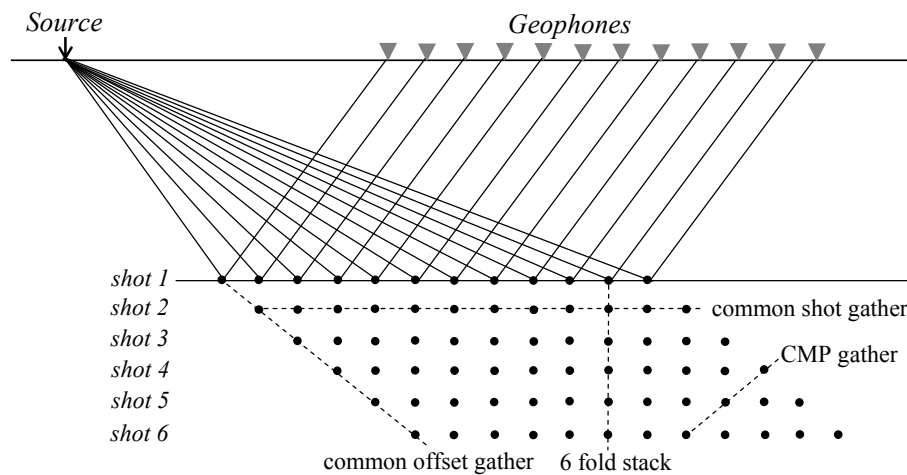


Figure 2.7 Stacking chart of multifold coverage showing common offset gather, common shot gather and CMP gather (Stone, 1994).

2.3 Seismic refraction method

The seismic refraction method assumes constant seismic velocity for each layer. Each layer is separated by a horizontal plane or by dipping interface. The velocity of a wave increases with depth. The seismic refraction method is based on Snell's law. Snell's law can be written as (Figure 2.3)

$$\frac{\sin \theta_1}{\sin \theta_2} = \frac{V_1}{V_2} \quad (2.9)$$

where θ_1 is the incident angle [degree], θ_2 is the refracted angle [degree], V_1 is the velocity of medium 1 [m/s] and V_2 is the velocity of medium 2 [m/s]. Seismic refraction exploration uses the travel times of the refracted waves to determine the velocity structure and layer thickness.

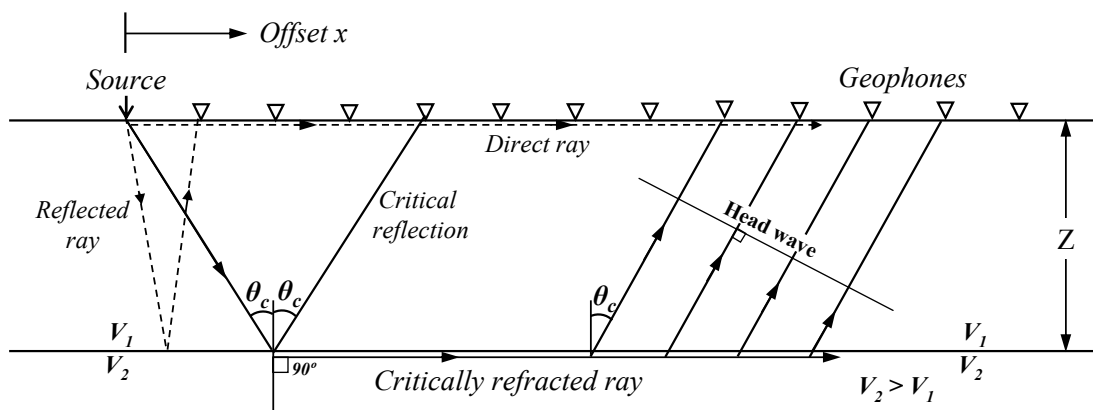


Figure 2.8 Theoretical raypath diagram seismic refraction and reflection (modified from Telford et al., 1990).

If the velocity of the upper layer is less than that of the lower layer and the refracted angle is 90 degrees, the incident angle is known as the critical angle. In this case, the refracted wave travels along the lower layer and returns to the surface at the same critical angle (Figure 2.8). If the velocity of the lower layer is less than that of the upper layer, critical refraction does not occur.

The travel time and distance can be plotted as a travel time-distance graph (Figure 2.9). The travel time-distance graph is used to calculate the velocity by

$$t = \frac{x_{cross}}{V_2} + \frac{2Z_1 \sqrt{V_2^2 - V_1^2}}{V_1 V_2} \quad (2.10)$$

where V_1 is the velocity of medium 1 [m/s], V_2 is the velocity of medium 2 [m/s], x_{cross} is the crossover distance [m], Z_1 is the thickness of the first layer [m] and t is the travel time of source to geophones [s].

In the case of two layers, the intercept time is the intersection on the time axis of travel time-distance curve. Velocities are calculated from slopes of a travel time-distance graph. The thickness of the first layer can be calculated using the following equation

$$t_i = \frac{2Z_1\sqrt{V_2^2 - V_1^2}}{V_1V_2} \quad (2.11)$$

where t_i is the intercept time [s].

Figure 2.9 shows the travel time-distance graph, the travel time of the direct wave gives the velocity of medium 1: slope = $1/V_1$, the travel time of the refracted wave is a straight line with slope $1/V_2$. The refracted wave is the first arrival for offsets greater than the crossover distance (x_{cross}). The refracted wave is observed only for offsets greater than critical distance (x_{crit}). The intercept time (t_i) can be found by extrapolating the refracted wave arrival time to $x = 0$. The depth of the interface can be determined by using

$$Z_1 = \frac{t_i V_1}{2 \cos \theta_c} = \frac{t_i V_1 V_2}{2 \sqrt{V_2^2 - V_1^2}} \quad (2.12)$$

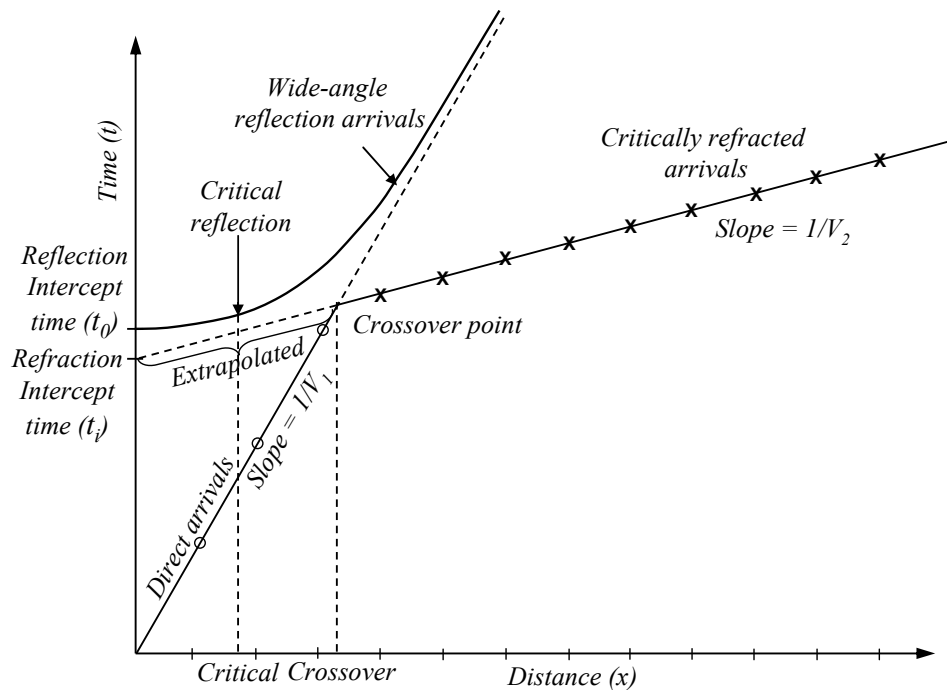


Figure 2.9 Travel time-distance graph of seismic reflection and refraction (modified from Sheriff and Geldart, 1995).

The intersection point of the straight lines for the direct wave and refracted wave is called crossover distance; x_{cross} can be calculated using the following equation

$$t_{\text{cross}} = \frac{x_{\text{cross}}}{V_1} \quad (2.13)$$

where t_{cross} is the travel time at the intersection point of the straight lines for the direct wave and refracted wave [s].

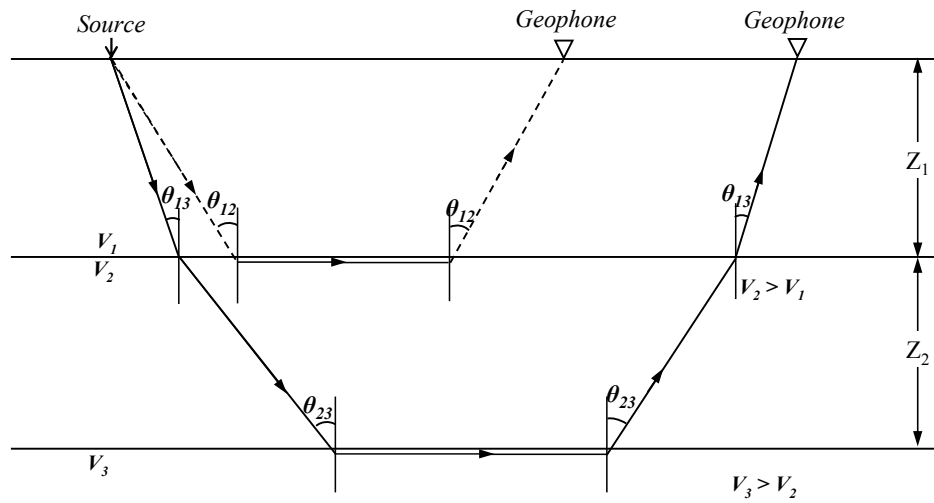


Figure 2.10 Raypath diagram of three layers case (modified from Boyd, 2003).

In case of three layers, Figure 2.10 shows a case of three layers (velocities V_1 and V_2) overlying the bottom refractor where the velocity is V_3 . The critical angle of refraction 1 (2.14) and the critical angle of refraction 2 (2.15) are

$$\sin \theta_c = \sin \theta_{12} = \frac{V_1}{V_2} \quad (2.14)$$

$$\sin \theta_{23} = \frac{V_2}{V_3} \quad (2.15)$$

where θ_{12} is the critical angle between layer 1 and layer 2 [degree] and θ_{23} is the critical angle between layer 2 and layer 3 [degree]. At the boundary between layer 1 and layer 2, Snell's law gives

$$\sin \theta_{13} = \frac{V_1}{V_2} \sin \theta_{23} = \frac{V_1}{V_3} \quad (2.16)$$

It can be shown that the travel time for the refraction can be calculated using the following equation

$$t = \frac{x}{V_3} + \frac{2Z_1 \cos \theta_{13}}{V_1} + \frac{2Z_2 \cos \theta_{23}}{V_2} \quad (2.17)$$

$$t = \frac{x}{V_3} + \frac{2Z_1 \sqrt{V_3^2 - V_1^2}}{V_1 V_3} + \frac{2Z_2 \sqrt{V_3^2 - V_2^2}}{V_2 V_3} \quad (2.18)$$

In case of multi parallel layers, the velocity and intercept time of each layer can be derived from the time-distance graph and then the thickness of each layer can be calculated using the following equation

$$t_n = \frac{x}{V_n} + \frac{2}{V_n} \sum_{i=1}^{n-1} Z_i \frac{\sqrt{V_n^2 - V_i^2}}{V_i} \quad (2.19)$$

where n is the number of layers.

In case of dipping layer, the dipping plane can be interpreted using split spread profiles. This can be used to calculate the thickness of the complex area. Figure 2.11 shows a raypaths and travel time curves for a dipping refractor. The travel time for the dipping layer is determined from Equation (2.20) and (2.21).

$$t_d = \frac{2Z_d \cos \theta_c}{V_1} + \frac{X}{V_1} \sin(\theta_c + \alpha) \quad (2.20)$$

$$t_u = \frac{2Z_u \cos \theta_c}{V_1} + \frac{X}{V_1} \sin(\theta_c - \alpha) \quad (2.21)$$

where t_d is the down dip travel time [s], t_u is the up dip travel time [s], Z_d is the depth of down dip [m], Z_u is the depth of up dip [m], V_1 is the interval velocity of the 1st layer [m/s], θ_c is the critical angle [degree], α is the dip angle [degree], and X is the distance of the geophone from the shot point [m].

Equation (2.20) and (2.21) can be used to calculate the slope of the straight lines by these equations as

$$\frac{1}{V_d} = \frac{\sin(\theta_c + \alpha)}{V_1} \quad (2.22)$$

$$\frac{1}{V_u} = \frac{\sin(\theta_c - \alpha)}{V_1} \quad (2.23)$$

where $1/V_d$ is the slope of down dip and $1/V_u$ is the slope of up dip.

Equation (2.22) and (2.23) can be used to determine θ_c and α as

$$\theta_c = \frac{1}{2} \left(\sin^{-1} \frac{V_1}{V_d} + \sin^{-1} \frac{V_1}{V_u} \right) \quad (2.24)$$

$$\alpha = \frac{1}{2} \left(\sin^{-1} \frac{V_1}{V_d} - \sin^{-1} \frac{V_1}{V_u} \right) \quad (2.25)$$

The following equations can be used to calculate layer thickness

$$t_{id} = \frac{2Z_d \cos \theta_c}{V_1} \quad (2.26)$$

$$t_{iu} = \frac{2Z_u \cos \theta_c}{V_1} \quad (2.27)$$

where t_{id} is the down-dip intercept time [s], and t_{iu} is the up-dip intercept time [s].

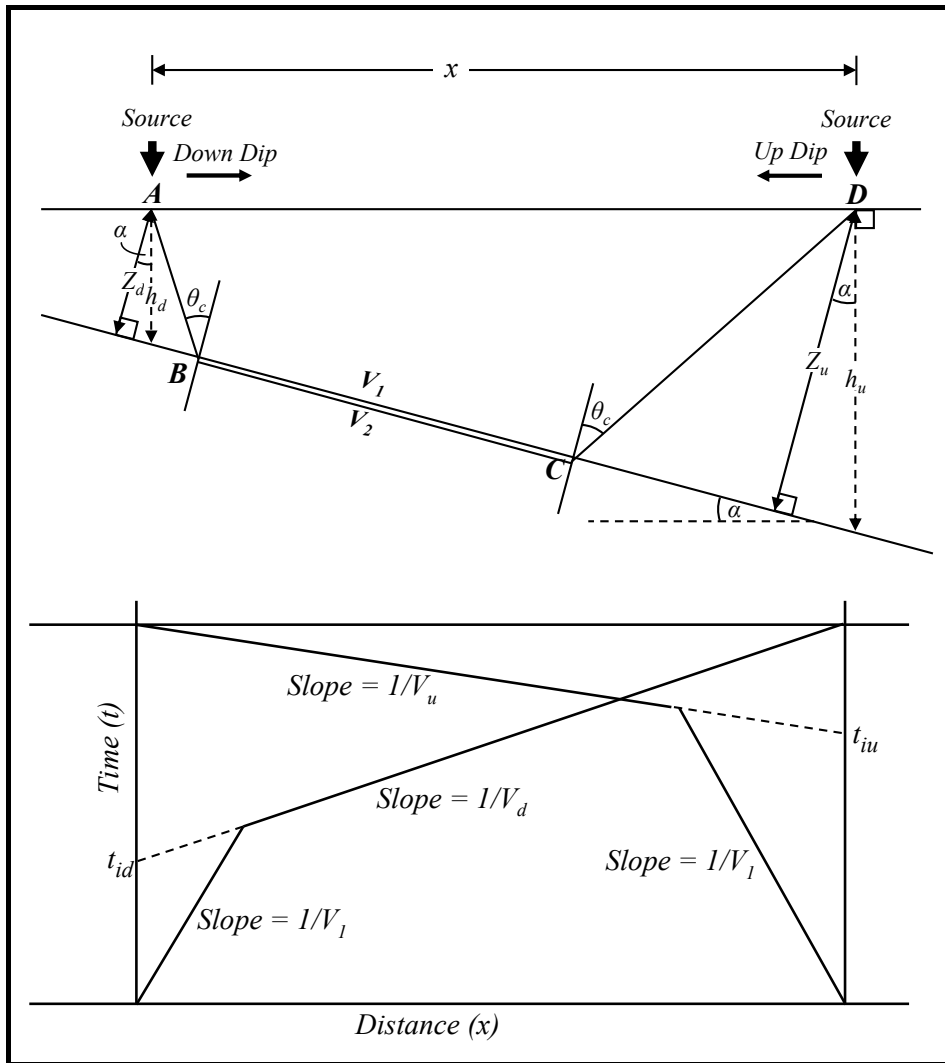


Figure 2.11 Raypaths and travel time curves for a dipping refractor (modified from Burger, 1992).

The following equations can be used to calculate the thickness as

$$h_d = \frac{Z_d}{\cos \alpha} \quad (2.28)$$

$$h_u = \frac{Z_u}{\cos \alpha} \quad (2.29)$$

where h_d is the thickness of down dip [m], and h_u is the thickness of up dip [m].

2.3.1 Seismic refraction data acquisition

Four seismic refraction survey lines were run over the Bo Yang district. Figure 2.12 shows the seismic refraction survey stations of each site. There are Wachiranukul School (SKR01), Mahavajiravudh School (SKR02), Chalathat Road (SKR03) and Samila Beach (SKR04). Table 2.2 shows the seismic refraction data acquisition.

Table 2.2 Seismic refraction data acquisition in the Bo Yang district.

Acquisition Parameter	SKR01	SKR02	SKR03	SKR04
Shot spacing (m)	18	18	18	12
Geophone spacing (m)	3	3	1.5	1
Shots stacked per shot record	10	10	10	10
Record length (ms)	256	256	512	512
Sampling interval (ms)	0.125	0.125	0.25	0.25
Survey length (m)	40	70	40	25
Line direction	N072E	N015W	N030W	N040E

The most common types of profiles that can be used in seismic refraction work are: (1) forward and reverse profiles consisting of a pair of shot points (SP) which surround a common geophone spread, (2) split profiles consisting of a single shot point surrounded by a pair of geophone spread and (3) in-offset profiles consisting of shot points at different distances on both sides of a common geophone spread. In this study, a new technique has been used to acquire and process data.

A number of geophones were placed on the ground along a straight line through the shot points to detect the direct and refracted waves. This technique is known as profile-shooting technique (it includes all the common type techniques in one profile). This technique is mainly used to determine the velocity and thickness of subsurface layers by picking the first arrival. The data acquisition consisting of seven shot points for every single profile.

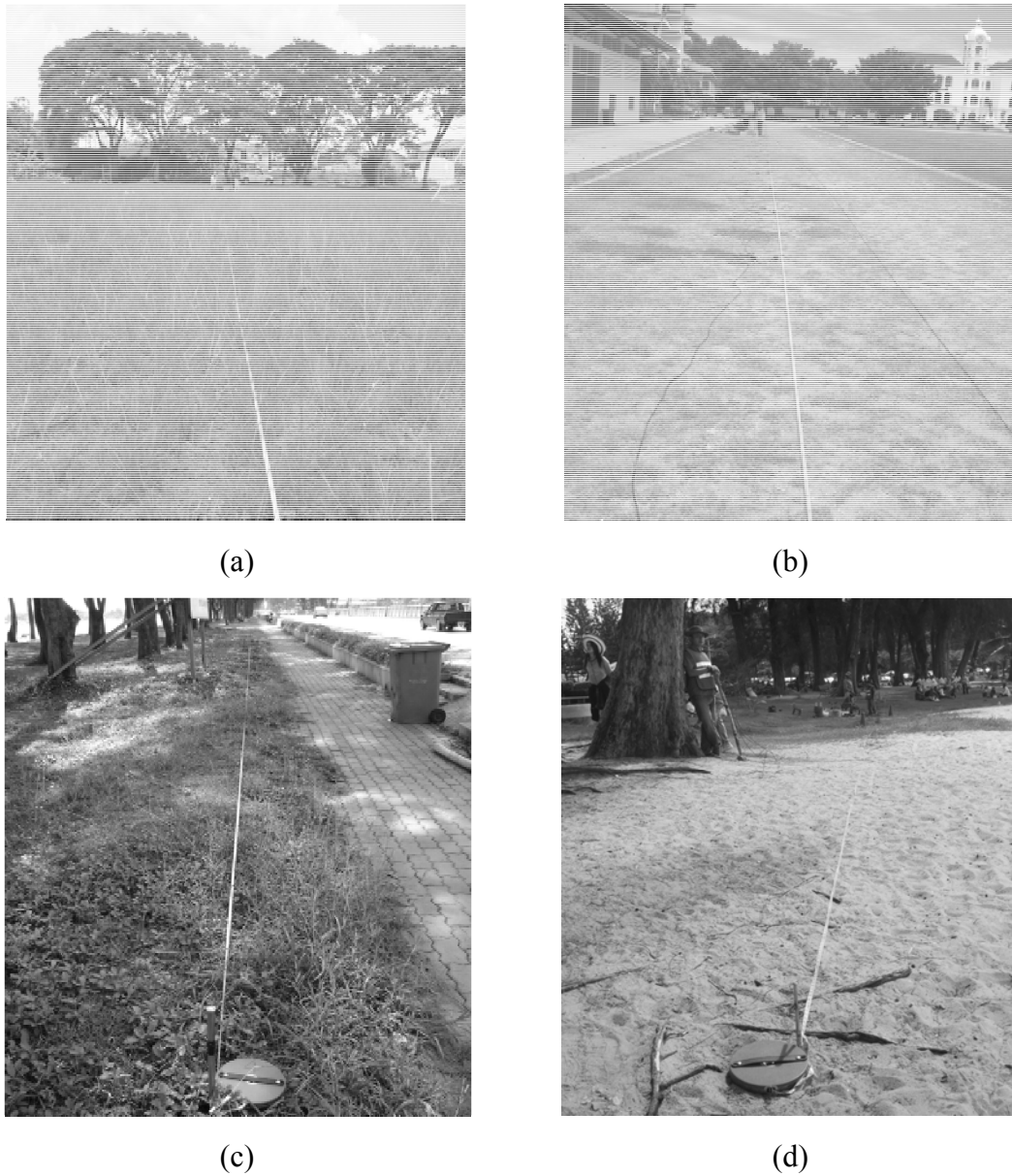


Figure 2.12 Seismic refraction survey stations (a) line SKR01, (b) line SKR02, (c) line SKR03 and (d) line SKR04.

Figure 2.13 shows shot record raw data of survey line SKR03. Shot spacing of each shot point is 18 m. The first shot is a normal shot within a 36.75 m distance before the first geophone (first geophone at zero m), the second shot at a 18.75 m distance before the first geophone, the third shot at a 0.75 m distance before the first geophone, the fourth one is a midpoint shot at a 17.25 m distance between geophone 12 and 13, the fifth shot is the reverse shot at a 0.75 m next to last

geophone, the sixth shot at a 18.75 m distance next to the last geophone and the last shot at a 36.75 m distance next to the last geophone.

2.3.2 Seismic refraction data processing

SIP Software by a registered trademark of Rimrock Geophysics Inc has been used for data processing of seismic refraction data. An initial model was created based on the time-distance graph. The program calculated the velocity of each layer. The depth of each layer beneath each geophone was determined. These depths were then interpolated between adjacent geophone positions. The program assumed that each layer encountered was horizontally continuous and that there were no lateral changes in velocity within any layer (Kutrubes et al., 2002).

Figure 2.14 shows determine the first arrival time (picking the first break) of the seismic wave at each geophone for every geophone spread. This step is the most important one and will determine the reliability of the resulting model. Create the data files for the interpretation program by using the first arrival data together with the elevation of each source points and geophones. Figure 2.15 shows the time distance graph of survey line SKR03. The layer assignment was made in time-distance graphs. Figure 2.16 shows depth and elevation of layers beneath shot points and geophones of survey line SKR03. These data were used to create a 2D velocity–depth model (Figure 2.17).

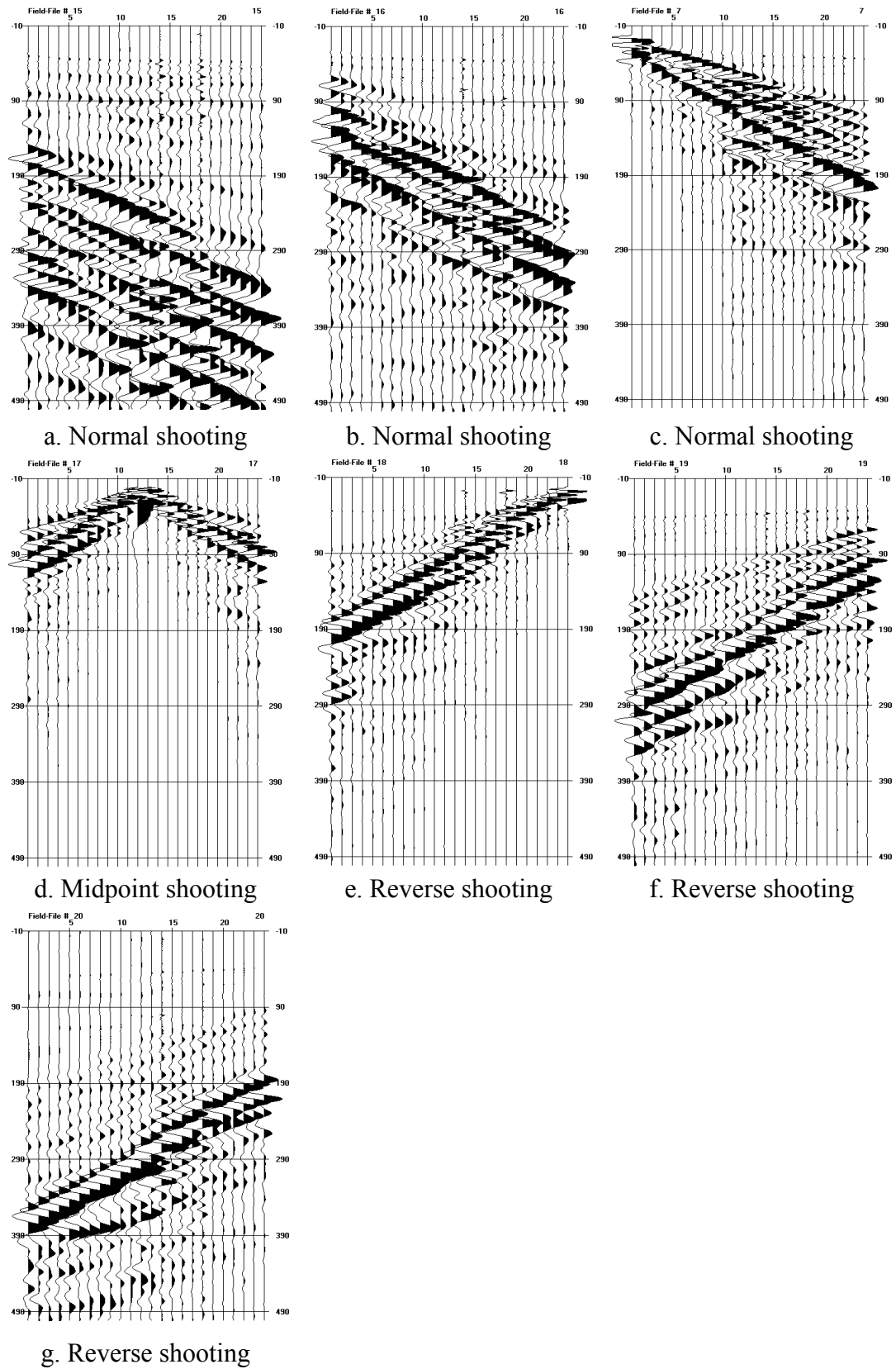


Figure 2.13 Shot record raw data of survey line SKR03.

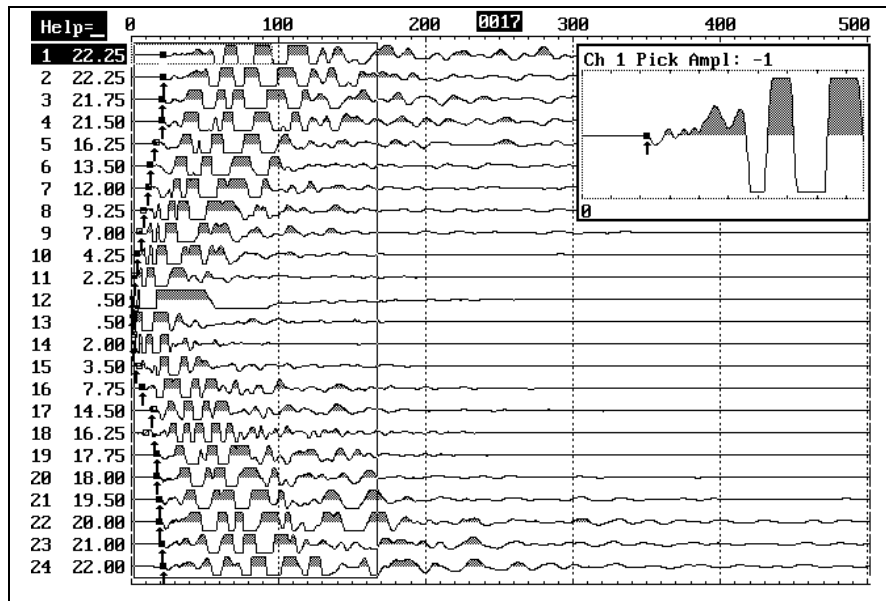


Figure 2.14 Example of picking the first break of shot record raw data of survey line SKR03.

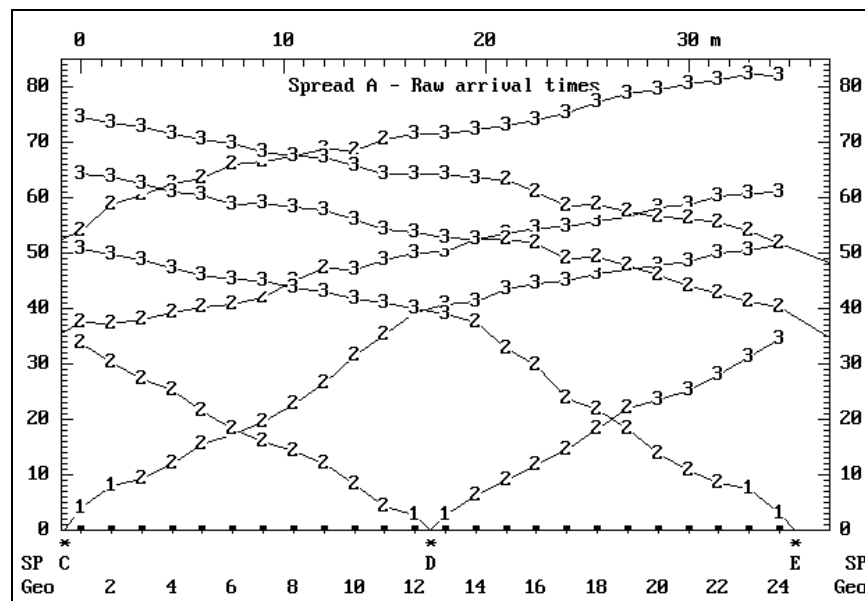


Figure 2.15 Time-distance graphs used as a layer assignment for each layer of survey line SKR03.

Spread A Depth and Elev of layers directly beneath SPs and Geos						
SP	Surface		Layer 2		Layer 3	
	X-Loc	Elev	Depth	Elev	Depth	Elev
C	-0.8	0.0	1.3	-1.3	8.7	-8.7
D	17.3	0.0	0.9	-0.9	8.5	-8.5
E	35.3	0.0	1.4	-1.4	7.9	-7.9

Geo	Surface		Layer 2		Layer 3	
	X-Loc	Elev	Depth	Elev	Depth	Elev
1	0.0	0.0	1.3	-1.3	8.7	-8.7
2	1.5	0.0	1.2	-1.2	8.7	-8.7
3	3.0	0.0	1.1	-1.1	8.9	-8.9
4	4.5	0.0	1.0	-1.0	9.0	-9.0
5	6.0	0.0	0.9	-0.9	9.1	-9.1
6	7.5	0.0	0.9	-0.9	9.1	-9.1
7	9.0	0.0	1.0	-1.0	9.1	-9.1
8	10.5	0.0	1.4	-1.4	8.9	-8.9
9	12.0	0.0	1.7	-1.7	8.8	-8.8
10	13.5	0.0	1.6	-1.6	8.8	-8.8
11	15.0	0.0	1.5	-1.5	8.7	-8.7
12	16.5	0.0	0.9	-0.9	8.5	-8.5
13	18.0	0.0	0.8	-0.8	8.4	-8.4
14	19.5	0.0	1.2	-1.2	8.5	-8.5
15	21.0	0.0	1.8	-1.8	8.7	-8.7
16	22.5	0.0	1.8	-1.8	8.8	-8.8
17	24.0	0.0	1.8	-1.8	9.0	-9.0
18	25.5	0.0	1.5	-1.5	9.1	-9.1
19	27.0	0.0	1.2	-1.2	9.1	-9.1
20	28.5	0.0	0.9	-0.9	8.0	-8.0
21	30.0	0.0	0.8	-0.8	7.5	-7.5
22	31.5	0.0	1.0	-1.0	7.5	-7.5
23	33.0	0.0	1.2	-1.2	7.9	-7.9
24	34.5	0.0	1.3	-1.3	7.9	-7.9

Velocities used to formulate the Depth Model

Spread A	Layer 1	Layer 2	Layer 3
Vertical	268	654	
Horizontal		654	1767

Figure 2.16 Depth and elevation of layers beneath shot points and geophones of survey line SKR03.

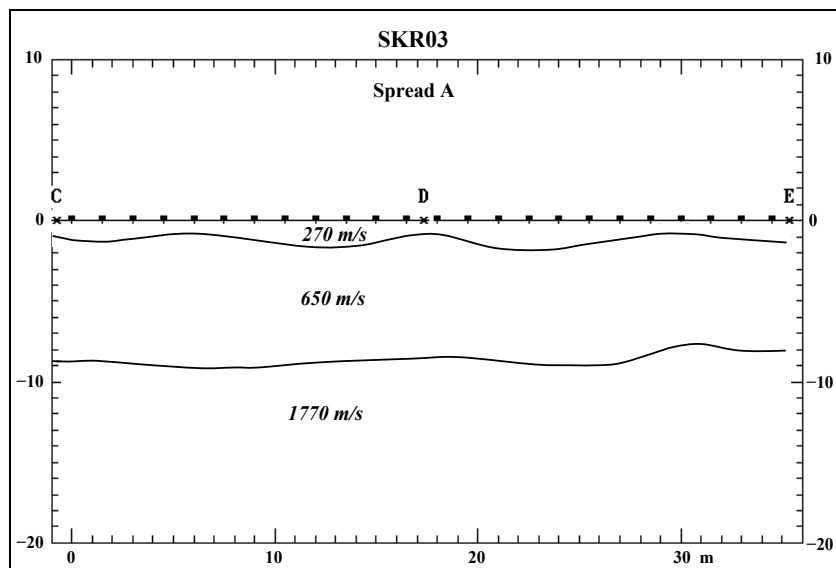


Figure 2.17 2D velocity–depth model of survey line SKR03.

2.4 Seismic reflection method

In general, the objective in seismic reflection surveys mainly is to map the depth, dip and strike of interfaces, which are usually parallel to the bedding. A second objective is to define stratigraphic variations from normal moveout measurements or from the amplitude and wave shape of reflection events (Sheriff, 1991).

Acoustic impedance (Z) is the product of the bulk density (ρ) and compressional wave velocity of the medium (V) and is defined as follows

$$Z = \rho V \quad (2.30)$$

Reflection coefficient (R) is the ratio of amplitude of the reflected wave to the incident wave. At the normal incidence of acoustic signal, where Z_1 and Z_2 are the acoustic impedances of the upper medium and the lower medium respectively, reflection coefficient is given by

$$R = \frac{\rho_2 V_2 - \rho_1 V_1}{\rho_2 V_2 + \rho_1 V_1} = \frac{Z_2 - Z_1}{Z_2 + Z_1} \quad (2.31)$$

Reflection of acoustic wave usually occurs at boundaries between layers of contrasting acoustic impedance. The acoustic impedance contrast between both sides of the reflecting surface affects the strength of reflected waves. Where the contrast between the media is large, the strength of reflected waves will be large too. The reflection coefficient can be positive or negative, depending on whether less dense rocks overlie more dense rocks, or vice versa. A large amplitude and strong reflection results in a large acoustic impedance contrast. A reflecting boundary appears as a trough in a seismic trace when $Z_2 > Z_1$ and as a peak when $Z_2 < Z_1$.

The transmission coefficient (T) can be calculated using the following equation

$$T = \frac{2\rho_1 V_1}{\rho_2 V_2 + \rho_1 V_1} = \frac{2Z_1}{Z_2 + Z_1} \quad (2.32)$$

In case of single horizontal reflector, the travel time and distance can be plotted as a travel time-distance graph (Figure 2.9). The basic geometry of the reflected ray path is shown in Figure 2.18 for the simple case of a single horizontal reflector lying at a depth Z beneath a homogeneous top layer of velocity V . The equation for the travel time t of the reflected ray from a source to a geophone at a horizontal offset, x is given by the ratio of the travel path length to the velocity

$$t^2 = \frac{x^2 + 4Z^2}{V^2} \quad (2.33)$$

The crossing with the time-axis ($x=0$) is the time, t_0 . With t_0 the expression for the travel time can be written as

$$t^2 = t_0^2 + \frac{x^2}{V^2} \quad (2.34)$$

In seismic reflection survey, the offset between the source and geophones is usually less than the depth of the interface ($x \ll Z$), and therefore the higher order terms can be written as

$$t_x = t_0 + \frac{x^2}{2V_1^2 t_0} \quad (2.35)$$

This equation indicates that the observed arrival time of the reflection is equal to the zero offset reflection time (t_0) plus an additional time due to the offset of the geophone. The difference in time ($t_x - t_0$) is the normal moveout (NMO) is given by re-arranging can be calculated using the following equation

$$t_x - t_0 = \frac{x^2}{2V_1^2 t_0} \quad (2.36)$$

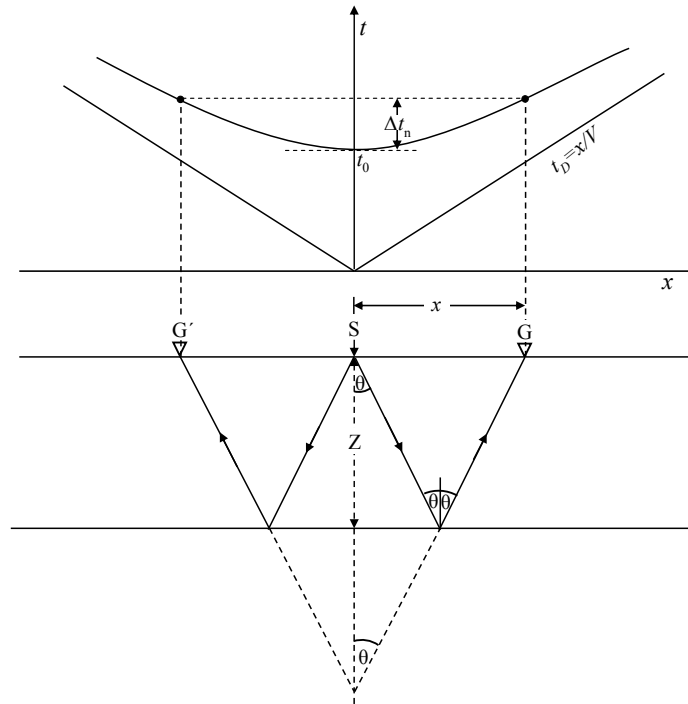


Figure 2.18 Geometry travel time curve for a horizontal reflector (modified from Sheriff and Geldart, 1995).

In case of multiple horizontal layers, when more than two layers are present the rays of the reflection are more complex. For the entire travel path, the average velocity is equal to the total distance traveled divided by the total travel time,

$$\bar{V} = \frac{\sum_{i=1}^n V_i \Delta t_i}{\sum_{i=1}^n \Delta t_i} \quad (2.37)$$

where \bar{V} is the average velocity [m/s], V_i is the velocity of the i^{th} layer [m/s] and t_i is the interval travel time through the i^{th} layer [m/s].

Another way to average velocity is to use the root-mean-square velocity, V_{rms} can be written as

$$V_{rms_n}^2 = \frac{\sum_{i=1}^n V_i^2 \Delta t_i}{\sum_{i=1}^n \Delta t_i} \quad (2.38)$$

Figure 2.19 shows reflected seismic waves that travel through multiple horizontal layers show an increase in travel time with increasing offset distance. For small offsets ($x \ll Z$), the total travel time for the wave reflected from interface n and recorded at offset x can be approximated by

$$t_{x,n} = \frac{\sqrt{4Z^2 + x^2}}{V_{rms_n}} \quad (2.39)$$

The normal moveout for each interface (Δt_n) is the difference between the observed travel time at offset x ($t_{x,n}$) and the travel time for the reflected wave at normal incidence, $x=0$ (t_n):

$$\Delta t_n = t_{x,n} - t_n = \frac{X^2}{2V_{rms_n}^2 t_n} \quad (2.40)$$

The interval velocity of each layer can be calculated from the root mean square velocity. The interval velocity of each layer must be calculated, the Dix equation is used

$$V_n^2 = \frac{V_{rms_n}^2 t_n - V_{rms_{n-1}}^2 t_{n-1}}{t_n - t_{n-1}} \quad (2.41)$$

where V_n is the interval velocity of the n^{th} layer [m/s], V_{rms_n} is the root-mean-square velocity of the n^{th} layer [m/s] and t_n is the measured travel time of the n^{th} layer [s].

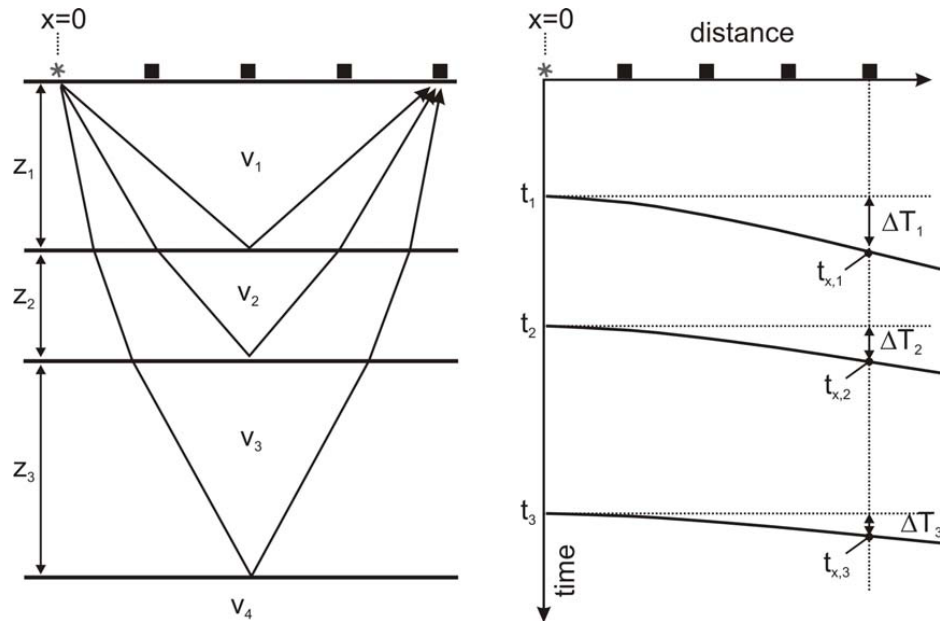


Figure 2.19 Reflected seismic waves that travel through multiple horizontal layers show an increase in travel time with increasing offset distance (Sheriff and Geldart, 1995).

In case of dipping reflector, when the bed is dipping in the direction of the profile, the geometry travel time curve for a dipping reflector shows in Figure 2.20, α being the dip and Z the distance normal to the bed. Application of the cosine law an expression for the travel times can be written as

$$\begin{aligned} V^2 t^2 &= x^2 + 4Z^2 - 4Zx \cos(90 + \alpha) \\ V^2 t^2 &= x^2 + 4Z^2 + 4Zx \sin \alpha \end{aligned} \quad (2.42)$$

The formula for dipping reflector follows analogue the case of the horizontal layer, on completing the squares, a hyperbolic expression is obtained

$$\frac{V^2 t^2}{(2Z \cos \alpha)^2} - \frac{(x + 2Z \sin \alpha)^2}{(2Z \cos \alpha)^2} = 1 \quad (2.43)$$

To obtain the dip (α) can solve for travel time (t) in Equation 2.42 can be calculated using the following equation

$$t = \frac{2Z}{V} \sqrt{1 + \frac{x^2 + 4Zx \sin \alpha}{4Z^2}}$$

$$t \approx t_0 \left(1 + \frac{x^2 + 4Zx \sin \alpha}{8Z^2} \right) \quad (2.44)$$

The travel time from two location x and $-x$, that both have the same distance from the shot point is not equal anymore caused by dipping reflector. The travel time difference between both points is called the dip moveout, can be calculated using the following equation

$$\Delta t_d = t_x - t_{-x} = \frac{2x \sin \alpha}{V} \quad (2.45)$$

For small dip angle, $\sin \alpha \approx \alpha$. Therefore the dip of the interface can be calculated using the following equation

$$\sin \alpha \approx \alpha \approx \frac{1}{2} V \left(\frac{\Delta t_d}{\Delta x} \right) \quad (2.46)$$

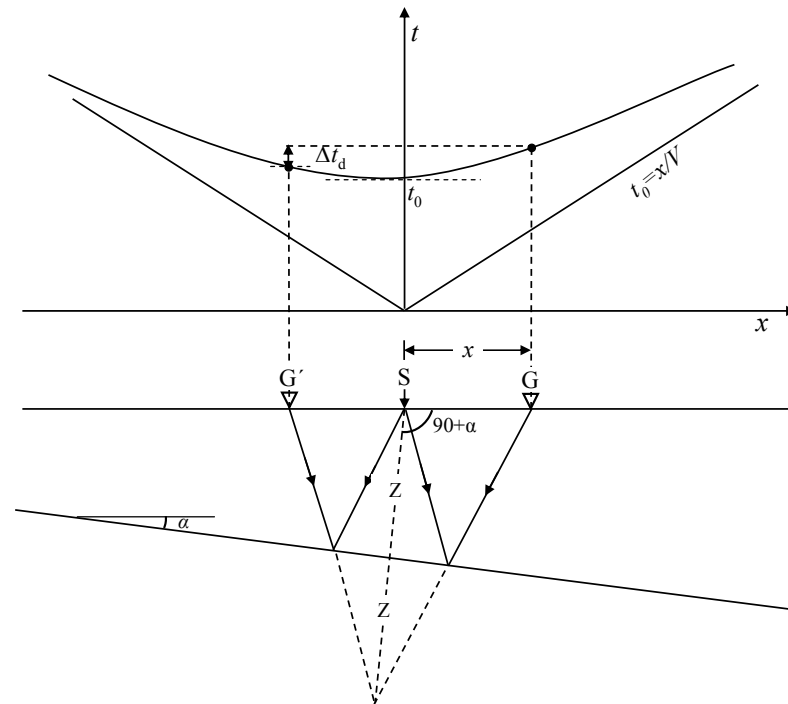


Figure 2.20 Geometry travel time curve for a dipping reflector (modified from Sheriff and Geldart, 1995).

2.4.1 Seismic reflection data acquisition

Six seismic reflection survey lines were run over the Bo Yang district. Figure 2.21 shows the seismic reflection survey stations of each site. They are Wachiranukul School (SKL01), Mahavajiravudh School (SKL02), Chalathat Road (SKL03), Rajamangala University of Technology Srivijaya (SKL04), Tinsulanonda Stadium (SKL05) and Samila Beach (SKL06). Table 2.3 shows the seismic reflection data acquisition.

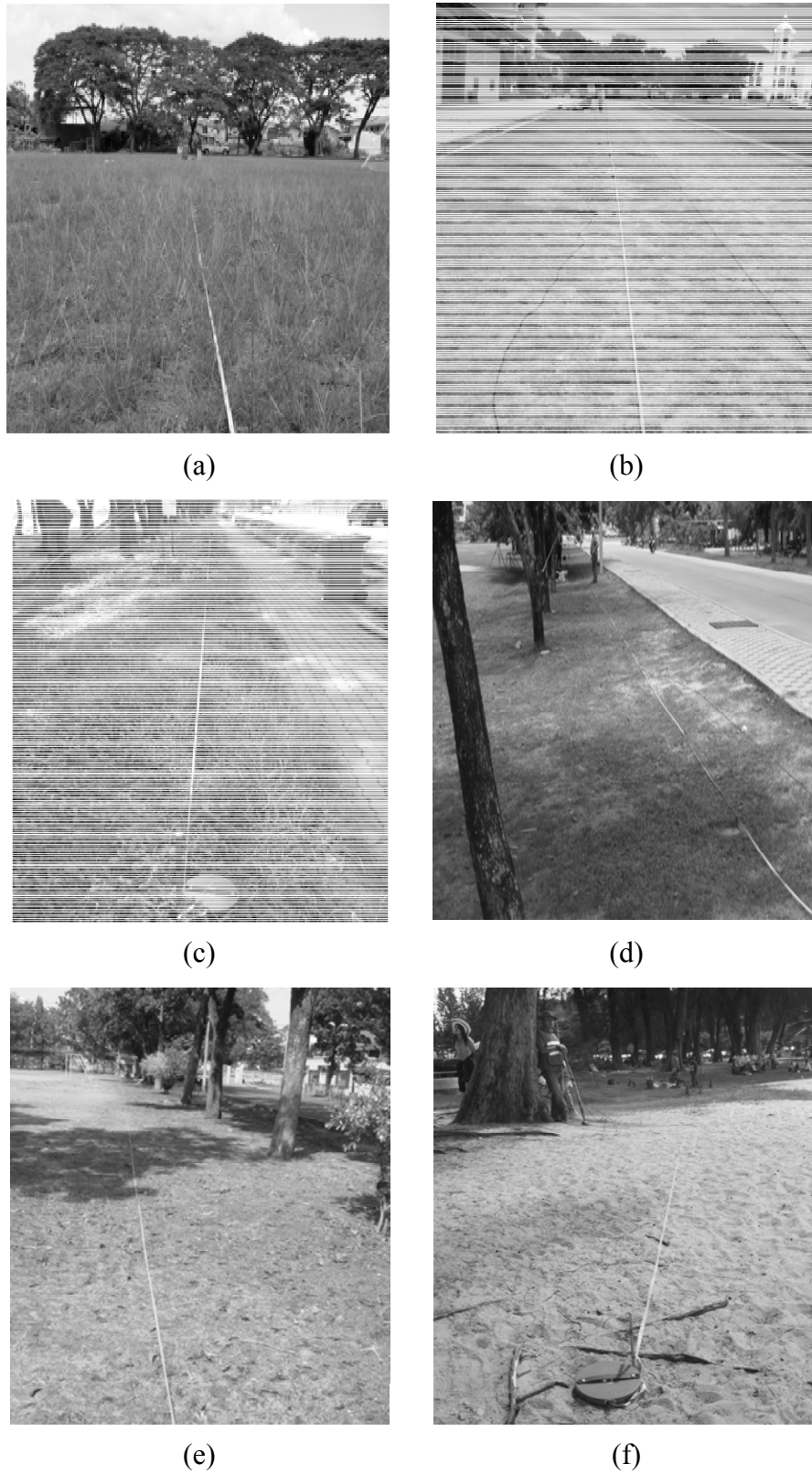


Figure 2.21 Seismic reflection survey stations (a) line SKL01, (b) line SKL02, (c) line SKL03, (d) line SKL04, (e) SKL05, and (f) SKL06.

The optimum offset determination is first step in seismic reflection survey to find the optimum offset in order to obtain the reflected wave, which is clearly separated from the refracted wave and the airwave arrival time in the record data (Figure 2.22). To distinguish the seismic reflection signal from noise in the field survey and during data processing, following general features of noise can be considered. Air waves usually contain higher frequencies than others and their velocity should be about 330 to 340 m/s. Ground roll is identified by a slow phase velocity (steep slope) and typically has a lower dominant frequency than near surface refractions or reflections. The offset-test distance can be defined as the distance between the source and first geophone (Figure 2.33); it was test at each site with 5, 10, and 15 meters. An optimum offset distance of 15 meters was chosen clearly reflected waves.

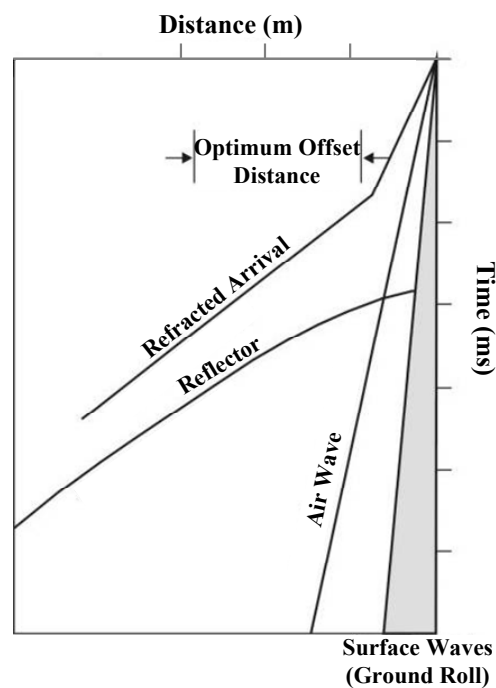


Figure 2.22 Time-distance graph show main phases that need to be considered for choosing the optimum offset in a field survey (from Pullan and Hunter, 1990).

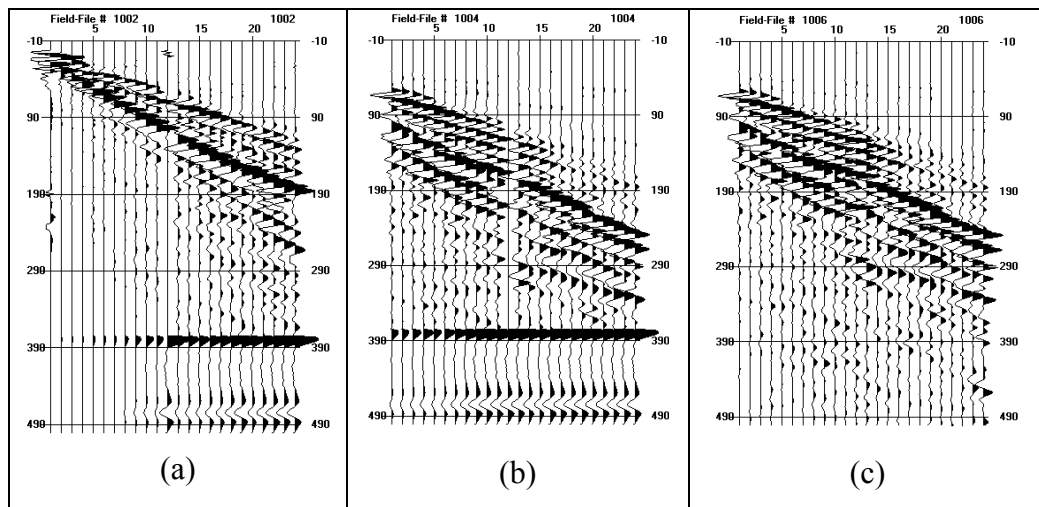


Figure 2.23 Series of test records recorded for the determination of the optimum offset (a) offset of 5 m (b) offset of 10 m and (c) offset of 15 m. An optimum offset of 15 m was chosen for the final records.

Table 2.3 Seismic reflection data acquisition in the Bo Yang District.

Acquisition Parameter	SKL01	SKL02	SKL03	SKL04	SKL05	SKL06
Shot interval (m)	3	3	1.5	1.5	1.5	1
Geophone interval (m)	3	3	1.5	1.5	1.5	1
Optimum Offset (m)	27	20.5	15	25	15	10
Shots stacked per shot record	10	10	10	20	15	10
Record length (ms)	256	256	512	512	256	512
Sampling interval (ms)	0.125	0.125	0.25	0.25	0.125	0.25
Shot-receiver configuration	Off-end	Off-end	Off-end	Off-end	Off-end	Off-end
Line direction	N072E	N015W	N030W	N050E	N060E	N040E
Survey length (m)	108	122.5	84	179	174	44

2.4.2 Seismic reflection data processing

Data processing is a necessary step before showing subsurface and interpreting the results. Figure 2.24 shows the following processing flow for seismic reflection data. GLOBE claritas and WinSeis15 software were used.

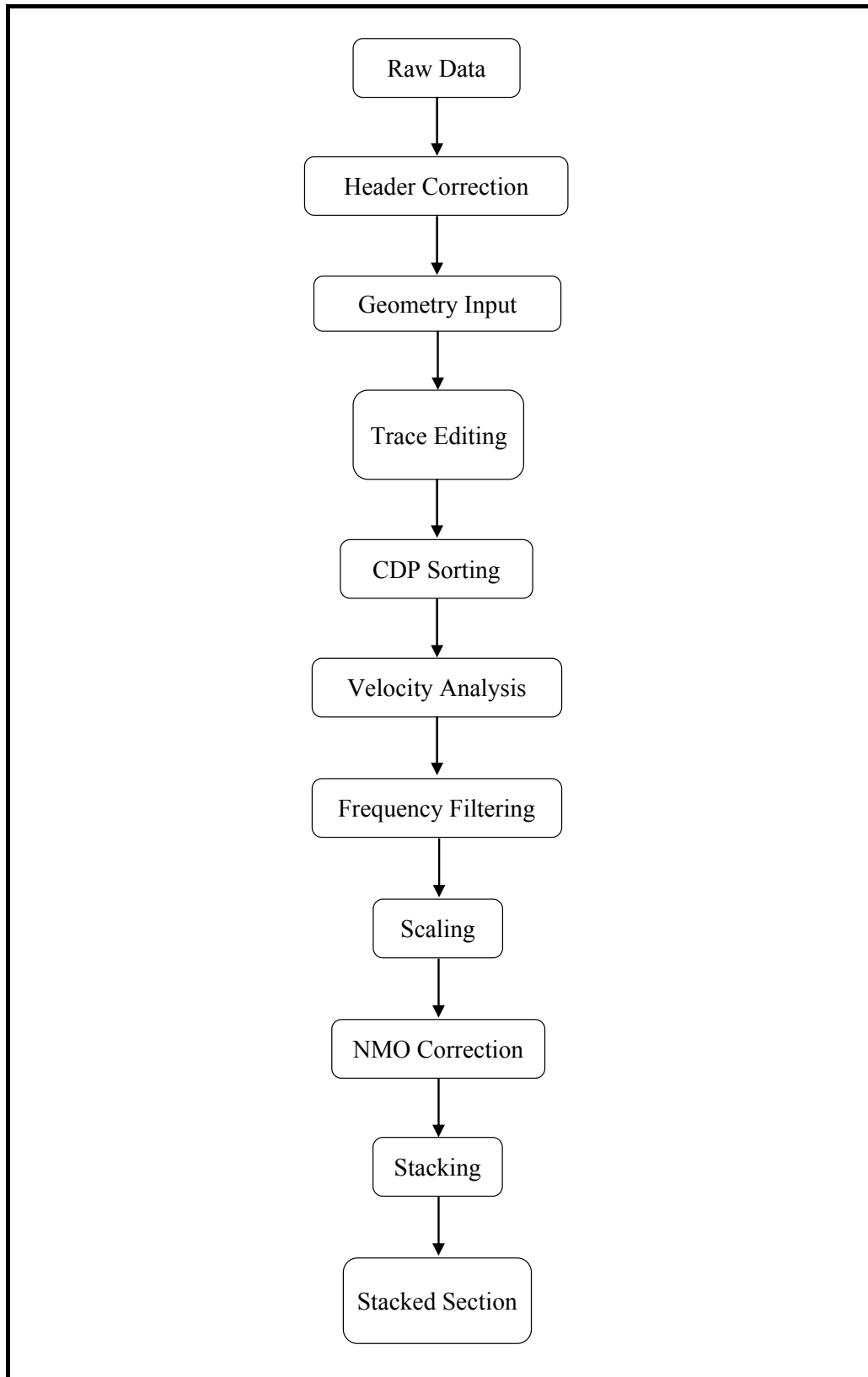


Figure 2.24 Processing flow for seismic reflection data.

2.4.2.1 Header correction

The SmartSeis™ S12 Seismograph was used for the Bo Yang survey. The data were recorded with 16-bits precision and 100 dB dynamic ranges. The SmartSeis™ S12 Seismograph recorded seismic data in SEG-2 seismic data formats. Convert input file from SEG-2 to SEG-Y format. Figure 2.25 shows the shot record raw data using 0.256 s of record length of survey line SKL05.

2.4.2.2 Geometry input

Input information such as field record number, shot stations, receiver stations, offset and CDP.

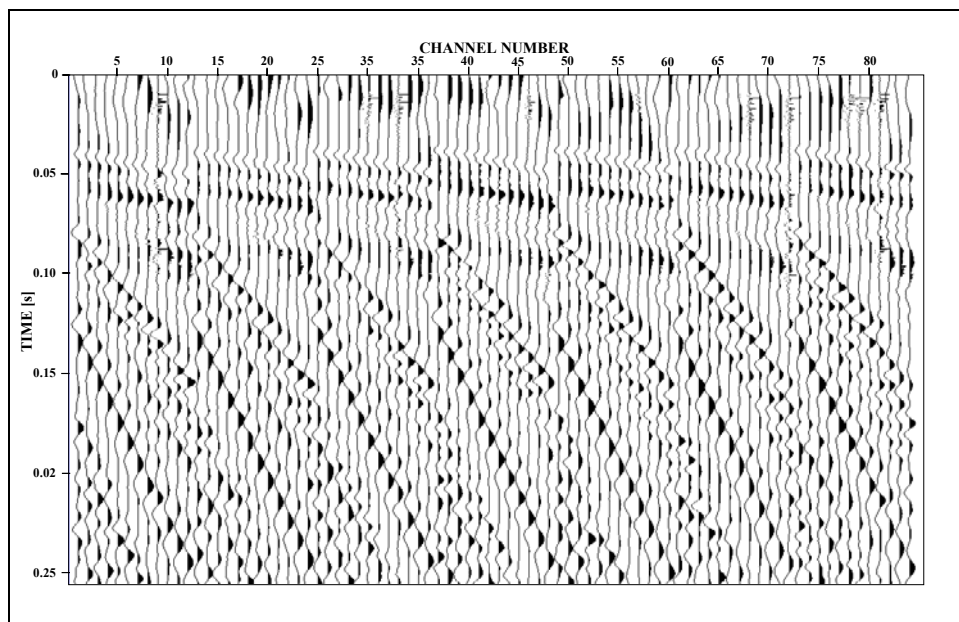


Figure 2.25 Shot record raw data of survey line SKL05.

2.4.2.3 Trace editing

This processing involves bad traces killing, first arrival muting and surgical muting.

2.4.2.3.1 Bad trace killing

The bad trace killing should be one of the first processes applied to the data. The process of trace killing refers to setting the amplitude that traces to zero (Baker, 1999). The bad trace killing shows in Figure 2.26 could be selected and killed one at time, but in most case a bad trace will be a bad connection or bad geophone at a particular receiver location that was not identified in the field.

Bad traces must be removed for two reasons. First, even when bad trace appears to contain some reflection information, it still has a lower signal to noise ratio (S/N) than the rest of the data and will therefore only serve to decrease S/N of the final section. Removing any trace with a lower S/N almost always better than assuming that important information will be lost if the trace is removed.

The second and most important reason bad traces should be edited is more subtle. Some bad traces can contain data spikes in which a single sample has the maximum amplitude and the adjacent samples are much smaller. This creates two problems: First, the spike will appear to have infinite frequency and may cause frequency-related processes to behave badly. Second, because the amplitude of the spike is anomalously high, it will not stack out under the assumption that it is random noise.

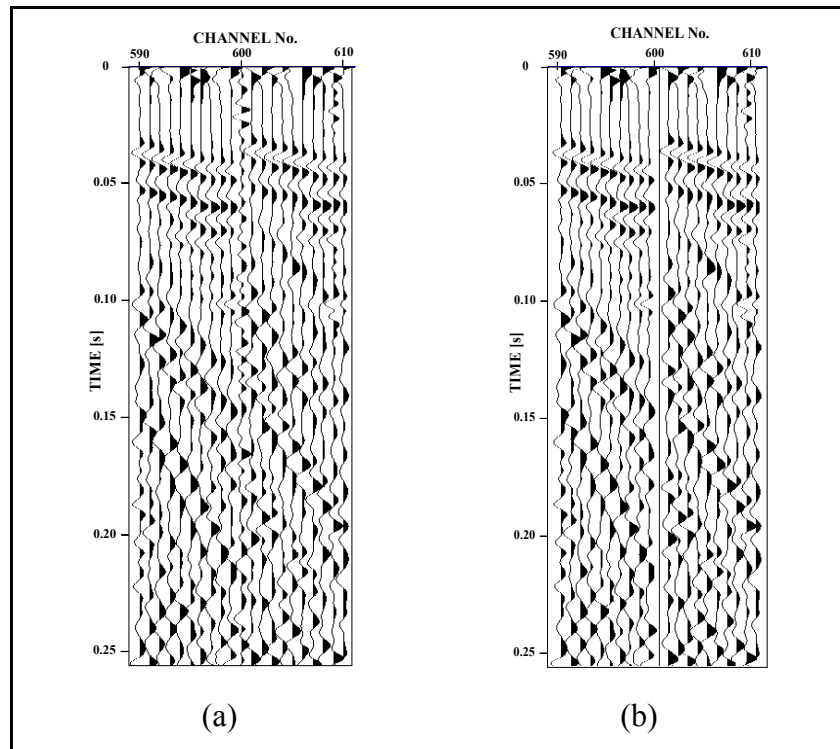
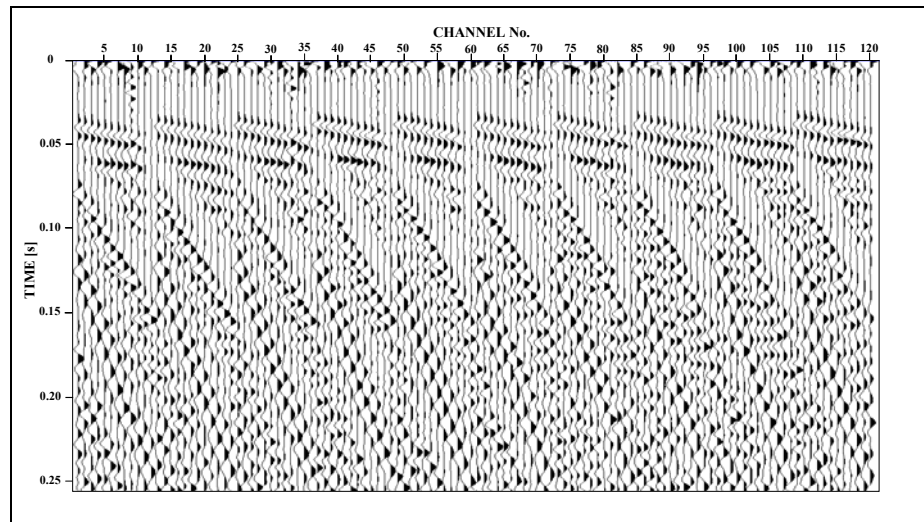


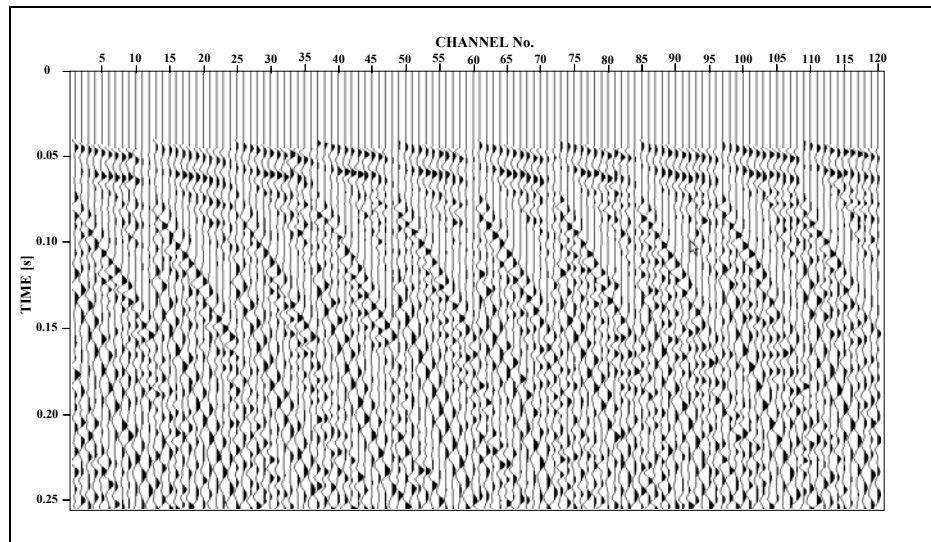
Figure 2.26 Shot record raw data (a) before and (b) after applying the trace edit process of survey line SKL06.

2.4.2.3.2 First arrival muting

The next step in the processing flow involves the muting refracted and direct wave energy. This is necessary on most data sets to ensure that refracted and/or direct wave energy does not appear coherent on CDP stacked sections. The high amplitude as well as the coherent nature of move out and stacked refraction energy, and in some situations it can easily be misinterpreted as shallow reflection energy. Figure 2.27 shows comparison between (a) shot record raw data without first arrival mute and (b) shot record raw data after applying the first arrival mute process of survey line SKL05.



(a)



(b)

Figure 2.27 Shot record raw data (a) before and (b) after applying the first arrival mute process of survey line SKL05.

2.4.2.3.3 Surgical muting

The final trace editing step involves the surgical removal of bad trace segments. Noises resulting from the air wave, electronic interference other than power line frequencies, and ground roll are generally constrained to isolated portions of a trace. High amplitude noise obviously dominating a well-defined time window should be removed.

2.4.2.4 CDP sorting

Traces are usually sorted into groups, or gathers, with all traces in a given type of gather having a certain common aspect. The most popular type of gather is the common depth point (CDP) gather. The number of traces in a CDP gather is called the fold. Figure 2.7 shows six fold CDP gathers.

2.4.2.5 Velocity analysis

The velocity analysis is the process of finding the stacking velocity to use for NMO correction and stacking process. NMO is the basis for determining velocities from seismic data. The correctness of the depth section depends on the stacking velocity.

For the Bo Yang seismic reflection data, two velocities analysis methods were used. First, velocity picking used to find out the rough velocity and for a first guess approximation of the stacking velocity of reflections. Second, constant velocity stack (CVS) used to pick velocity function which indicate best stack section.

The method of constant velocity stack is the common midpoint gather that has been repeatedly NMO corrected using a range of constant velocity values. The constant velocities used in the CVS method should be considered the range of velocities needed to stack the data and the spacing between trial stacking velocities. In choosing a range, consideration should be given to the fact that dipping events and useful out-of-plane reflections may have anomalously high stacking velocities. In choosing the spacing of constant velocities, because it is moveout not velocities, that is the basis for velocity estimation. Thus, it is better to scan in increments of equal Δt_{NMO} than equal to V_{NMO} . This prevents over sampling of the high velocity events and under sampling of the low velocity events. A good way to choose is to pick it so that the moveout difference between adjacent trial velocities at the maximum offset to be stacked is approximately one-third of the dominant period of the data.

2.4.2.6 Frequency filtering

Frequency filters are the most important filters in digital signal processing. The energy of reflections is usually present in a certain frequency range. Specific noise sources and background noise are commonly present in a different

frequency range. These frequency differences allow noise and reflection information to be separated.

2.4.2.6.1 Fourier transformation

The basis of a digital frequency filter is the Fourier transformation, which transforms a time queue from time domain, amplitude as function of time, to the frequency domain, amplitude as function of frequency. In a time shot record, there is usually an unexpected noise that interferes with the reflection signal. This noise cannot be directly suppressed because the reflection signal would be affected too. A forward Fourier transform is used to solve this problem by transforming the seismic signal from a time domain into a frequency domain. This cuts field data frequency domain noise. The equation of forward Fourier transform is (Krebes, 1989)

$$G(f) = \int_{-\infty}^{\infty} g(t)e^{-2\pi ift} dt \quad (2.47)$$

where $G(f)$ is the frequency domain of wave train function, $g(t)$ is the time domain of wave train function, f is the seismic signal frequency, t is the apparent reflector time and i is the mathematics imaginary part.

The output of these transforms is an easy way to reject any noise in the frequency domain that is different in bandwidth from that of the reflection signal. The equation of inverse Fourier transform is (Krebes, 1989)

$$g(t) = \int_{-\infty}^{\infty} G(f)e^{2\pi ift} df \quad (2.48)$$

The function $G(f)$ in frequency domain represents the amplitude and phase difference of the sine or cosine function with the frequency f . Noise frequency is rejected by defining the bandwidth frequency of a signal.

2.4.2.6.2 Band-pass filter

Most filters are applied in the frequency domain. The desired band-pass filter is based on a characteristic of seismic field data. Seismic data are usually generated from the same source type for each survey field, so seismic data from each field usually are not different in their bandwidth frequencies. From the frequency spectrum of a seismograph, the bandwidth of the signal can be defined. Band-pass filters put the amplitude range of unwanted frequencies to zero. Table 2.4 shows the best band-pass filters with truncation frequency that contains dominant signal frequency bandwidth of the Bo Yang survey. Figure 2.28 Shows shot record raw data without filtering and after applying band-pass filtering results of survey line SKL05.

Table 2.4 Best band-pass filters with truncation frequency that contains dominant signal frequency bandwidth of the Bo Yang survey.

Line \ Fq.	Low truncation frequency (Hz)	Low pass frequency (Hz)	High pass frequency (Hz)	High truncation frequency (Hz)
SKL01	20	50	150	250
SKL02	20	100	150	200
SKL03	20	50	150	250
SKL04	20	50	150	250
SKL05	20	100	200	250
SKL06	20	100	150	250

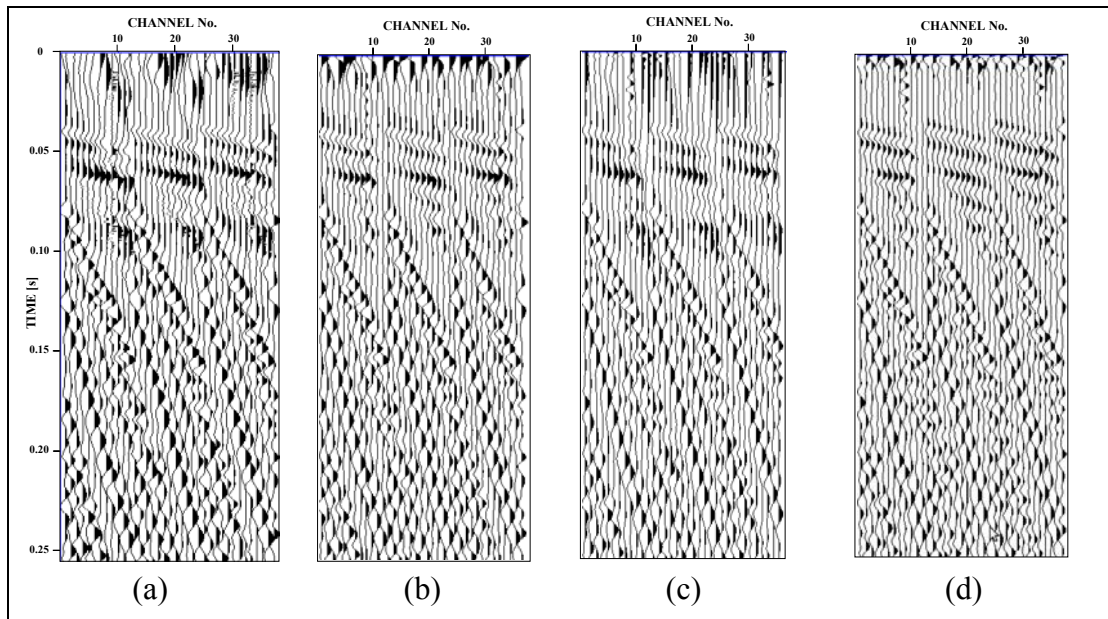


Figure 2.28 Shot record raw data, (a) without filtering, (b) after applying band-pass filtering with a filter function of 10-20-200-300 Hz, (c) band-pass filtering with a filter function of 20-50-150-250 Hz and (d) band-pass filtering with a filter function of 20-100-150-250 Hz of survey line SKL05.

2.4.2.7 Scaling

Scaling is the process whereby amplitudes of data are increased for display or processing purposes. Two factors affect the amplitudes of reflection data and associated noise: the amplitude of a spherical wave front is inversely proportional to its distance from the source, and higher frequencies are attenuated faster than lower frequencies. Through the combination of these two effects, reflections (which typically have higher frequency and lower amplitude than ground roll and refractions) are attenuated with distance from the source. Gain corrections are used, therefore, to enhance the visible appearance of reflections, with a higher gain correction being needed for deeper reflections. Three main types of gain correction are constant gain, automatic gain control (AGC) and spherical divergence gain.

The Bo Yang seismic reflection data used automatic gain control (AGC) correction to make reflections visible. When any gain is applied, amplitude information is being altered. When true amplitude analysis is to be performed, AGC

must not be applied because AGC is not a reversible linear process, such as it is not possible to extract true amplitude information from data that has had AGC applied. The critical parameter specified in the AGC process is the length of the AGC window. This length is the time-band or window within which the amplitudes are normalized. One factor associated with window length is that, within the window, the highest amplitude information most strongly affects normalization. Thus, if the AGC window is too big, very little change in the data will be observed. If the AGC window is too small, everything will be changed, and the data will be very noisy. Figure 2.29 shows the shot record raw data and a series of AGC gained sections.

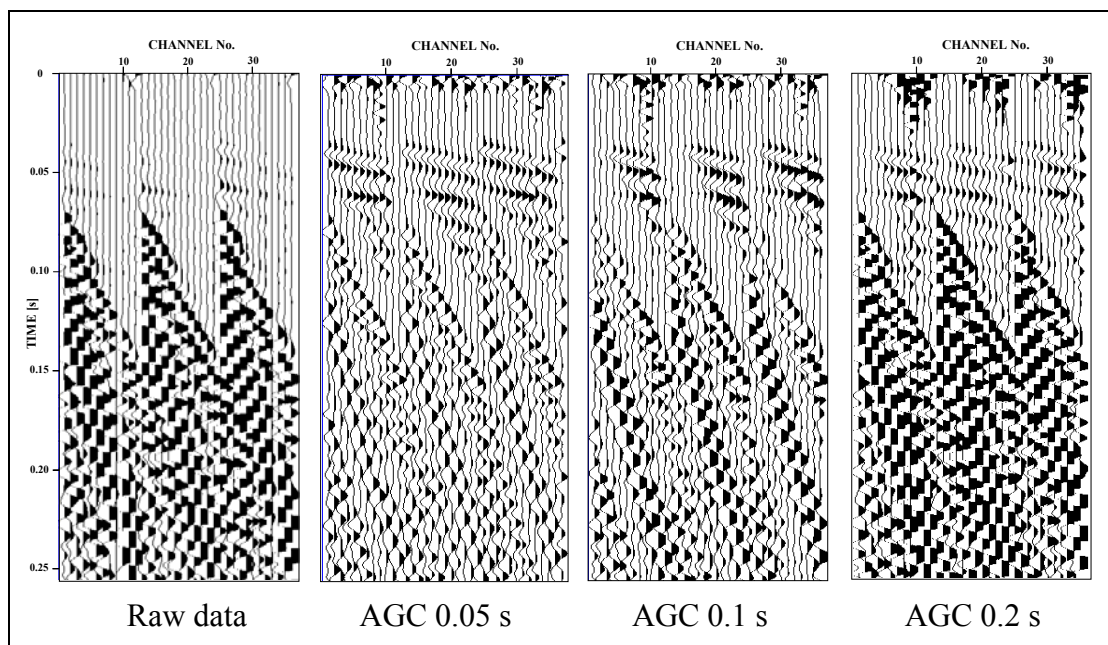


Figure 2.29 Shot record raw data and series of AGC gained section with window lengths 0.05, 0.1, 0.2 s of survey line SKL05.

2.4.2.8 NMO correction

The travel time along the raypath from shot position to depth point, then back to receiver position is t_x . The travel time equation as a function of offset, can be calculated using the following equation

$$t_x^2 = t_0^2 + \frac{x^2}{V^2} \quad (2.49)$$

where t_x is two-way travel time for an offset x [s], x is the distance between source and receiver position on the surface [m], V is the velocity of medium above the reflecting interface [m/s], and t_0 is the two-way travel time along the vertical path [s].

The equation describes a hyperbola in a plane of two-way time versus offset. Figure 2.30 is an example of traces in a common midpoint gather. The velocity that best flattens the reflection hyperbola is the velocity that best corrects for normal moveout before stacking the traces in the gather. The difference between the two-way travel time at a given offset, t_x , and the two-way zero-offset travel time, t_0 , is called normal moveout. NMO time can be calculated using the following equation (Yilmaz, 1989)

$$\Delta t_{NMO} = t_x - t_0 = \sqrt{t_0^2 + \frac{x^2}{V^2}} - t_0 \quad (2.50)$$

where Δt_{NMO} is the difference between the two-way travel time at the offset and the two-way zero-offset travel time [s], t_x is two-way travel time at the offset [s], t_0 is the two-way zero-offset travel time [s], x is the distance between source and receiver position on the surface [m] and V is the stacking velocity [m/s].

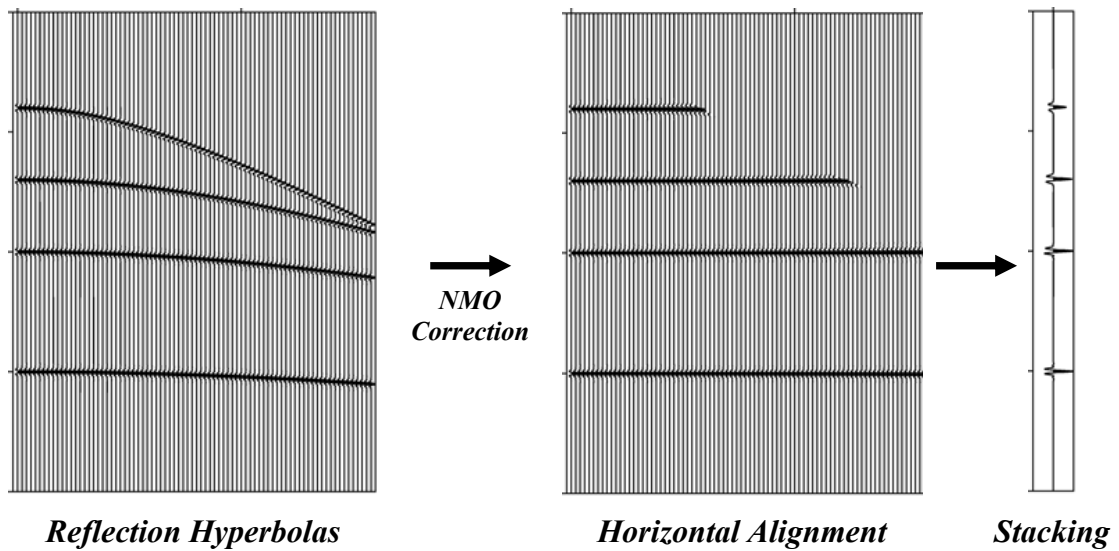


Figure 2.30 Principle of NMO correction, the reflections are aligned using the correct velocity, such that the events are horizontally, then all the separate traces are stacked (summed).

The normal moveout velocity is estimated and travel times are corrected to remove the influence of offset. Traces in the NMO corrected gather then are summed to obtain a stack trace at the particular common midpoint location. The NMO corrections increase with offset and decrease with reflector depth. They are also smaller for larger velocity values. The reflector hyperbola is corrected for offset of the correct medium velocity used in the NMO equation. If a velocity higher than the actual medium velocity is used, then the hyperbola is not completely flattened. This causes an undercorrection, the reflection curves downward. On the other hand, if a lower velocity is used, overcorrection results, the reflection curves upward (Figure 2.31).

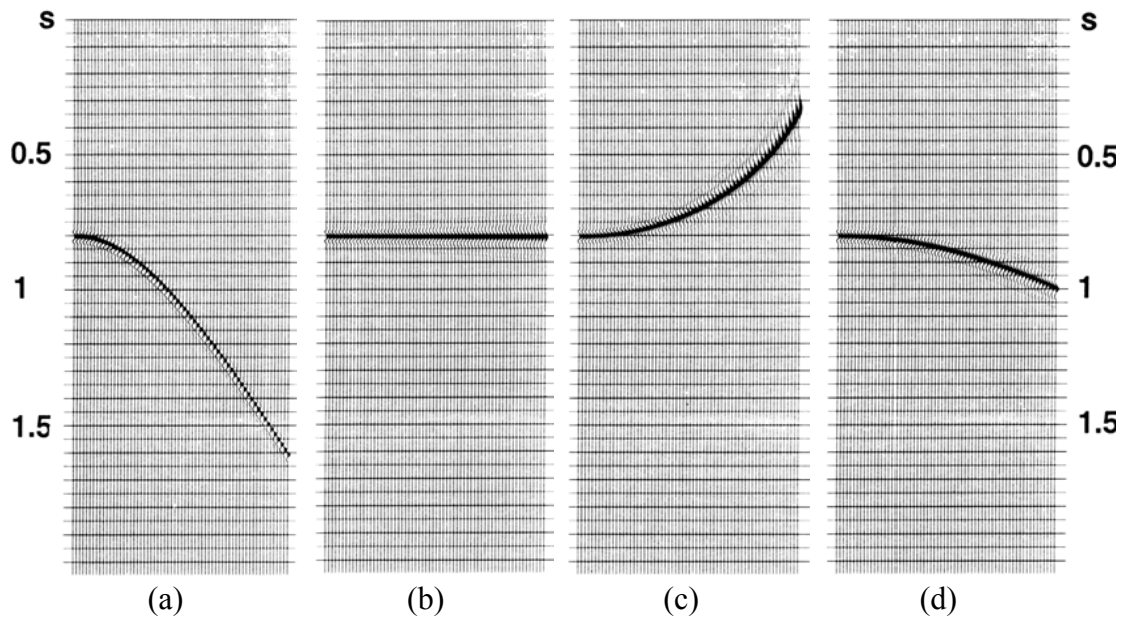


Figure 2.31 NMO correction of a reflection, (a) reflection is not corrected, (b) corrected with proper velocity, (c) correction velocity is too low and (d) correction velocity is too high (Yilmaz, 1987).

2.4.2.9 Stacking

Stacking is a seismic technique to summation together in formation on each trace of CDP gather after NMO correction to obtain one stacked trace for each gather into the same position. This method enhances reflections, reduces random noise and increase the S/N ratio. Figure 2.32 shows the stacked section of survey line SKL05.

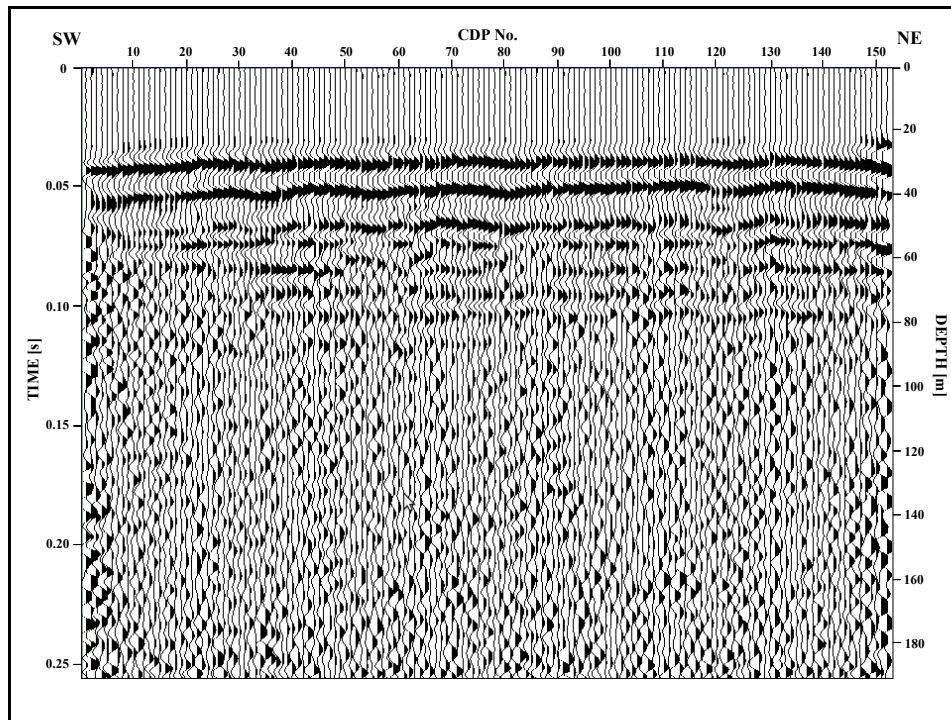


Figure 2.32 Stacked section of survey line SKL05.

2.5 Vertical electrical sounding method

The purpose of vertical electrical sounding (VES) surveys is to determine the subsurface resistivity distribution by making measurements on the ground. From these measurements the true resistivity of the subsurface can be estimated. The ground resistivity is related to various geological parameters, such as the mineral and fluid content, porosity, and degree of water saturation in the rock. Typical resistivity values of the different types of materials are shown in Table 2.5. These values are only the general resistivity value range for the materials listed. VES surveys have been the most important geophysical method of water prospecting in many such areas.

Table 2.5 Resistivity values of water and sediments (modified from Zohdy et al, 1993).

Resistivity ($\Omega.m$)	Sediments	Fluid in sediments
0.5 – 2.0	Very porous sand, saturated clay	Seawater; very saline water
2.0 – 4.5	Porous sand, saturated clay	Saline water
4.5 – 10.0	Sandy saturated, sandy clay	Salty brackish water
10.0 – 15.0	Sandy clay, sandy gravel	Brackish water
15.0 – 30.0	Sand, gravel, some clay	Poor quality fresh water
30.0 – 70.0	Sand, gravel, minor clay	Intermediate quality fresh water
70.0 – 100.0	Sand, gravel, no clay	Good quality fresh water
> 100.0	Coarse sand, gravel, no clay	Very good quality fresh water

Resistivity measurements are normally made by injecting current into the ground through two current electrodes, called C1 and C2, and measuring the resulting voltage difference at two potential electrodes called P1 and P2. The apparent resistivity can be calculated using the following equation

$$\rho_a = k \frac{V}{I} \quad (2.51)$$

where ρ_a is the apparent resistivity [$\Omega.m$], k is the geometric factor which depends on the arrangement of the four electrodes [m], V is the potential difference [V] and I is the current [A].

The calculated resistivity value is not the true resistivity of the subsurface, but an apparent value which is the resistivity of a homogeneous ground which will give the same resistance value for the same electrode arrangement. The relationship between the apparent resistivity and the true resistivity is a complex

relationship. To determine the true subsurface resistivity, an inversion of the measured apparent resistivity values using a computer program must be carried out (Loke, 2000).

The arrangement of current electrodes and potential electrodes is variable. Over the years, many variations have been tried; however, only four are in popular use (Figure 2.33). These four are a) Wenner array, all electrodes equally spaces, b) Schlumberger array, the current electrodes are spaced much father apart than the potential electrodes, c) Pole-dipole (three-point) array, one of the current electrodes is fixed at a great distance from the other three, and d) Dipole-dipole array, the current electrodes close together and potential electrodes close together, but the two sets are relatively far apart.

Wenner, Schlumberger and Dipole-dipole arrays are commonly used in vertical electrical sounding surveys. Wenner and Dipole-dipole arrays are usually applied for environment problem, archeological problem or landfill problem, whereas Schlumberger array is commonly used in groundwater exploration (Telford et al., 1990).

In this work, vertical electrical sounding with Schlumberger electrode array (Figure 2.34) was carried out in Bo Yang district for determining groundwater layer. The apparent resistivity (ρ_a) of the Schlumberger array can be determined from the following equation

$$\rho_a = \frac{\pi(L^2 - l^2)}{2l} \cdot \left(\frac{V}{I}\right) \quad (2.52)$$

where L is half current electrode spacing [m], l is half potential electrode spacing [m] and V/I is reading taking from resistivity meter [ohm].

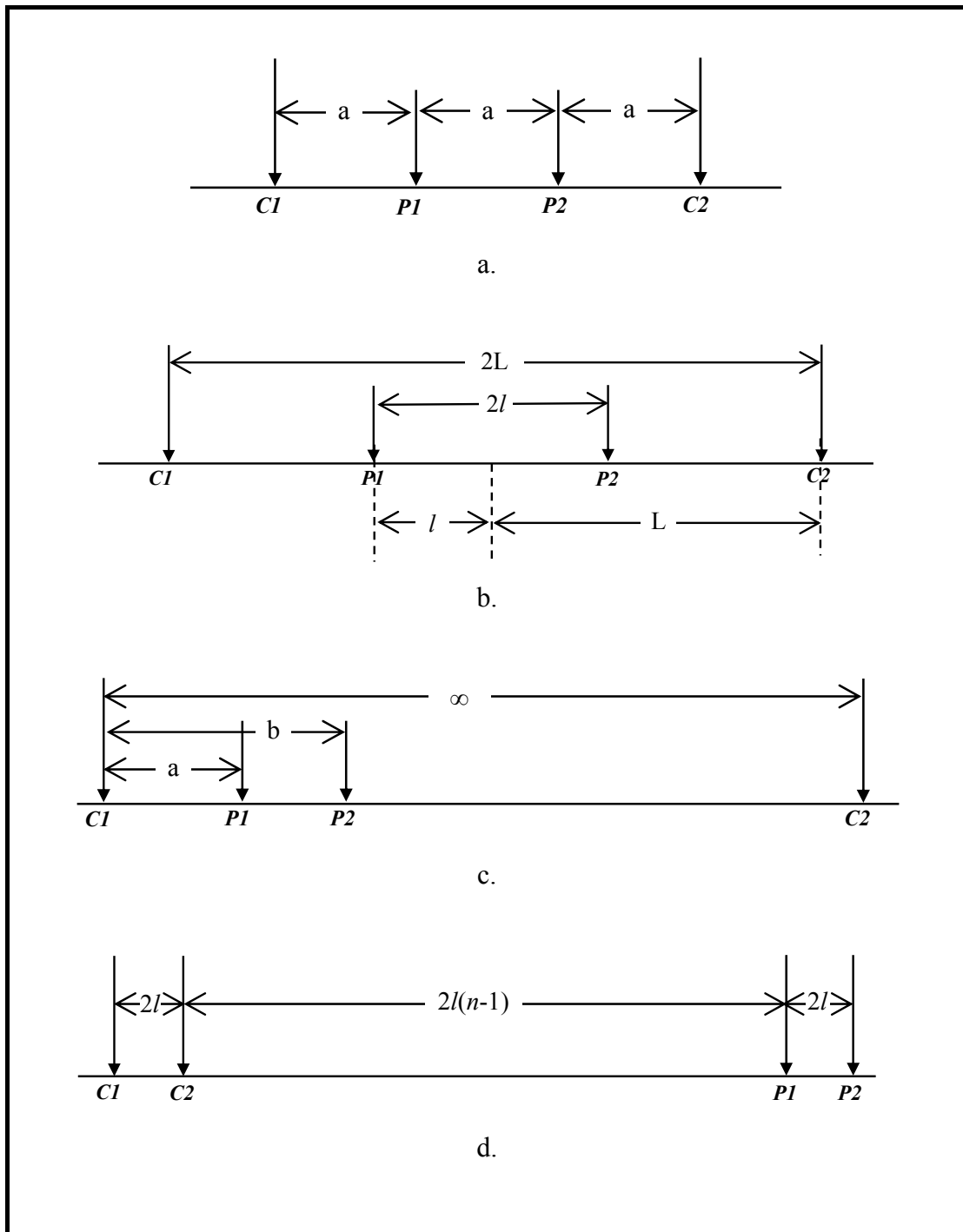


Figure 2.33 Electrode arrays in common use. (a) Wenner, (b) Schlumberger, (c) Pole-dipole and (d) Dipole-dipole (modified from Telford et al., 1990).

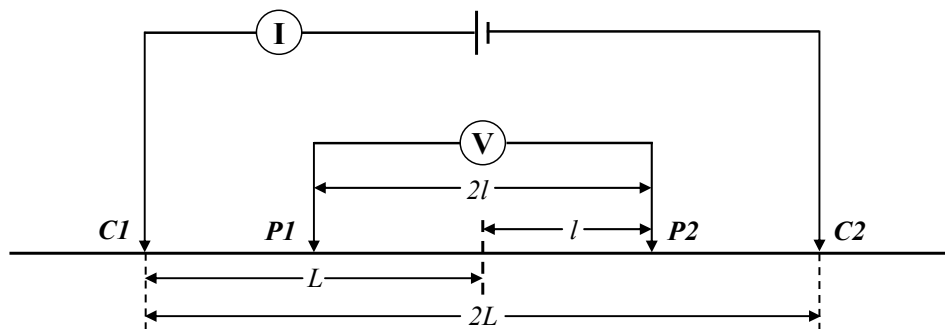


Figure 2.34 Schlumberger electrodes array.

2.5.1 Vertical electrical sounding data acquisition

The Bo Yang data acquisition used the following survey equipment:

1. A resistivity meter, ABEM Terrameter SAS 1000, for measuring ground resistivity (Figure 2.35).
2. Measuring tapes and two rolls of string for assigning positions of electrodes
3. Hammers used for forcing current and potential electrodes into ground.
4. GPS for determining locations of VES points.
5. Four rolls of electrical cables for connecting current and potential electrodes with resistivity meter (SAS 1000).
6. Car battery (12V-20A) for a direct current power supply of the resistivity meter (SAS 1000)
7. Two big steel electrodes for injecting current into ground and two potential electrodes for measuring voltage difference at the ground surface.



Figure 2.35 Resistivity meter, ABEM Terrameter SAS 1000.

Data acquisition is the first and most important step in obtaining the best subsurface data. The VES measurement was conducted at 12 VES stations with ABEM Terrameter SAS 1000 in Bo Yang district. All VES stations were measured using the Schlumberger array at half current electrode spacing ($AB/2$) of 1.5, 2, 3, 4.5, 7, 10, 15, 20, 30, 45, 60, 90, 150, 225, 350 and 500 meters. This survey started with half potential electrode spacing ($MN/2$) of 0.5, 2, 6, 10, 20, 30 and 50 meters.

Determine locations of VES stations select line of measurement and placing four electrodes on the ground surface along the straight line. Connecting electrodes to the resistivity meter SAS 1000 via electric cables. Switching on power started a measurement and reading the resistance (R) value. After the values and the electrode separations for the first separation were recorded, the procedure was repeated until measurements were recorded at all designed electrode separations. Field data from all of VES locations are shown in Appendix A.

2.5.2 Vertical electrical sounding data processing

The VES data were processed by using a personal computer. The VES was performed to provide information on the variation in subsurface conditions with depth. The VES data were analyzed by plotting measured resistivity versus electrode

spacing. These resistivity curves were correlated to theoretical model curves to determine the subsurface stratigraphy. In this study, the resistivity data were modeled using the IPI2WIN program to obtain one-dimensional inverse modeling algorithm. The resistivity of different layers and their corresponding thicknesses were reproduced by a number of iterations until the model parameters of all the sounding curves were totally resolved with minimum root mean square errors. Figure 2.36 shows the VES model of survey point SKV09.

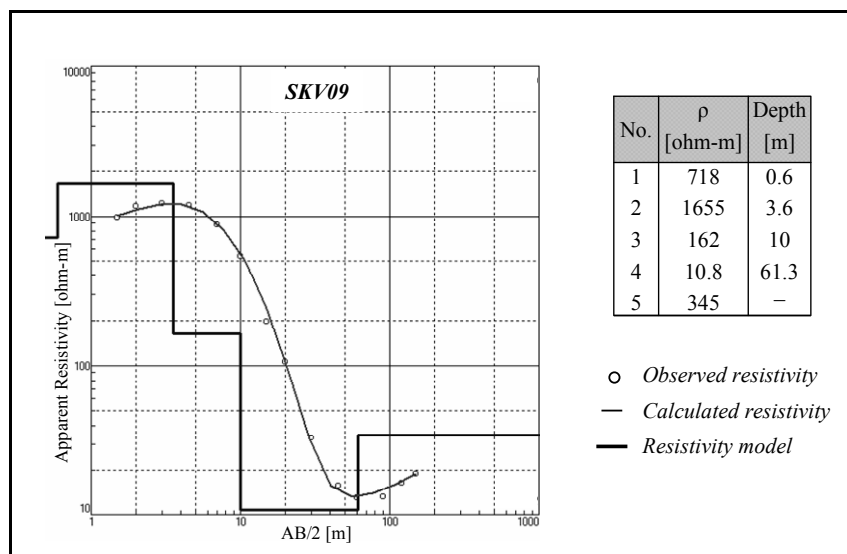


Figure 2.36 VES model of survey point SKV09.

CHAPTER 3

RESULTS

This chapter presents the results of seismic refraction measurement, seismic reflection measurement and vertical electrical sounding measurement for study sites in Bo Yang district.

3.1 Geology and hydrogeology

Songkhla Province is underlain stratigraphically by a variety of rocks ranging in age from the oldest rock of Cambrian, to the youngest Quaternary that of beach /alluvial deposits (Figure 3.1). The Bo Yang district is a part of the Songkhla province. Geology of the study area is Quaternary age, Quaternary deposits comprise all of the younger unconsolidated deposits, terrace/alluvial and beach/alluvial deposits. Terraces, alluvial fans, alluvial deposits of unconsolidated gravels, sands, silts and clay characterize the former sequence. The latter sequence is composed mainly of unconsolidated beach deposits, consisting of beach sands, silts and clay. However, alluvial gravel, clayey estuarine and tidal flat deposits are also common. The distributions are extensive, especially in the intermountain basins, undulated terrains, as well as along the minor and major stream courses in the area. The upper units are governed in both the coastal range zones.

The hydrogeologic unit of Bo Yang is beach-sand deposits in the coastal plain of southern regions of the Gulf of Thailand. Unconsolidated deposits can be divided into four types; (a) Recent beach-sand deposits, (b) Old beach-sand deposits, (c) Lagoon deposits and (d) Estuary deposits. The groundwater source in coastal area is groundwater in sand layer, which accumulated along the beach and stored in the sand dunes or sand ridges in old beach-sand (Department of Mineral Resources, 2007).

The groundwater resources in Bo Yang consist of groundwater stored in unconsolidated and consolidated sedimentary. Groundwater in the study area is the floodplain deposits aquifer (Qfd) consisting of sand, gravel, silt and clay.

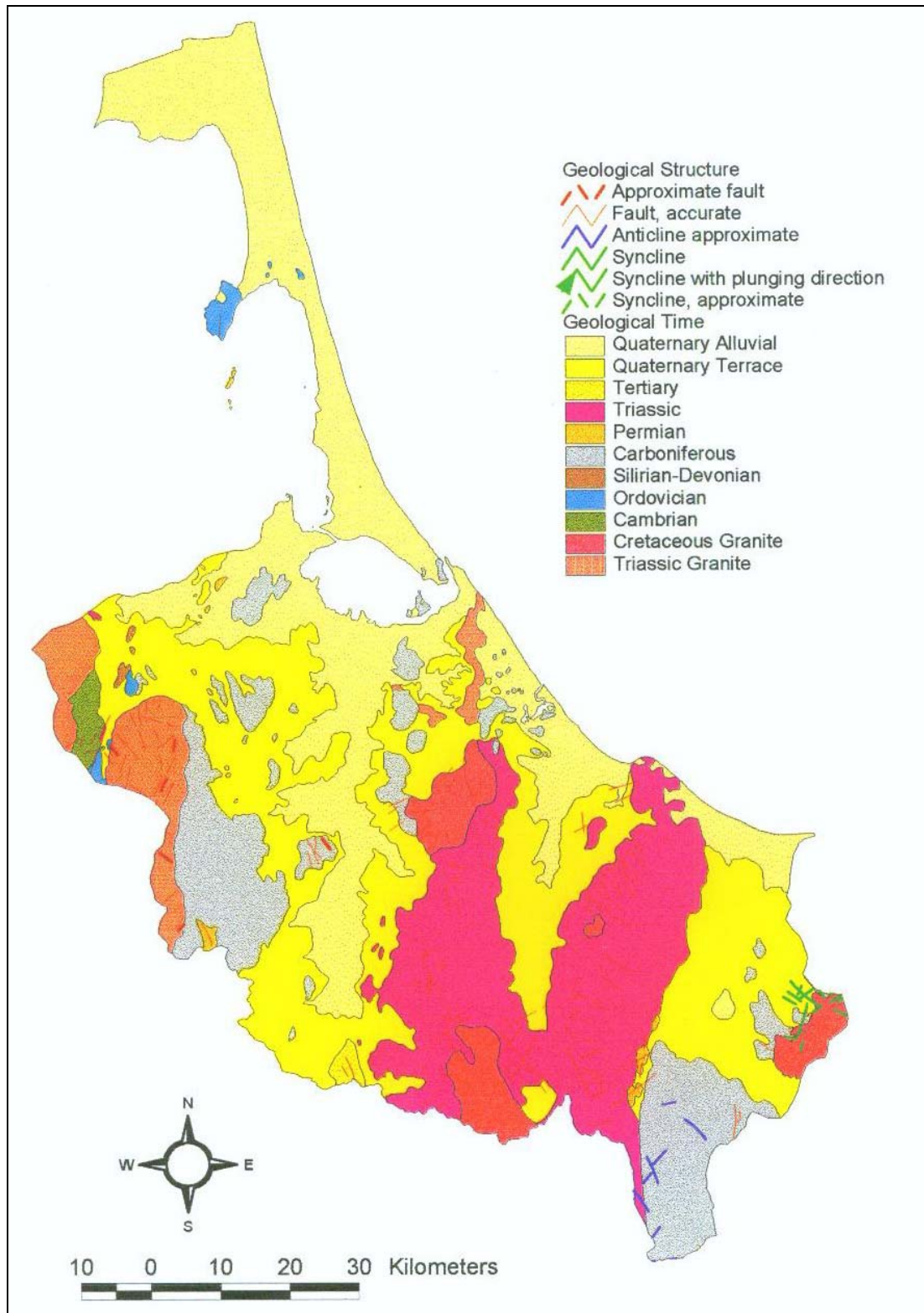


Figure 3.1 Geological map of Songkhla Province (from Department of Mineral Resources, 2007).

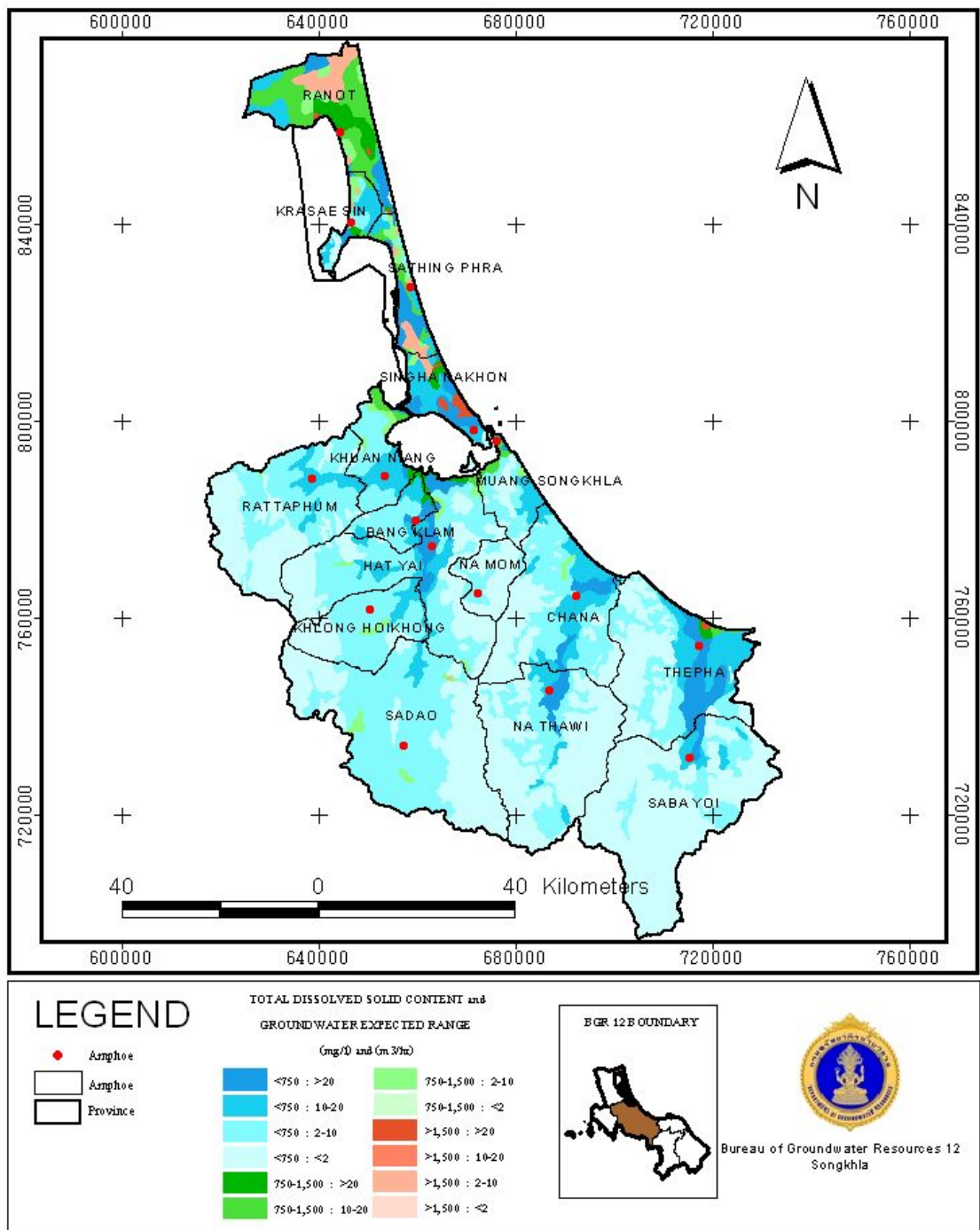


Figure 3.2 Total dissolved solids and groundwater expected yield map of Songkhla Province (Bureau of Groundwater Resources 12 Songkhla, 2005).

The total dissolved solids (TDS) are a measure of the combined content of all inorganic and organic substances contained in a liquid in: molecular, ionized or micro-granular (colloidal sol) suspended form. Generally the operational definition is that the solids must be small enough to survive filtration through a sieve the size of two micrometer. Total dissolved solids are normally discussed only for freshwater systems, as salinity comprises some of the ions constituting the definition of TDS. The principal application of TDS is in the study of water quality for streams, rivers and lakes, although TDS is not generally considered a primary pollutant (e.g. it is not deemed to be associated with health effects) it is used as an indication of aesthetic characteristics of drinking water and as an aggregate indicator of the presence of a broad array of chemical contaminants.

Table 3.1 Classification of water base on the total dissolved solids (TDS) (modified from Wendell, 2007).

Types of water	TDS (mg/l)
Fresh water	<1,500
Brackish water	1,500 – 5,000
Saline water	>5,000

Fresh groundwater comes in contact with saline groundwater at the seaward margins of coastal aquifers. The seaward limit of freshwater in a particular aquifer is controlled by the amount of freshwater flowing through the aquifer, the thickness and hydraulic properties of the aquifer and adjacent confining units, and the relative densities of saltwater and freshwater, among other variables. Because of its lower density, freshwater tends to remain above the saline (saltwater) zones of the aquifer, although in multilayered aquifer systems, seaward flowing freshwater can discharge upward through confining units into overlaying saltwater. Fresh water is defined as water having TDS concentration less than 1,500 mg/l, brackish water has TDS concentration of about 1,500–5,000 mg/l and saline water has TDS concentration more than 5,000 mg/l (Table 3.1).

The groundwater expected yield is the amount of water that can be withdrawn from it without producing an undesired effect. Figure 3.2 shown the total

dissolved solids and groundwater expected yield map of Songkhla Province, the study area has a TDS concentration of about 750–1,500 mg/l and have groundwater expected yield in range 10 – 20 m³/hr.

3.2 Results of SK01 site

The SK01 site located at Wachiranukul School with measurements on one line oriented W–E consisting of seismic refraction, seismic reflection, and VES surveys (Figure 3.3).

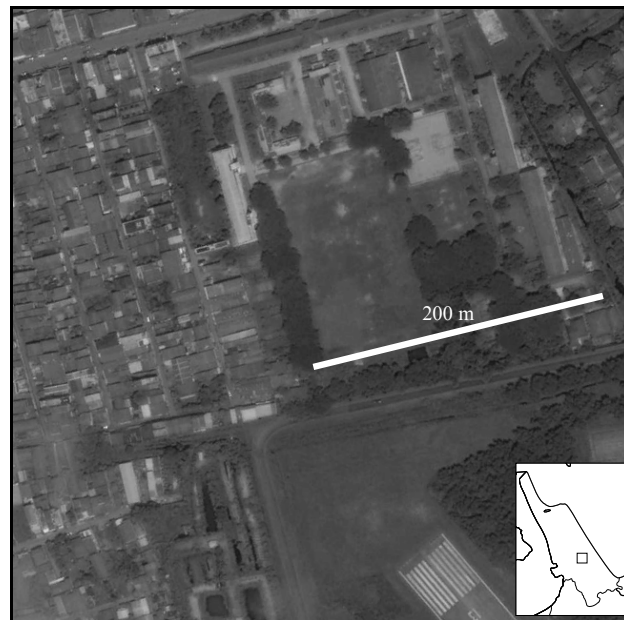


Figure 3.3 Location of seismic refraction (*SKR01*), seismic reflection (*SKL01*) and VES (*SKV01*) profiles at SK01 site.

Figure 3.4 shows that the 2D velocity–depth model has three layers and an increase in velocity with depth. The interpretation of the velocity–depth models was based on the relation between velocity and material in Table 2.1. Layer 1 has a P–wave velocity of 360 m/s and a depth between 0 m to 2 m. Layer 2 has a P–wave velocity of 760 m/s and depth between 2 m to 8.4 m. Layer 3 has a P–wave velocity of 1,400 m/s and a depth more than 8.4 m.

The SK01 site is located near the Songkhla Naval Base Airport. During the survey noise from helicopters starting and landing every hour caused significant noise in the seismic data. Figure 3.5 shows the seismic section of the survey line SKL01 along the Wachiranukul School football field; the line runs in a W–E direction and is about 200 m length. The first reflector appears at depth of about 28 m with a P–wave velocity of 1,500 m/s.

Figure 3.6 shows the VES model of SKV01 interpreted as a four layer model. Layer 1 has a resistivity value of 597 ohm-m and 3 m depth. Layer 2 has a resistivity value of 56.5 ohm-m and 8.9 m depth. Layer 3 has a resistivity value of 8.1 ohm-m and 60.1 m depth. Layer 4 has a resistivity value of 21.1 ohm-m and more than 60.1 m depth.

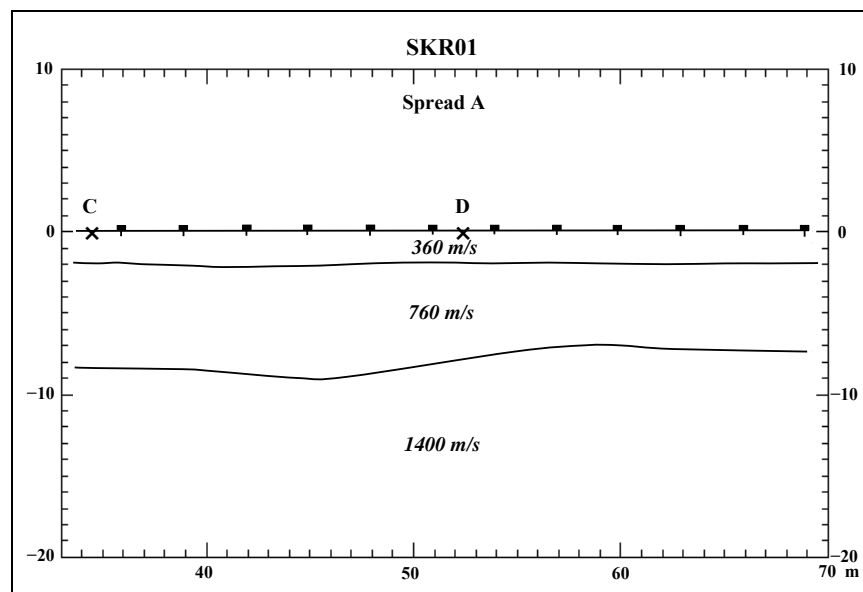


Figure 3.4 2D velocity–depth model of survey line SKR01.

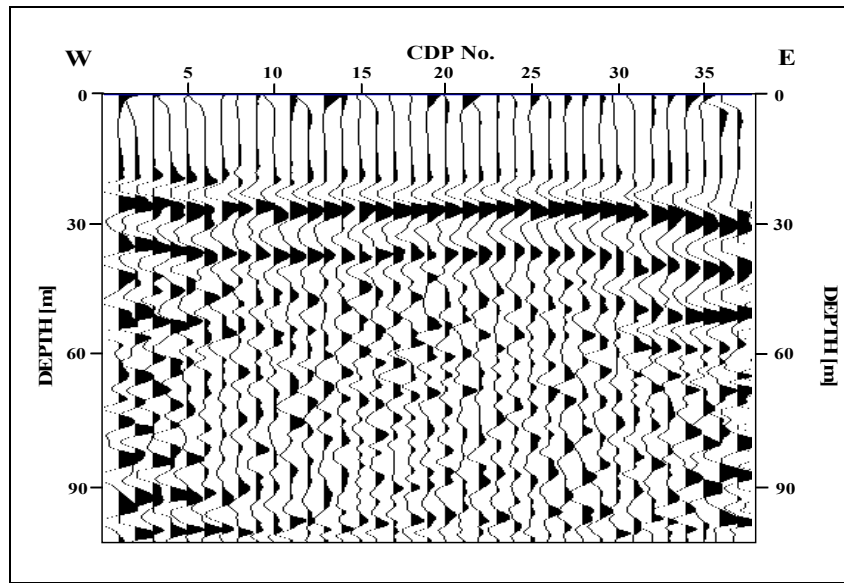


Figure 3.5 Seismic section of survey line SKL01.

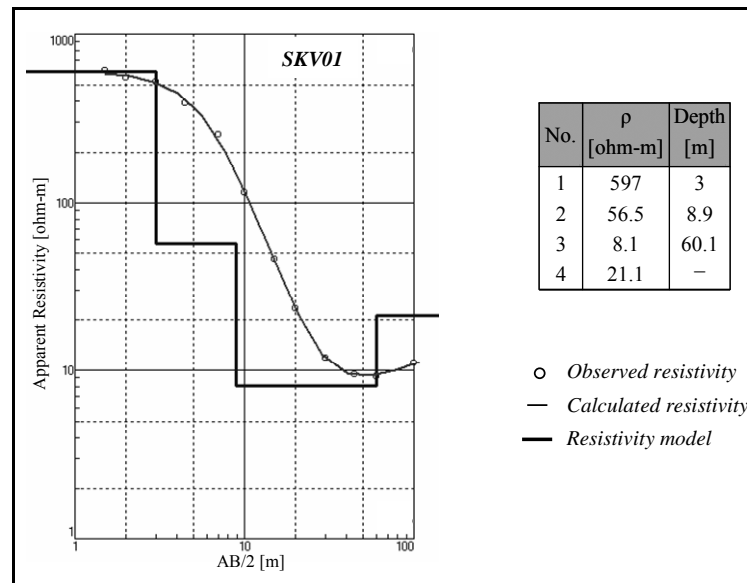


Figure 3.6 VES model of survey point SKV01.

3.3 Results of SK02 site

The SK02 site located at Mahavajiravudh School has measurements on one line oriented N–S consisting of seismic refraction, seismic reflection and VES surveys with one line oriented W–E consisting of a VES survey (Figure 3.7).

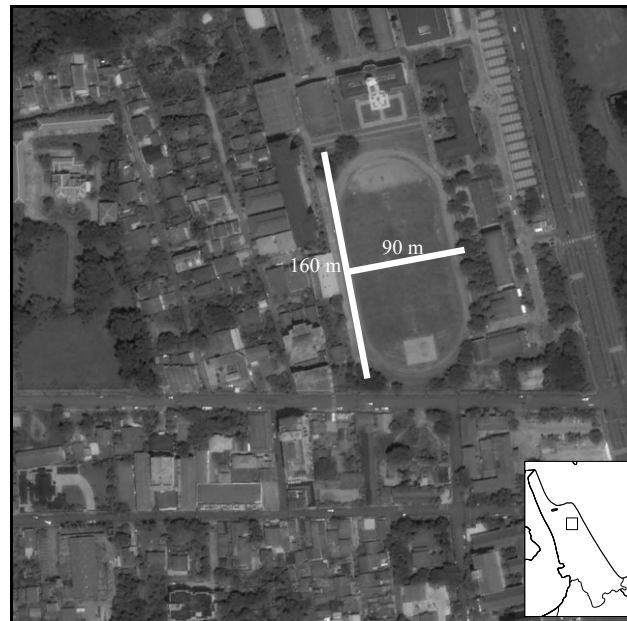


Figure 3.7 Location of seismic refraction (*SKR02*), seismic reflection (*SKL02*) and VES (*SKV02*, *SKV03*) profiles at *SK02* site.

Figure 3.8 shows that the 2D velocity–depth model has three layers. Layer 1 has a P–wave velocity of 500 m/s and a depth between 0 m to 4.0 m. Layer 2 has a P–wave velocity 910 m/s and a depth between 4.0 m to 10.6 m. Layer 3 has a P–wave velocity of 1,490 m/s and a depth more than 10.6 m.

Figure 3.9 shows the seismic section of survey line *SKL02* along the Mahavajiravudh School football field; the line runs in a N–S direction and is about 150 m long. The first reflector appears at a depth of about 52 m with a velocity of 1,500 m/s. During the survey was significant seismic noise from traffic and other human activities. Therefore the quality of the data set was not very good. The discontinuity of the reflector between 30 and 40 m can be attributed to that.

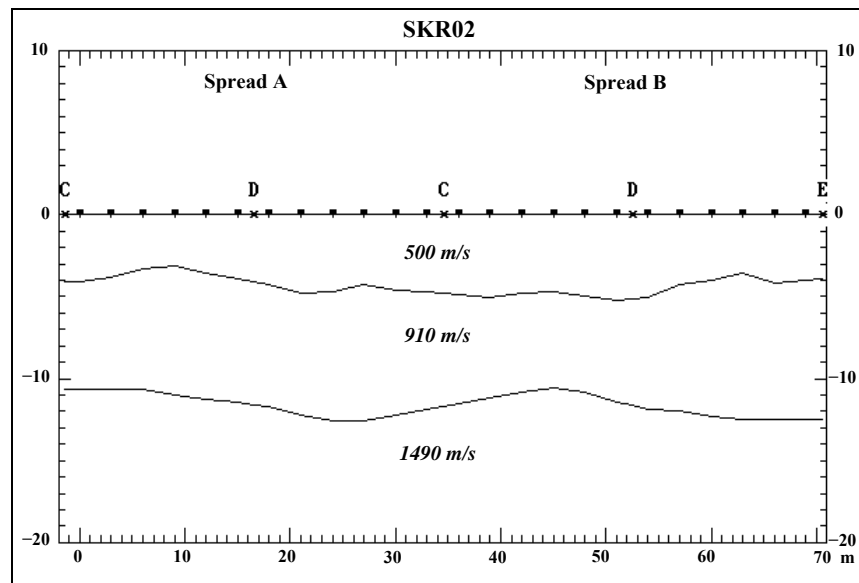


Figure 3.8 2D velocity–depth model of survey line SKR02.

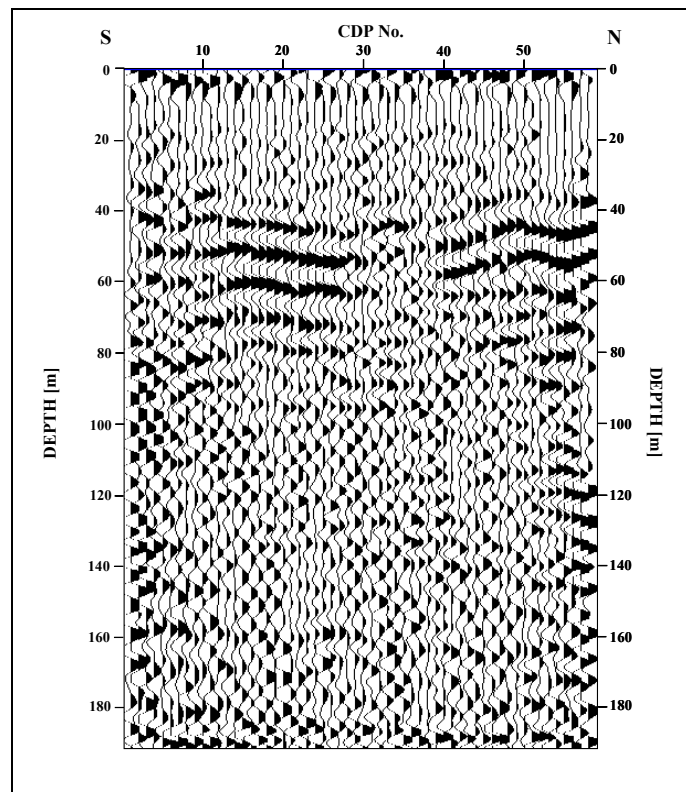


Figure 3.9 Seismic section of survey line SKL02.

Figure 3.10 shows the VES model of SKV02 interpreted as a five layer model. Layer 1 has a resistivity value of 74.8 ohm-m and 0.9 m depth. Layer 2 has a resistivity value of 235 ohm-m and 1.9 m depth. Layer 3 has a resistivity value of 21 ohm-m and 19 m depth. Layer 4 has a resistivity value of 8.6 ohm-m and 40.2 m depth. Layer 5 has a resistivity value of 143 ohm-m and more than 40.2 m depth.

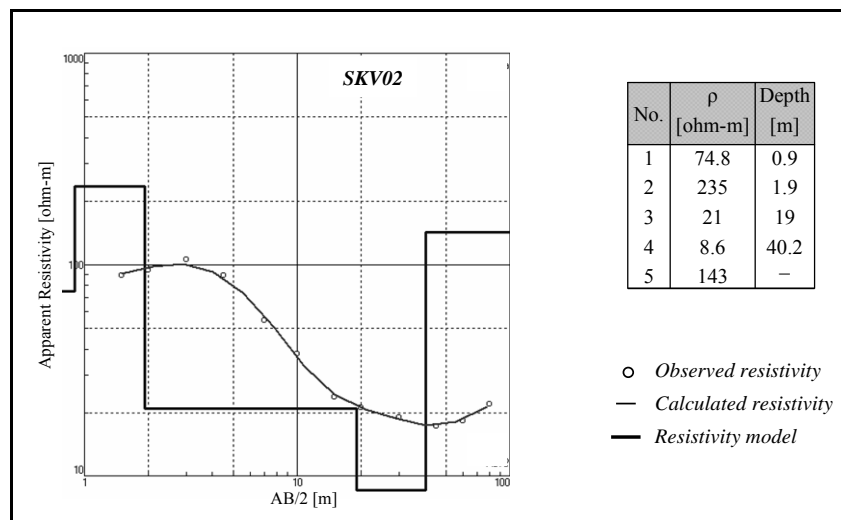


Figure 3.10 VES model of survey point SKV02.

Figure 3.11 shows the VES model of SKV03 interpreted as a four layer model. Layer 1 has a resistivity value of 56 ohm-m and 0.5 m depth. Layer 2 has a resistivity value of 372 ohm-m and 3.7 m depth. Layer 3 has a resistivity value of 36.2 ohm-m and 15.1 m depth. Layer 4 has a resistivity value of 3.6 ohm-m and a depth of more than 15.1 m.

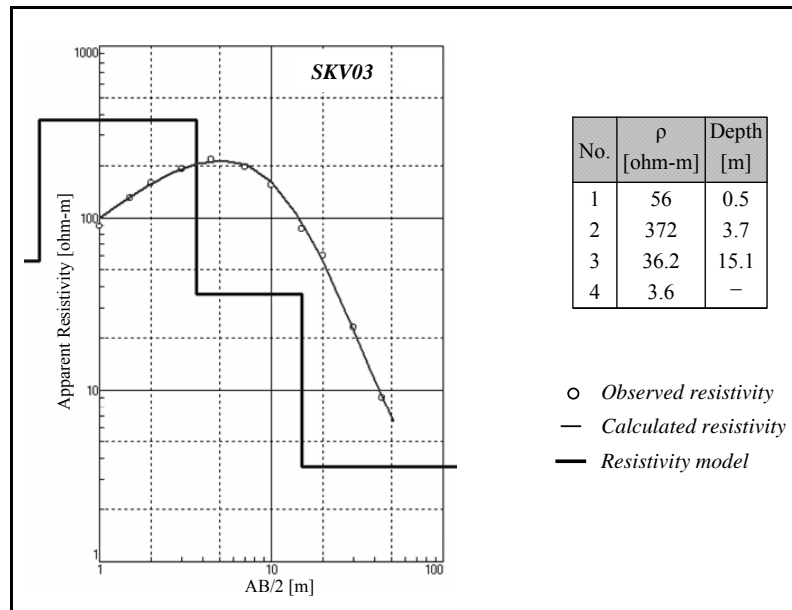


Figure 3.11 VES model of survey point SKV03.

3.4 Results of SK03 site

The SK03 site is located at Chalathat Road with measurements on one line oriented NW–SE consisting of seismic refraction, seismic reflection and VES surveys. At the Songkhla Naval Base Airport there were measurements on one line of a VES survey (Figure 3.12).

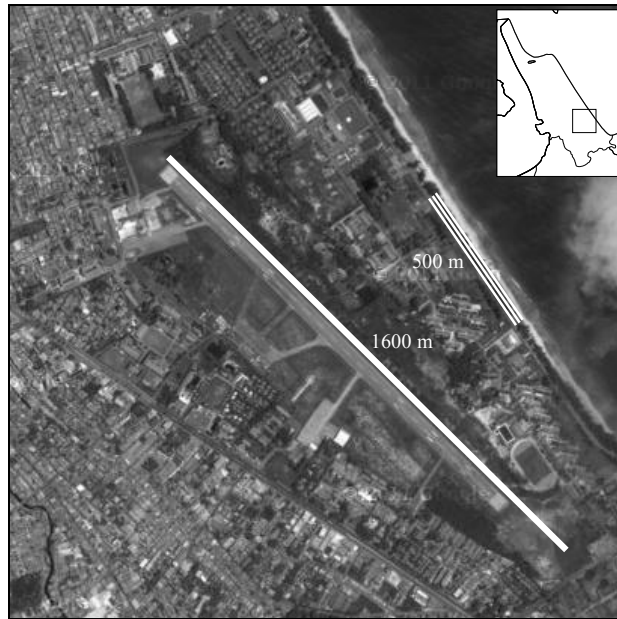


Figure 3.12 Location of seismic refraction (*SKR03*), seismic reflection (*SKL03*) and VES (*SKV04*, *SKV05*, *SKV06*, *SKV07*) profiles at SK03 site.

Figure 3.13 shows the 2D velocity–depth model that has three layers. Layer 1 has a P–wave velocity of 270 m/s and a depth between 0 m to 1.3 m. Layer 2 has a P–wave velocity of 650 m/s and a depth between 1.3 m to 8.8 m. Layer 3 has a P–wave velocity of 1,200 m/s and a depth of depth more than 8.8 m.

Figure 3.14 shows the seismic section of survey line SKL03 along the Chalathat Road; the line runs in a NW–SE direction and is about 100 m length. The first strong reflector appears at depth of about 30 m with velocity 1,200 m/s. The second reflector appears at depth of about 52.5 m with velocity 1,600 m/s

Figure 3.15 shows the VES model of SKV04 is interpreted as a four layer model. Layer 1 has a resistivity value of 263 ohm-m and 2.5 m depth. Layer 2 has a resistivity value of 33.4 ohm-m and 7.8 m depth. Layer 3 has a resistivity value of 4.2 ohm-m and 30.3 m depth. Layer 4 has a resistivity value of 156 ohm-m and more than 30.3 m depth.

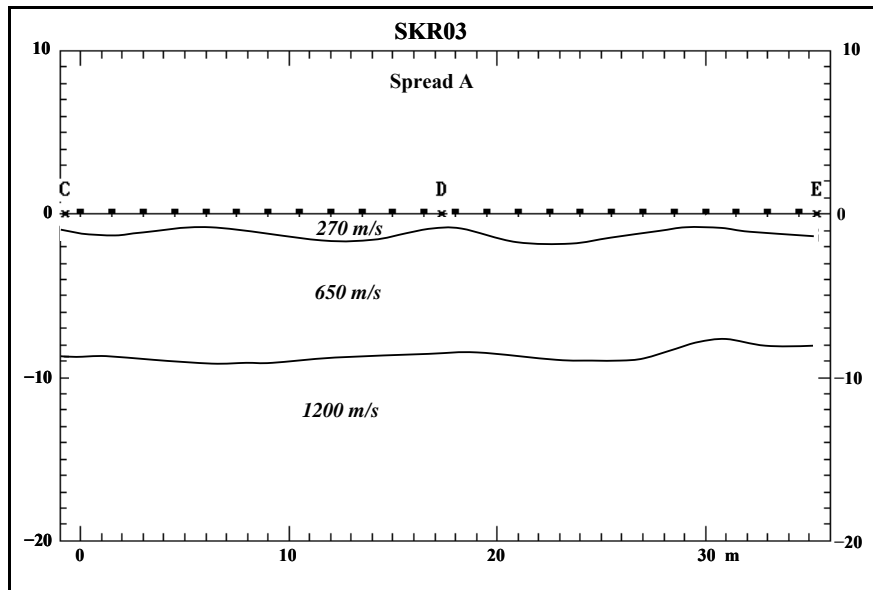


Figure 3.13 2D velocity–depth model of survey line SKR03.

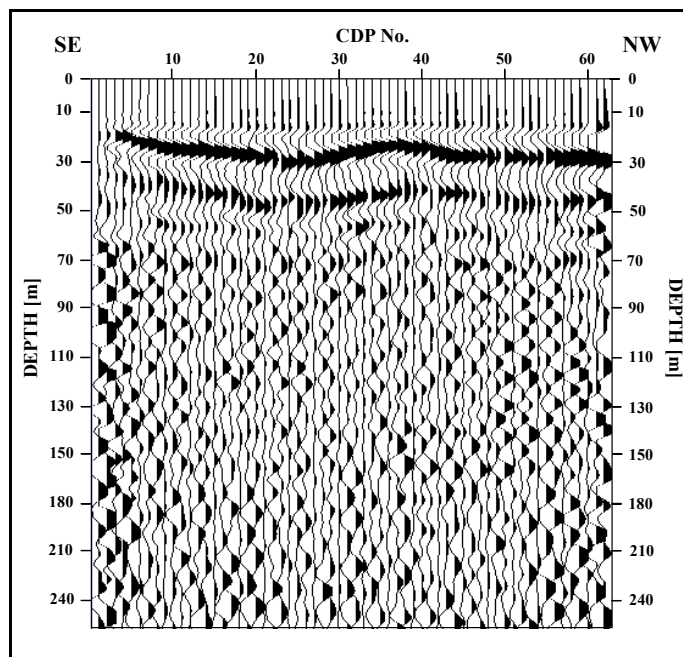


Figure 3.14 Seismic section of survey line SKL03.

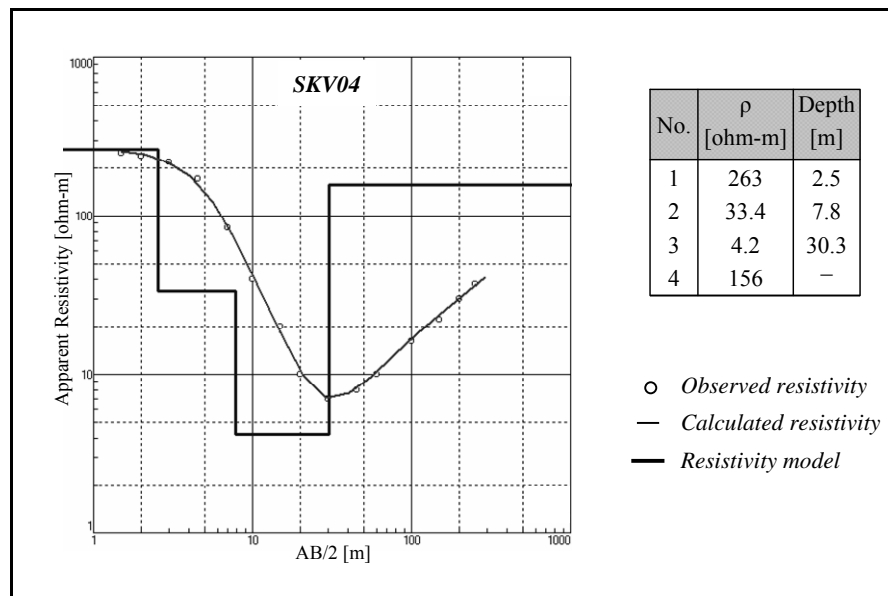


Figure 3.15 VES model of survey point SKV04.

Figure 3.16 shows the VES model of SKV05 is interpreted as a five layer model. Layer 1 has a resistivity value of 1,053 ohm-m and 1.2 m depth. Layer 2 has a resistivity value of 269 ohm-m and 4.2 m depth. Layer 3 has a resistivity value of 52.2 ohm-m and 13.2 m depth. Layer 4 has a resistivity value of 5.3 ohm-m and 55.4 m depth. Layer 5 has a resistivity value of 45.5 ohm-m and more than 55.5 m depth.

Figure 3.17 shows the VES model of SKV06 is interpreted as a four layer model. Layer 1 has a resistivity value of 560 ohm-m and 1.4 m depth. Layer 2 has a resistivity value of 95.3 ohm-m and 6.3 m depth. Layer 3 has a resistivity value of 6 ohm-m and 33 m depth. Layer 4 has a resistivity value of 154 ohm-m and more than 33 m depth.

Figure 3.18 shows the VES model of SKV07 is interpreted as a five layer model. Layer 1 has a resistivity value of 4,894 ohm-m and 0.7 m depth. Layer 2 has a resistivity value of 767 ohm-m and 3.6 m depth. Layer 3 has a resistivity value of 50.5 ohm-m and 19 m depth. Layer 4 has a resistivity value of 4.2 ohm-m and 68.6 m depth. Layer 5 has a resistivity value of 140 ohm-m and more than 68.6 m depth.

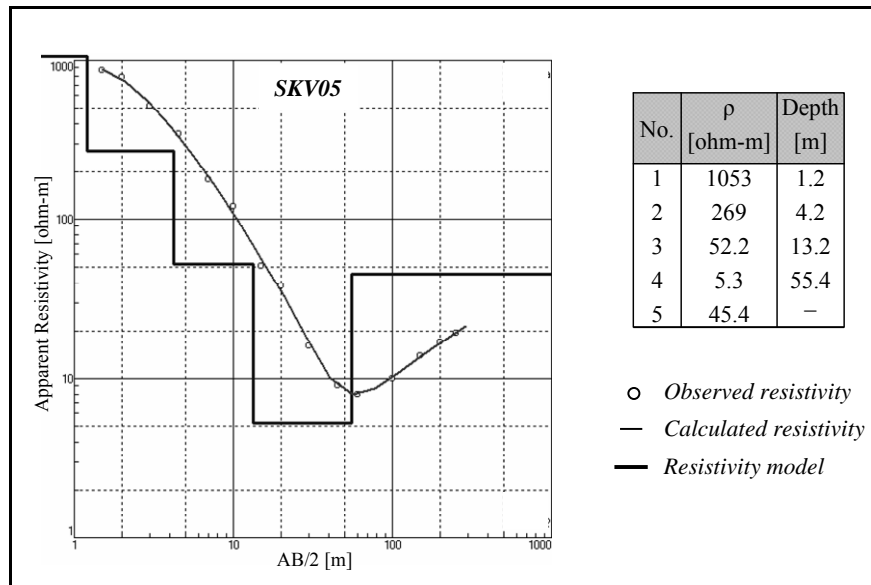


Figure 3.16 VES model of survey point SKV05.

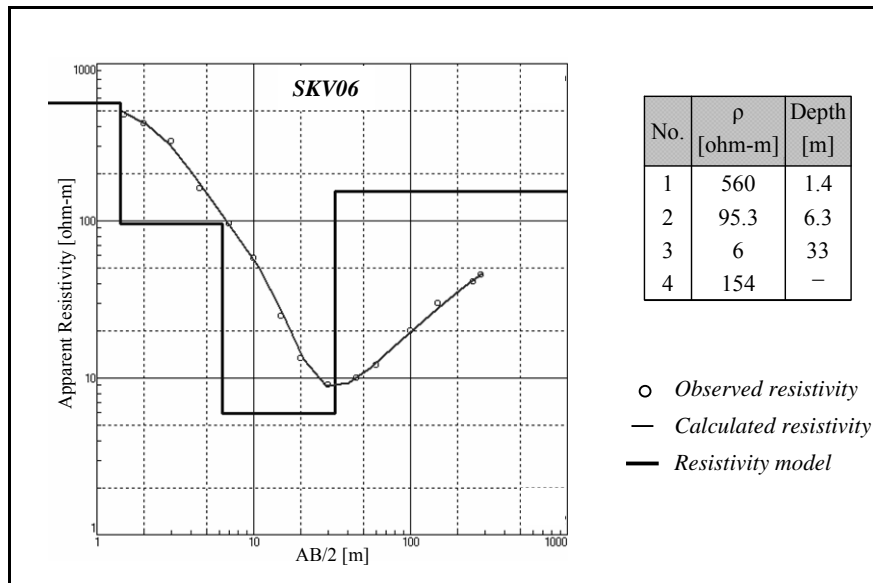


Figure 3.17 VES model of survey point SKV06.

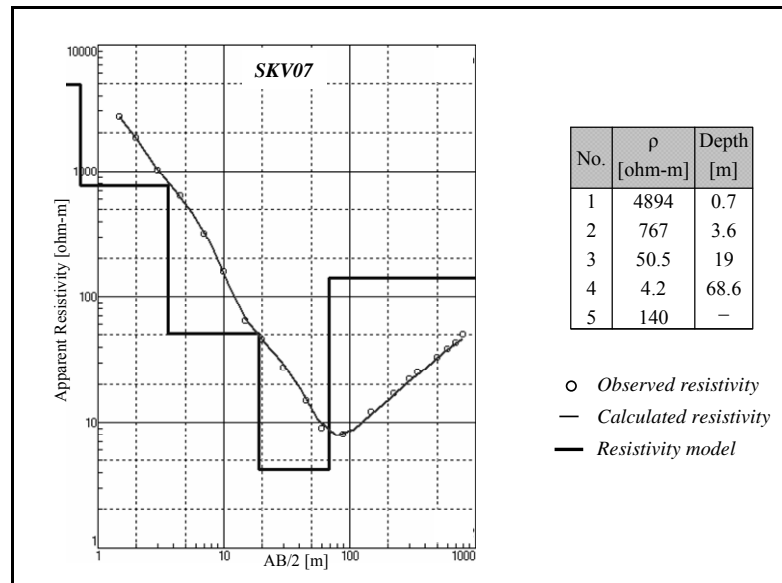


Figure 3.18 VES model of survey point SKV07.

3.5 Results of SK04 site

The SK04 site is located at Rajamangala University of Technology Srivijaya and measurements were carried out along one line oriented SW–NE consisting of a seismic reflection survey (Figure 3.19).

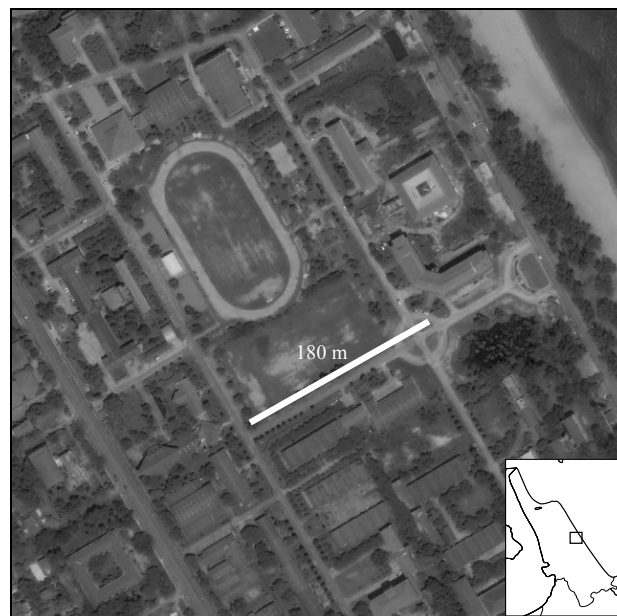


Figure 3.19 Location of seismic reflection (SKL04) profiles at SL04 site.

Figure 3.20 shows the seismic section of survey line SKL04 along the the Rajamangala University of Technology Srivijaya; the line runs in a NE–SW direction and has a length of about 200 m. The first strong reflector appears at depth of about 40 m with a P–wave velocity of 1,200 m/s. The second reflector appears at depth of about 80 m with a velocity of 1,800 m/s. The third reflector appears at depth of about 120 m with velocity of 2,200 m/s.

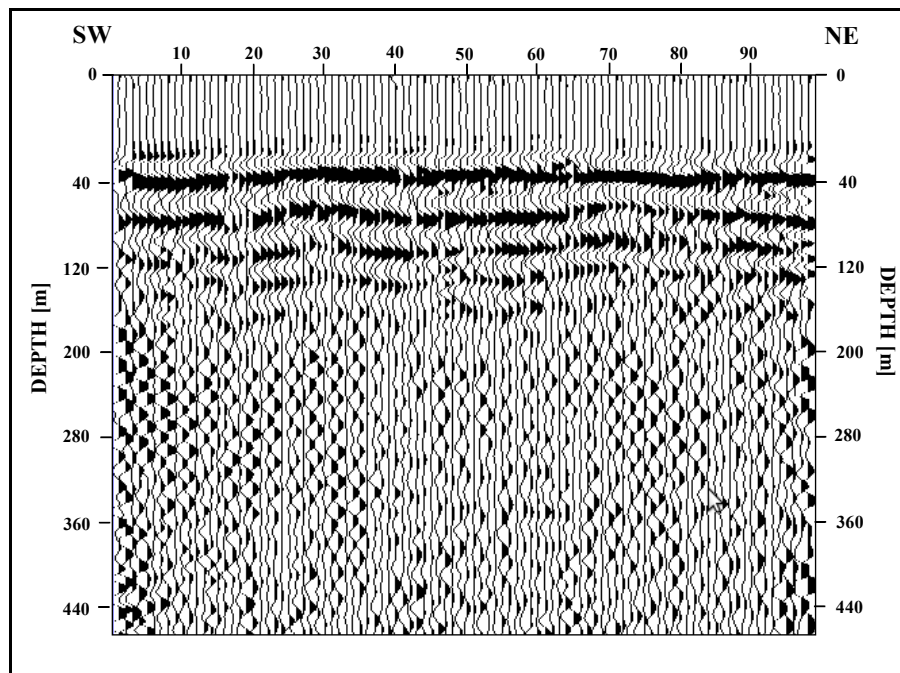


Figure 3.20 Seismic section of survey line SKL04.

3.6 Results of SK05 site

The SK05 site is located at the Tinsulanonda Stadium with measurements on one line oriented SW–NE consisting of seismic reflection and VES surveys; one line of VES survey measured along the beach in front of the Tinsulanonda Stadium (Figure 3.21).



Figure 3.21 Location of seismic reflection (*SKL05*) and VES (*SKV09*, *SKV10*) profiles at SK05 site.

Figure 3.22 shows the seismic section of survey line SKL05 along the Tinsulanonda Stadium; the line runs in a NE–SW direction and is about 300 m long. The first strong reflector appears at depth of about 28 m with a P–wave velocity of 1,000 m/s. The second strong reflector appears at depth of about 50 m with a velocity of 1,500 m/s.

Figure 3.23 shows the VES model of SKV09 interpreted as a five layer model. Layer 1 has a resistivity value of 718 ohm-m and 0.6 m depth. Layer 2 has a resistivity value of 1,655 ohm-m and 3.6 m depth. Layer 3 has a resistivity value of 162 ohm-m and 10 m depth. Layer 4 has a resistivity value of 10.8 ohm-m and 61.3 m depth. Layer 5 has a resistivity value of 345 ohm-m and more than 61.3 m depth.

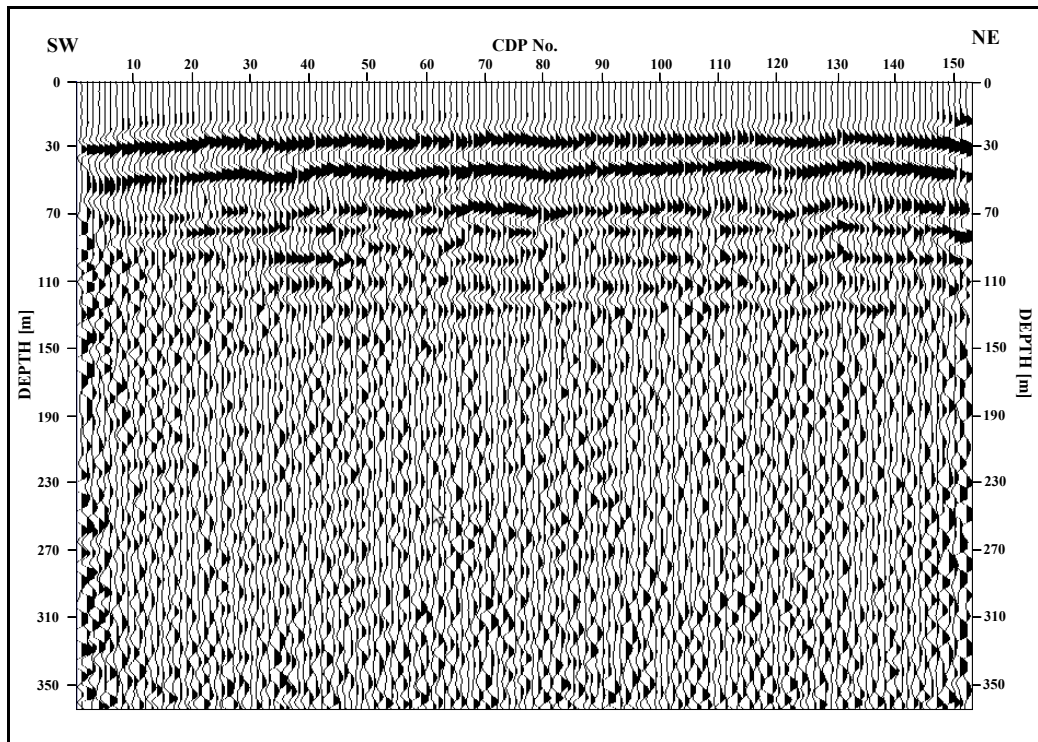


Figure 3.22 Seismic section of survey line SKL05.

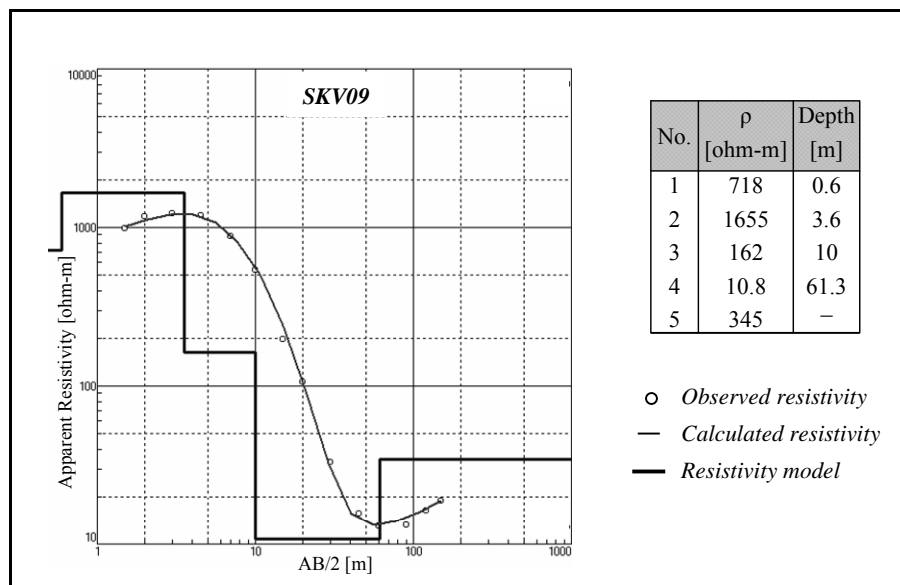


Figure 3.23 VES model of survey point SKV07.

Figure 3.24 shows the VES model of SKL10 interpreted as a four layer model. Layer 1 has a resistivity value of 759 ohm-m and 2.4 m depth. Layer 2 has a resistivity value of 50.2 ohm-m and 13.1 m depth. Layer 3 has a resistivity value of 5 ohm-m and 89.1 m depth. Layer 4 has a resistivity value of 40.4 ohm-m and more than 89.1 m depth.

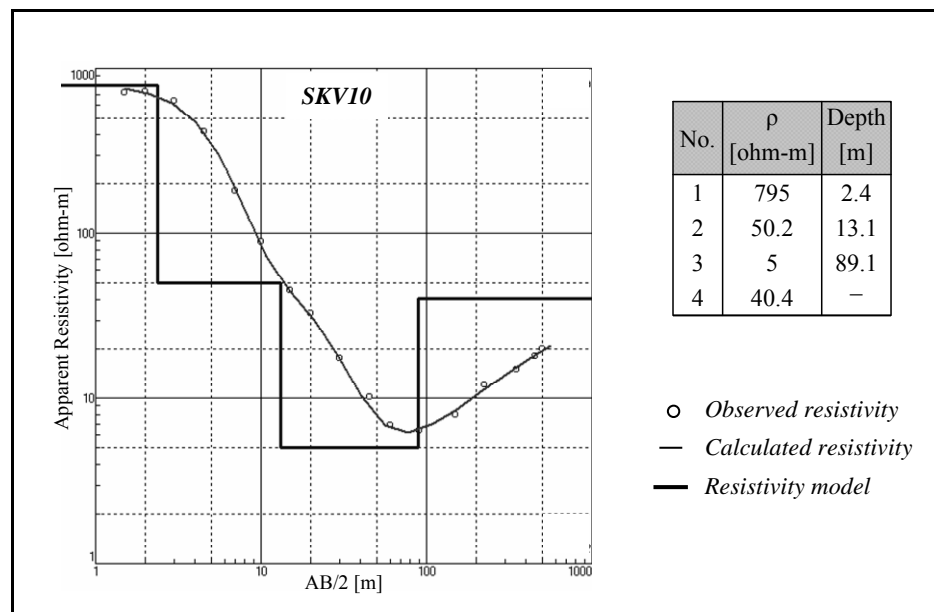


Figure 3.24 VES model of survey point SKV10.

3.7 Results of SK06 site

The SK06 site located at Samila Beach; measurements were on one line oriented SW–NE consisting of seismic refraction, seismic reflection and VES surveys (Figure 3.25).

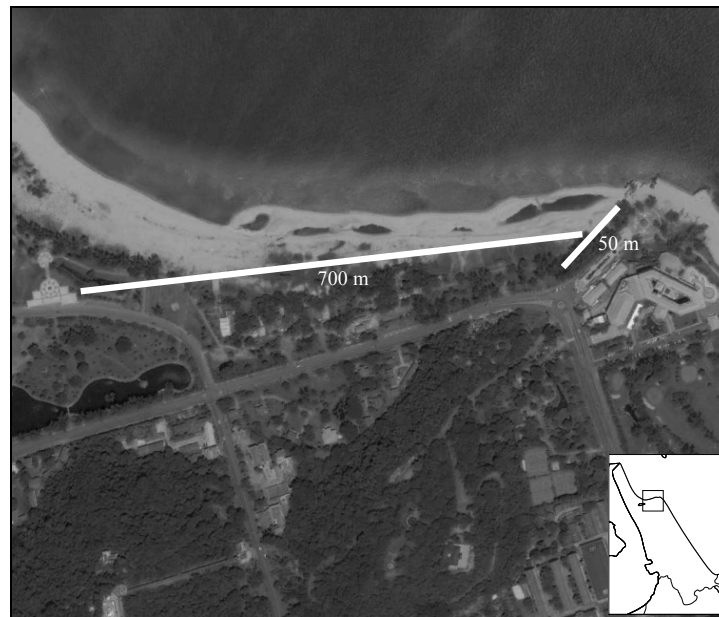


Figure 3.25 Location of seismic refraction (SKR04), seismic reflection (SKL06) and VES (SKV08) profiles at SK06 site.

Figure 3.26 shows that the 2D velocity–depth model has three layers. Layer 1 has a P–wave velocity of 370 m/s and a depth between 0 m to 2.8 m. Layer 2 has a P–wave velocity of 1,560 m/s and a depth between 2.8 m to 9.8 m. Layer 3 has a P–wave velocity of 3,920 m/s and depth more than 9.8 m.

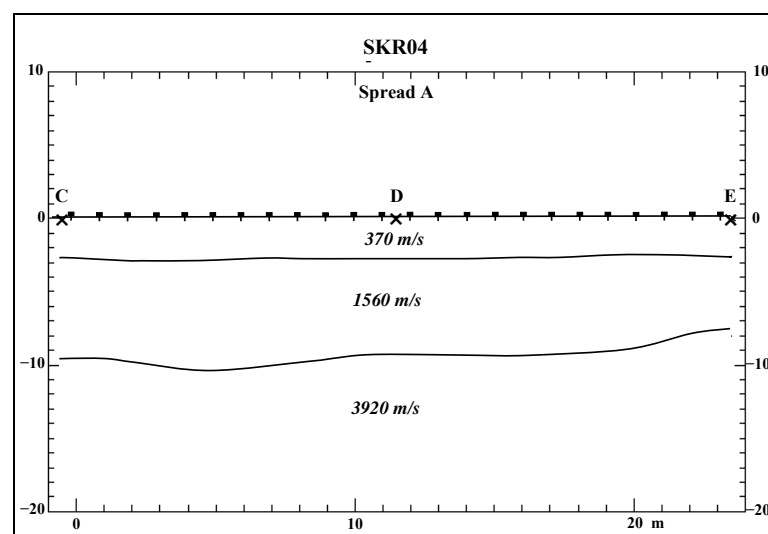


Figure 3.26 2D velocity–depth model of survey line SKR04.

Figure 3.27 shows the seismic section of survey line SKL04 along the Samila Beach; the line runs in a NE–SW direction and is about 60 m long. The first strong reflector appears at a depth of about 20 m with a P–wave velocity of 1,200 m/s. The second reflector appears at depth of about 30 m with a velocity of 1,600 m/s. The third weak reflector appears at a depth of 50 m with a velocity of 2,000 m/s.

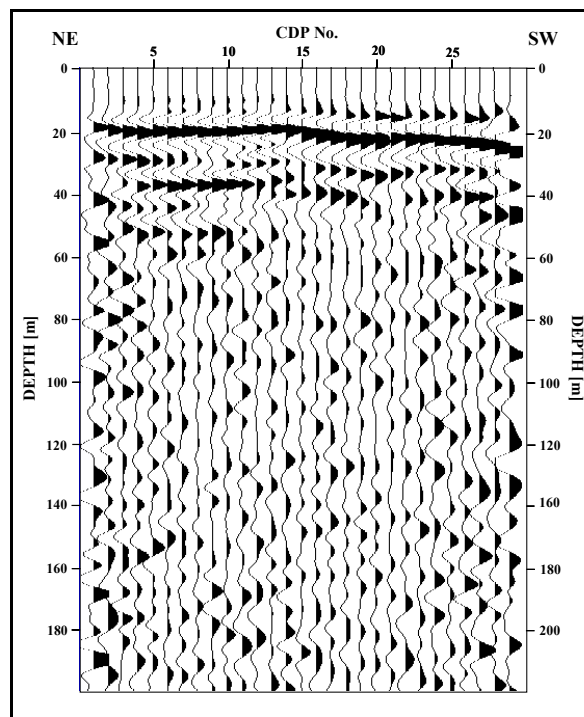


Figure 3.27 Seismic section of survey line SKL06.

Figure 3.28 shows the VES model of SKV08 interpreted as a five layer model. Layer 1 has a resistivity value of 971 ohm-m and 0.8 m depth. Layer 2 has a resistivity value of 10.4 ohm-m and 3.7 m depth. Layer 3 has a resistivity value of 1.8 ohm-m and 8.7 m depth. Layer 4 has a resistivity value of 8.1 ohm-m and 80.5 m depth. Layer 5 has a resistivity value of 34.2 ohm-m and more than 80.5 m depth.

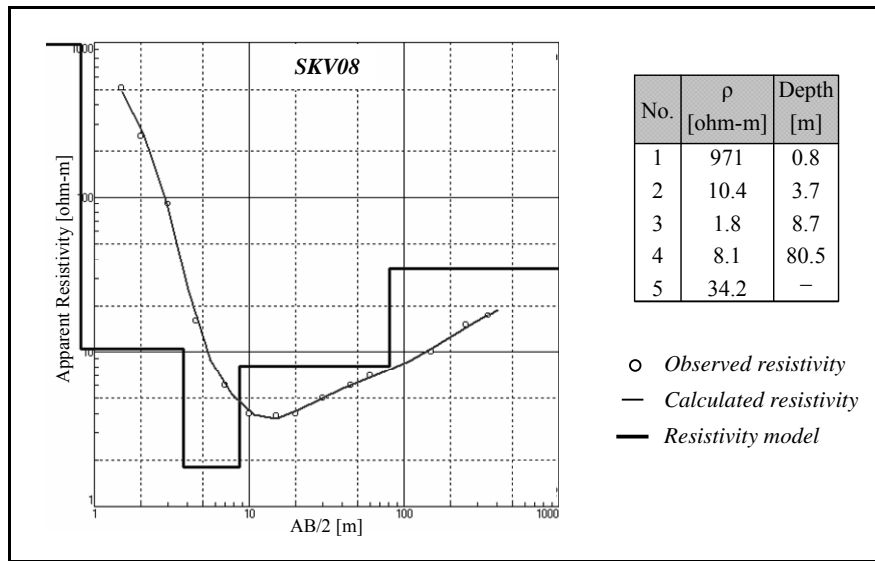


Figure 3.28 VES model of survey point SKV08.

3.8 Results of SK07 site

The SK07 site located at Laem Son On with measurements on two lines oriented NW–SE consisting only of VES surveys (Figure 3.29).

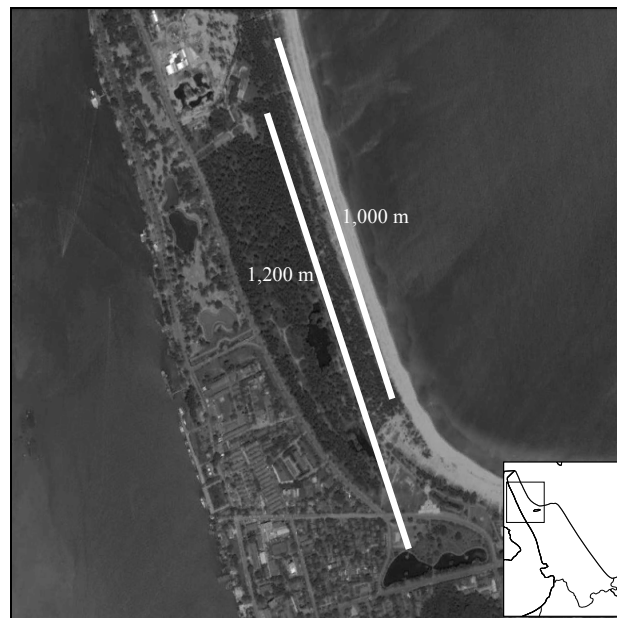


Figure 3.29 Location of VES (SKV11, SKV12) profiles at SK07 site.

Figure 3.30 shows the VES model of SKV11 interpreted as a four layer model. Layer 1 has a resistivity value of 428 ohm-m and 0.5 m depth. Layer 2 has a resistivity value of 2,168 ohm-m and 2.7 m depth. Layer 3 has a resistivity value of 44.4 ohm-m and 11.2 m depth. Layer 4 has a resistivity value of 6.4 ohm-m and 72.6 m depth. Layer 5 has a resistivity value of 22.5 ohm-m and more than 72.6 m depth.

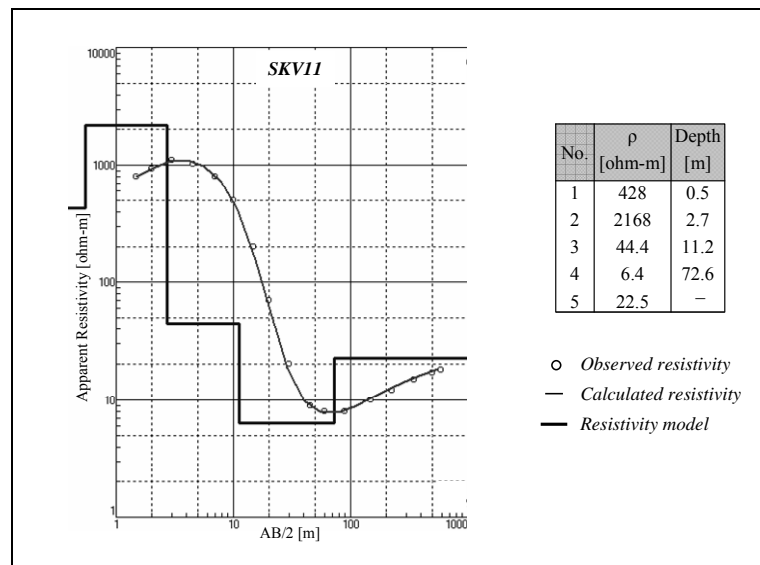


Figure 3.30 VES model of survey point SKV11.

Figure 3.31 shows the VES model of SKV12 interpreted as a four layer model. Layer 1 has a resistivity value of 4,547 ohm-m and 1.5 m depth. Layer 2 has a resistivity value of 93.2 ohm-m and 4.3 m depth. Layer 3 has a resistivity value of 2.5 ohm-m and 78.7 m depth. Layer 4 has a resistivity value of 263 ohm-m and more than 78.7 m depth.

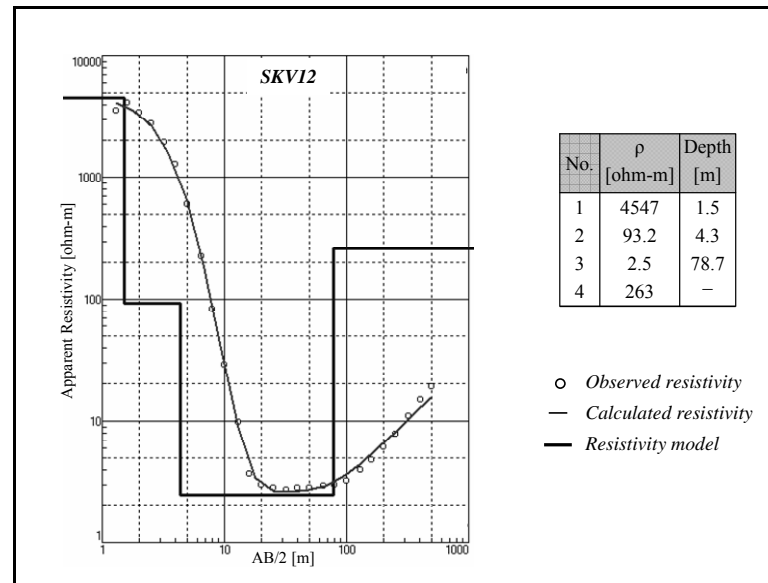


Figure 3.31 VES model of survey point SKV12.

3.9 Borehole information

Borehole data were available to calibrate the geophysical data interpretation. These data came from the Department of Groundwater Resources and the Provincial Groundwater Office. There are seven drilling locations in the study area. The borehole data in the study area only has a few and shallow data. Further, most of the data are older, up to 40 years, as most of the drilling activities are carried out at that time. Currently, hardly any drilling is been done in the study area.

Well number TH405 (676345E, 796961N)

Figure 3.32 shows the borehole data of log of boring number TH405 at Songkhla Provincial Administration Organization. The borehole data has total depth 30 m. Layer 1 has a depth between 0 m to 4.5 m and identified as sand. Layer 2 has a depth between 4.5 m to 7.8 m and identified as clay/sand. Layer 3 has depth between 7.8 m to 12 m and identified as sand. Layer 4 has depth between 12 m to 30 m and identified as clay.

Well number TH230 (676735E, 7947562N)

Figure 3.33 shows the borehole data of well number H230 at Ramkhamhaeng Camp. The borehole data has a total depth of 12.2 m. Layer 1 has a depth between 0 m to 4.5 m and identified as sand. Layer 2 has a depth between 4.5 m to 12.2 m and identified as clay.

Well number H1383 (678468E, 793788N)

Figure 3.34 shows the borehole data well number H1383 at Songkhla Rajanagarindra Psychiatric Hospital. The borehole data has a total depth of 27.4 m. Layer 1 has a depth between 0 m to 5 m and identified as sand. Layer 2 has a depth between 5 m to 8 m and identified as sand mixes black clay. Layer 3 has a depth between 8 m to 15 m and identify as clay. Layer 4 has a depth between 15 m to 24.5 m and identify as black clay mixes sand. Layer 5 has a depth between 24.5 m to 27.5 m and identify as granite.

Well number H49 (676550E, 796850N)

Figure 3.35 shows the borehole data well number H49 at Mahavajiruvudh School. The borehole data has a total depth of 17 m. Layer 1 has a depth between 0 m to 4.5 m and identified as sand. Layer 2 has a depth between 4.5 m to 9 m and identified as clay (very sandy). Layer 3 has a depth between 9 m to 12 m and identify as sand. Layer 4 has a depth between 12 m to 17 m and identify as clay.

Well number H237 (676863E, 794952N)

Figure 3.36 shows the borehole data well number H237 at Ramkhamhaeng Camp. The borehole data has a total depth of 69 m. Layer 1 has a depth between 0 m to 3 m and identified as sand. Layer 2 has a depth between 3 m to 15 m and identified as clay. Layer 3 has a depth between 15 m to 38 m and identify as clay. Layer 4 has a depth between 38 m to 67 m and identify as gravel.

Well number H186 (676294E, 796586N)

Figure 3.37 shows the borehole data of well number H186 at Woranari Chaloeem School. The borehole data has a total depth of 15 m. Layer 1 has a depth

between 0 m to 4.5 m and identified as sand. Layer 2 has a depth between 4.5 m to 9 m and identified as clay. Layer 3 has a depth between 9 m to 12.5 m and identify as sand. Layer 4 has a depth between 12.5 m to 15.5 m and identify as clay.

Well number H43 (676250E, 795550N)

Figure 3.38 shows the borehole data of well number H43 at Songkhla Vocational Education College. The borehole data has a total depth of 29 m. Layer 1 has a depth between 0 m to 3 m and identified as sand. Layer 2 has a depth between 3 m to 15.5 m and identified as clay. Layer 3 has a depth between 15.5 m to 29 m and identify as clay.

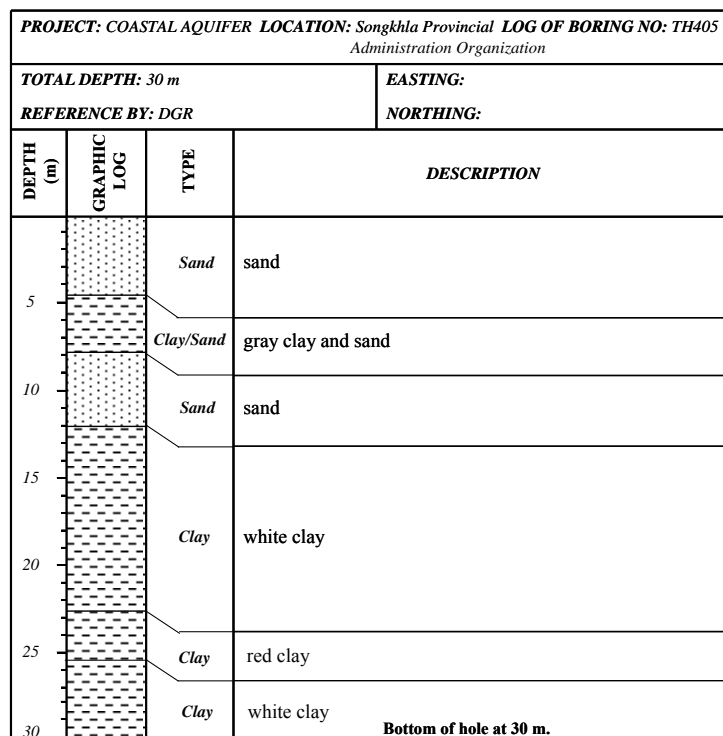


Figure 3.32 Borehole data of log of boring number TH405.

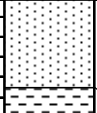
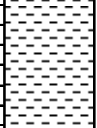
PROJECT: COASTAL AQUIFER LOCATION: Ramkhamhaeng Camp LOG OF BORING NO: H230			
TOTAL DEPTH: 12.20 m		EASTING:	
REFERENCE BY: DGR		NORTHING:	
DEPTH (m)	GRAPHIC LOG	TYPE	DESCRIPTION
5		Sand	dirty gray, size ranged from fine to coarse, angular to rounded, poorly sorted; composed mostly of quartz, muscovite, weathered feldspars, and dark minerals
10		Clay	greenish gray, silty, slightly plastic, moderately compacted; calcareous matters and muscovite in places
Bottom of hole at 12.20 m.			

Figure 3.33 Borehole data of log of boring number H230.

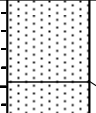
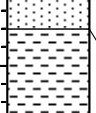
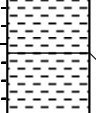
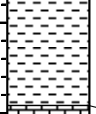

PROJECT: COASTAL AQUIFER LOCATION: Songkhla Rajanagarindra LOG OF BORING NO: H1383			
<i>Psychiatric Hospital</i>			
TOTAL DEPTH: 27.44 m		EASTING: 678468	
REFERENCE BY: DGR		NORTHING: 793788	
DEPTH (m)	GRAPHIC LOG	TYPE	DESCRIPTION
5		Sand	sand
10		Sand	sand mixes black clay
15		Clay	black clay
20		Clay	black clay mixes sand
25		Granite	granite
Bottom of hole at 27.44 m.			

Figure 3.34 Borehole data of log of boring number H1383.

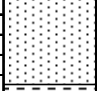
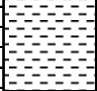
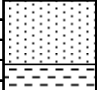
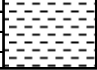
PROJECT: COASTAL AQUIFER LOCATION: Mahavajiravudh Sch. LOG OF BORING NO: H49			
TOTAL DEPTH: 16.77 m		EASTING: 676550	
REFERENCE BY: DGR		NORTHING: 796850	
DEPTH (m)	GRAPHIC LOG	TYPE	DESCRIPTION
5		Sand	plae yellowish brown, medium to very coarse, angular to sub-rounded, poorly sorted, composed of quartz of various colors; with chert fragments
10		Clay	dark yellowish brown, very sandy, partially limonitic, compacted, non-plastic, with some shells fragments
15		Sand	same as at 0' - 15', but color changed to dark yellwish brow
		Clay	dark yellowish brown to dark olive gray, shaly, limonitic, compacted plastic
Bottom of hole at 16.77 m.			

Figure 3.35 Borehole data of log of boring number H49.

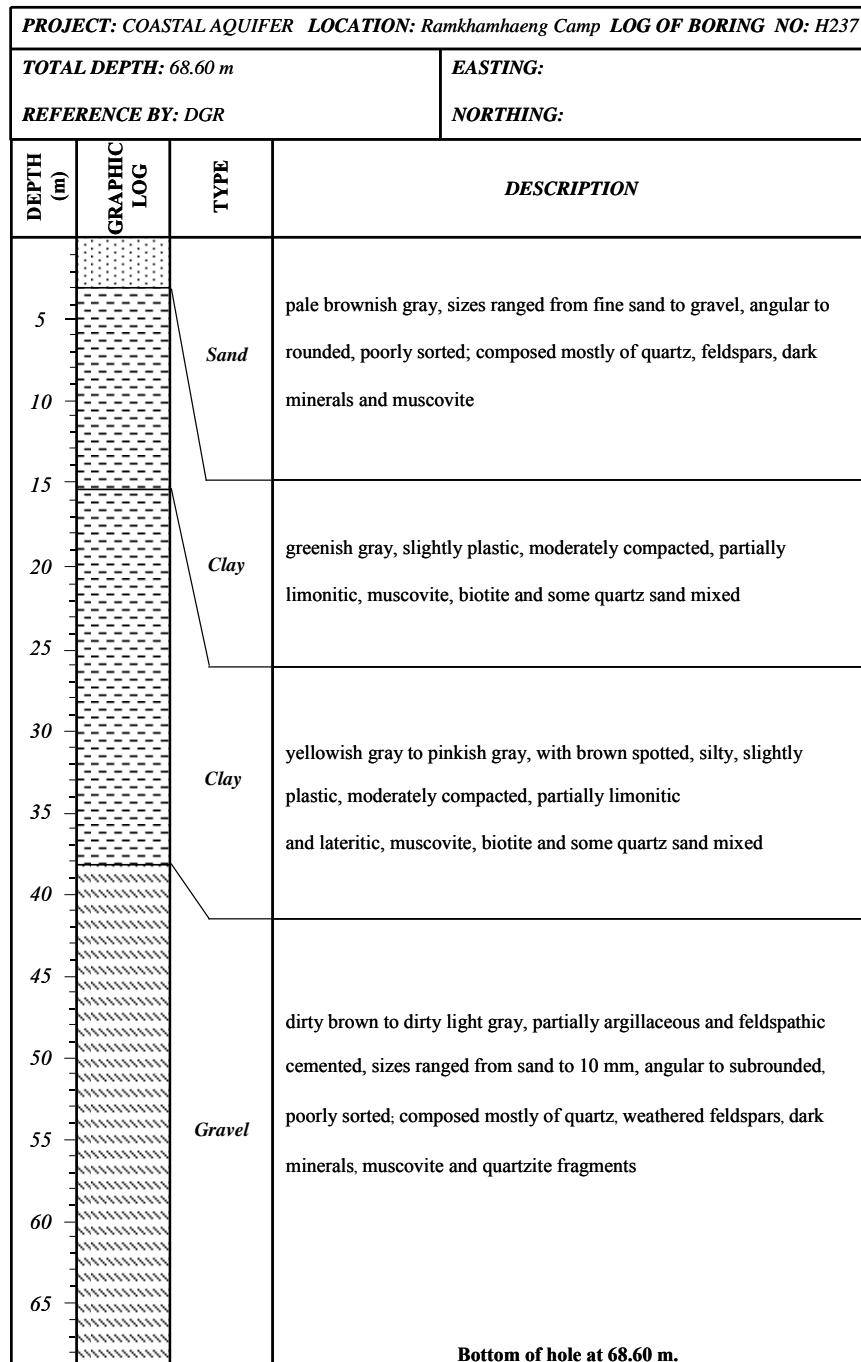


Figure 3.36 Borehole data of log of boring number H237.

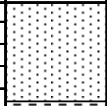
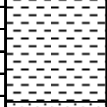
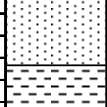
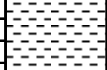
PROJECT: COASTAL AQUIFER LOCATION: Woranari Chaloem Sch. LOG OF BORING NO: H186			
TOTAL DEPTH: 15.24 m		EASTING: 676294	
REFERENCE BY: DGR		NORTHING: 796586	
DEPTH (m)	GRAPHIC LOG	TYPE	DESCRIPTION
5		<i>Sand</i>	whitish gray, sizes ranged from silt to fine sand, rather good sorting; composed mostly of quartz, feldspar and dark mineral
10		<i>Clay</i>	dirty gray, sandy, very slightly plastic, partially compacted; composed mostly of quartz, feldspar, dark minerals and fragments of shell
15		<i>Sand</i>	gray to dirty brown, sizes ranged from fine sand to coarse sand; composed mostly of quartz and fragment of shell, medium
		<i>Clay</i>	dirty brown, sandy, slightly plastic, rather compacted, limonitic Bottom of hole at 15.24 m.

Figure 3.37 Borehole data of log of boring number H186.

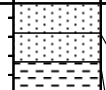
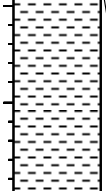
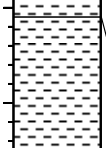
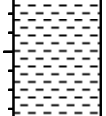
PROJECT: COASTAL AQUIFER LOCATION: Songkhla Vocational LOG OF BORING NO: H0043 <i>Education College</i>			
TOTAL DEPTH: 28.9 m		EASTING: 676250	
REFERENCE BY: DGR		NORTHING: 795550	
DEPTH (m)	GRAPHIC LOG	TYPE	DESCRIPTION
5		<i>Sand</i>	dark olive gray, very fine to fine sub-angular to rounded
10		<i>Sand</i>	yellowish gray, fine to very coarse, sub-angular to rounded, poorly sorted, composed of quartz of various colors; with chert fragment
15		<i>Clay</i>	dark greenish gray, silty limonitic, composed, slightly plastic; with some mica's
25		<i>Clay</i>	yellowish brown to greenish gray, sandy, limonitic, composed, non-plastic Bottom of hole at 28.96 m.

Figure 3.38 Borehole data of log of boring number H230.

Table 3.2 Borehole data show the location and screen interval.

BORING NO.	LOCATION	SCREEN INTERVAL (m)
H49	Mahavajiravudh School	6–12
TH405	Songkhla Provincial Administration Organization	18–22, 26–28
H186	Woranari Chaloem School	6–12
H43	Songkhla Vocational Education College	16.5–25.5
H230	Ramkhamhaeng Camp	3–6
H237	Ramkhamhaeng Camp	12–42
H1383	Songkhla Rajanagarindra Psychiatric Hospital	6–12
H1502*	Songkhla Provincial Administration Organization	12–16
H1503*	Wichianchom School	25–28
H1504*	3 rd Naval Police Regiment	32–40
H1505*	Songkhla Vocational Education College	48–52
H1506*	Phathammarong Museum	8–12
H1507*	Songkhla Provincial Agriculture Office	12–16
H1780*	no location available	92–106
TH201*	no location available	18–26
TH202*	no location available	19–27
TH203*	Songkhla Naval Base	44–50
TH204*	Songkhla Naval Base	41–45
TH261*	Miniciple 4 School	40–48
TH262*	Miniciple 4 School	12–20, 26–32
TH263*	no location available	28–32
TH280*	no location available	8–22.5
TH281*	no location available	40–44
TH318*	Woranari Chaloem School	8–16
H44*	Songkhla Rajanagarindra Psychiatric Hospital	15–22.5

* Borehole has only screen interval but no lithology data.

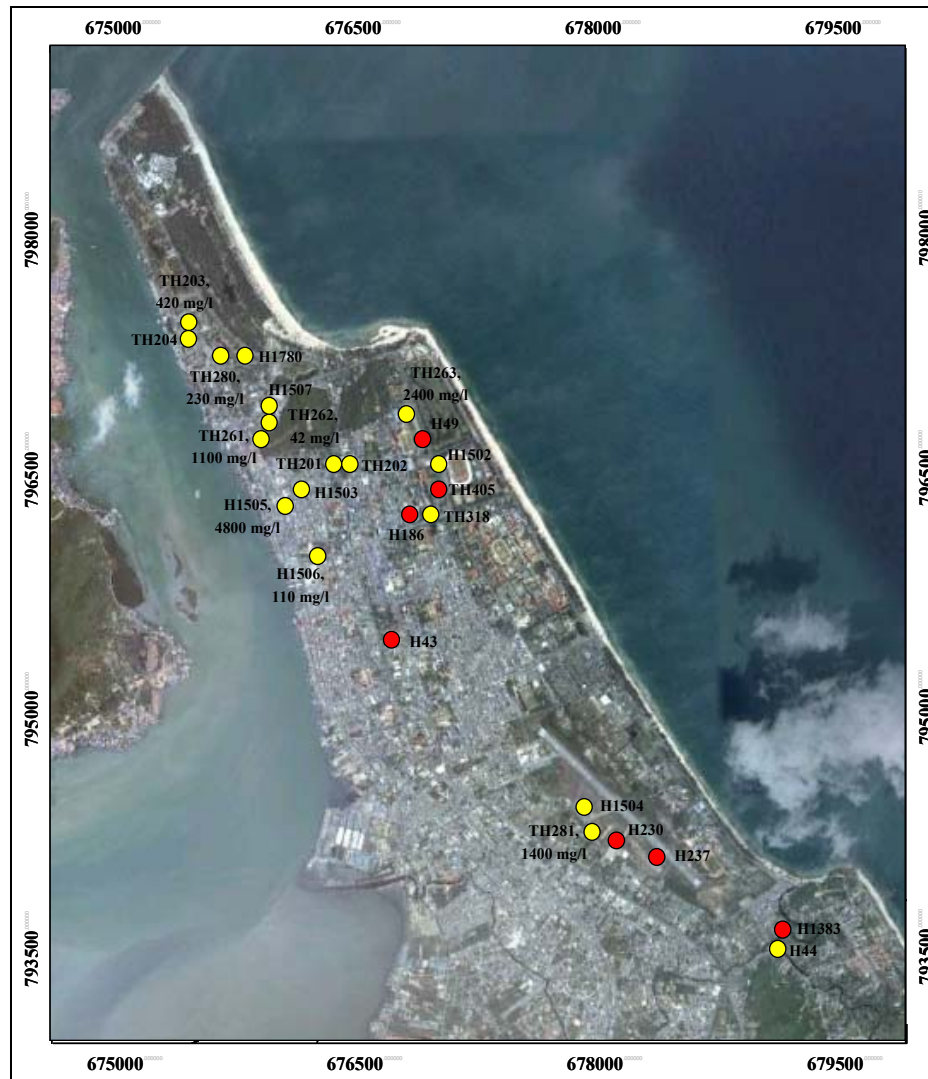


Figure 3.39 Location and chloride distribution of borehole in the study area (red points) shows the location of borehole have a lithology log (yellow points) shows the location of borehole not have lithology log (base map from GoogleEarth).

Borehole data show the location and screen interval (Table 3.2) of all borehole data in the study area for support the interpretation of geophysics surveys. Figure 3.39 shows the location and chloride distribution of borehole in the study area, (red points) shows the location of borehole has a lithology log, (yellow points) shows the location of borehole no lithology log. The chemical analysis of chloride concentrations groundwater samples of each borehole (DGR, 1970) are used to support the saline water intrusion in the groundwater system.

CHAPTER 4

DISCUSSION AND CONCLUSION

4.1 Geophysical investigations in a city

The study area is mainly located in the city with housing and traffic. A main problem was the limitation of the space and length with access to the subsurface, which was needed for the geophysical investigations. Therefore, survey lines were mostly in the football field of schools, in the stadium and at the nearby beach. Another area was the military airfield, where with the permission of the Royal Thai Army, Navy, and Airforce, geophysical investigation could be carried out. Another main problem was seismic noise due to road traffic and starting and landing low-flying helicopters. The last one triggered automatic stacking during a seismic survey. The effect of the road related noise on the seismic survey was minimized by an increased number of stacks, up to 20.

4.2 Data integration for specific sites

SK01 site

The survey line in SK01 site was placed perpendicular to the coast. The correlation between seismic refraction data (Figure 4.1a) and VES data (Figure 4.1b) can characterize three layers of the subsurface. The first layer interpreted to be loose sand. The second layer interpreted to be sand and the third layer is clay.

The integrated interpretation of the seismic reflection, seismic refraction (Figure 4.1c) and VES data (Figure 4.1 d) can characterize the subsurface structure and saline intrusion in this site. The near surface layer is loose sand has a depth less than 2 m. The second layer is sand has a depth between 2 m to 8 m, this layer is the first aquifer that can be confirmed by the screen interval from the borehole data near this site, well number H230 (3–6 m). The quality of the groundwater within the first aquifer was identified to be intermediate freshwater. The third layer is thick clay has a depth between 8 m to 30 m. The fourth layer is sand (water saturated) has a depth between 30 m to 40 m, this layer is the second aquifer that can be confirmed by

the screen interval from the borehole data near this site, well number H1504 (32–40 m). The quality of the groundwater within the second aquifer was identified to be brackish water.

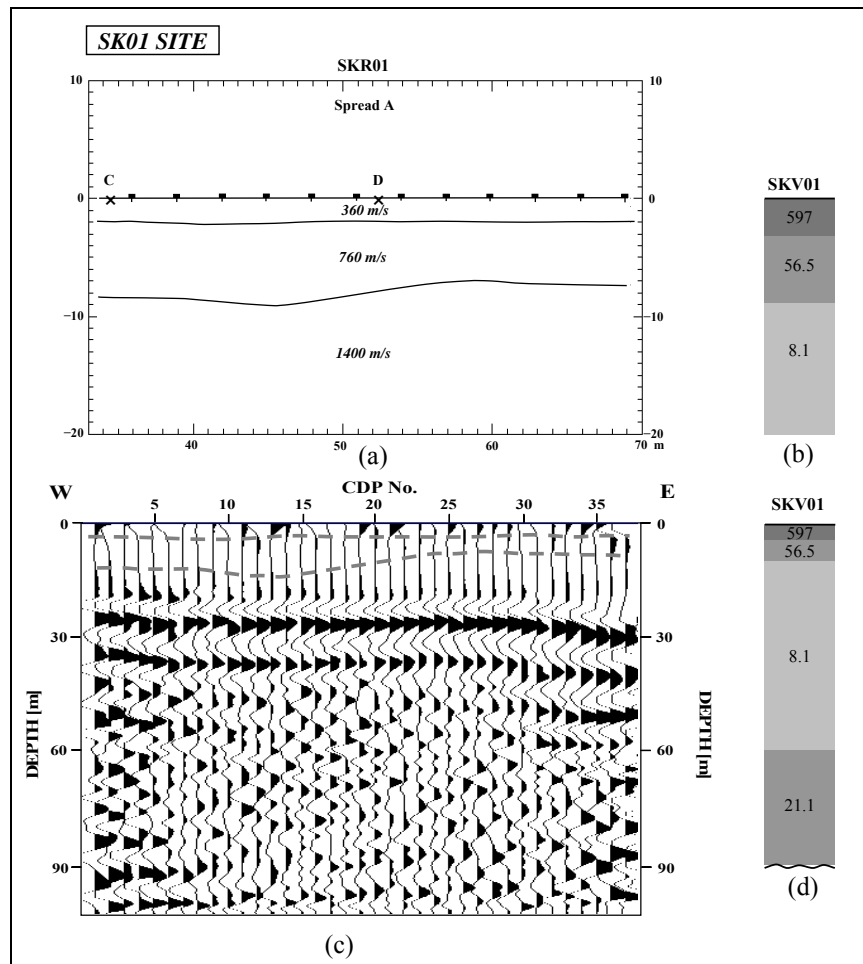


Figure 4.1 Correlation between (a) seismic refraction data (b) VES data and (c) integrated interpretation of seismic reflection and seismic refraction of SK01 site.

SK02 site

The survey line in SK02 site was placed parallel to the coast and has borehole data from well number H49. The correlation between seismic refraction data (Figure 4.2a), VES data (Figure 4.2b) and borehole data (Figure 4.2c) found to be correlated with the seismic refraction, can characterize three layers of the subsurface. The first layer is loose sand. The second layer is sand/clay and the third layer is clay.

The integrated interpretation of seismic reflection and seismic refraction (Figure 4.2d) in comparison with VES (Figure 4.2e) and borehole data (Figure 4.2 f) can characterize the subsurface structure and saline intrusion in this site. The near surface layer is loose sand has a depth of less than 4 m. The second layer is sand and has a depth between 4 m to 12 m; this layer is the first aquifer that can be confirmed by the screen interval from the borehole data at this site with well number H49 (6–12 m). The quality of the groundwater within the first aquifer was identified to be poor quality freshwater. The third layer is thick clay has a depth between 12 m to 40 m.

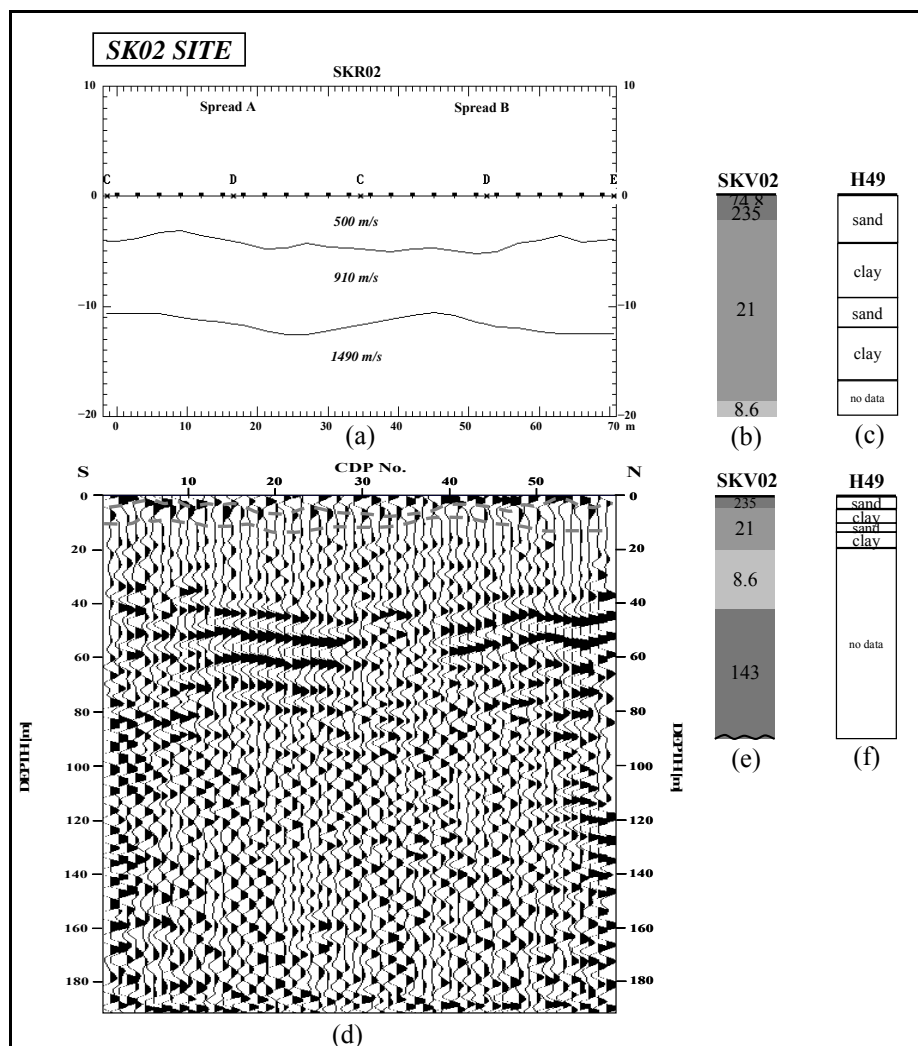


Figure 4.2 Correlation between (a) seismic refraction data (b) VES data and (c) integrated interpretation of seismic reflection and seismic refraction of SK02 site.

SK03 site

The survey line in SK03 site was placed parallel to the coast. The correlation between seismic refraction data (Figure 4.3a) and VES data (Figure 4.3b), which found to correlate to the seismic refraction, can be characterized as three layers of the subsurface. The first layer is beach sand or loose sand, the second layer is sand, and the third layer is clay.

The integrated interpretation of seismic reflection, seismic refraction (Figure 4.3c) and VES data (Figure 4.3 d) can characterize the subsurface structure and saline intrusion at this site. The near surface layer is beach sand or loose sand has a depth of less than 2 m. The second layer is sand and has a depth between 2 m to 8 m, this layer is the first aquifer, which can be confirmed by the screen interval from the borehole data near this site, well number H230 (3–6 m). The quality of the groundwater within the first aquifer can be identified to be intermediate quality freshwater. The third layer is thick clay and has a depth between 8 m to 30 m. The fourth layer is sand (water saturated) and has a depth between 30 m to 50 m; this layer is the second aquifer that can be confirmed by the screen interval of the borehole data near this site from well number H1504 (32–40 m) and TH281 (40–44 m). The quality of the groundwater within the second aquifer was identified to be very good quality freshwater.

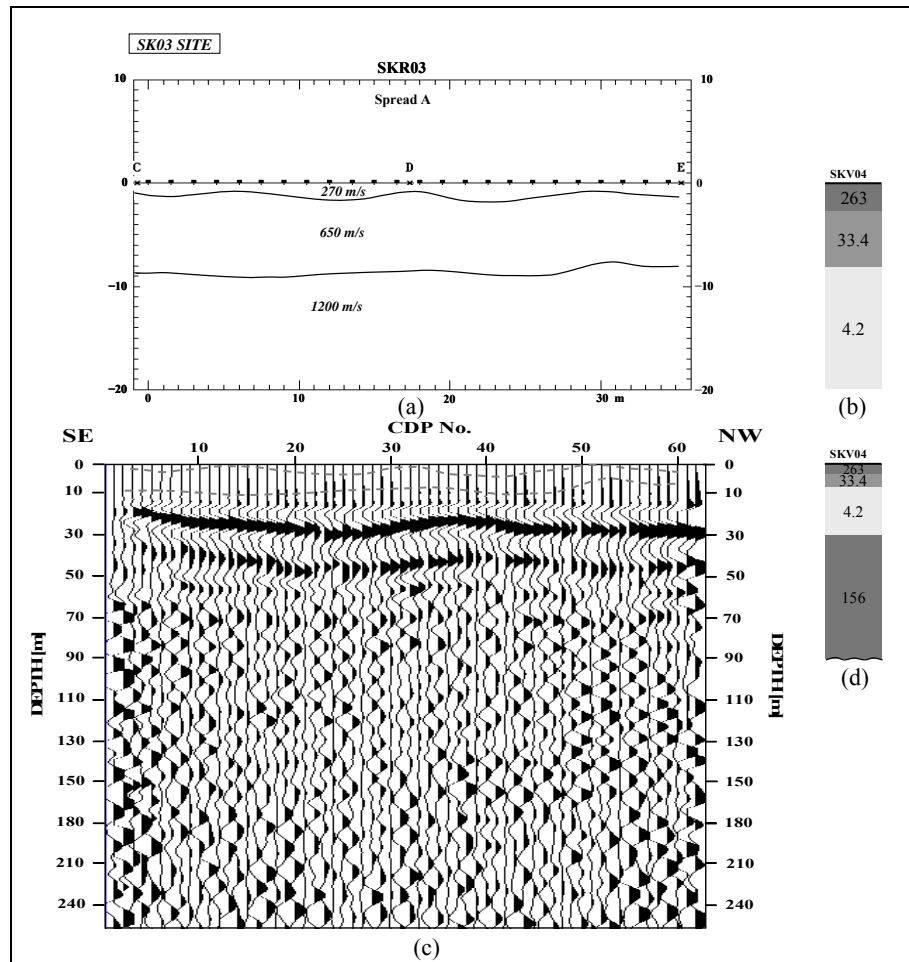


Figure 4.3 Correlation between (a) seismic refraction data (b) VES data and (c) integrated interpretation of seismic reflection and seismic refraction of SK03 site.

SK04 site

The survey line in SK04 site was placed perpendicular to the coast. In this site there is only one seismic reflection survey. The seismic reflection can be characterized by three layers of the subsurface. The first layer is apparently sand at a depth of about 40 m. The second layer is apparently clay at depth of about 80 m. The third layer may be sand, at depth of about 120 m.

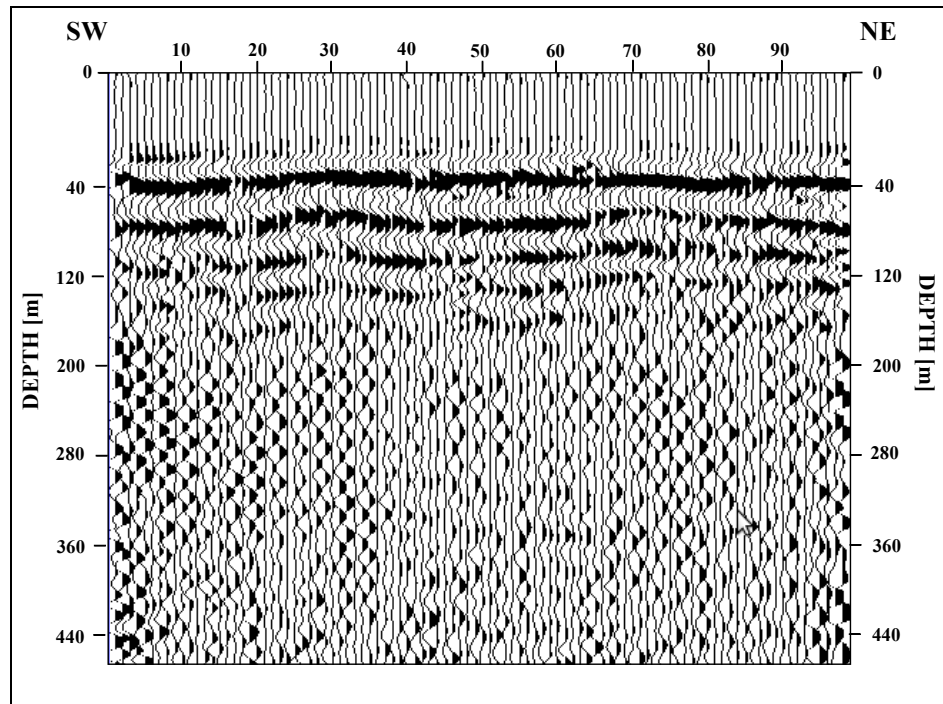


Figure 4.4 Seismic section of survey line SKL04.

SK05 site

The survey line in SK05 site was placed perpendicular to the coast and has borehole data from well number TH405. A correlation between seismic reflection data (Figure 4.5a), VES data (Figure 4.5b) and borehole data (Figure 4.5c) showed a good correlation with the VES in order to characterize the layers of the subsurface.

The integrated interpretation of seismic reflection and VES data can characterize the subsurface structure and saline intrusion at this site. The near surface layer is sand has a depth of less than 4 m. The second layer is sand has a depth between 4 m to 10 m; this layer is the first aquifer. The quality of the groundwater within the first aquifer was identified to be very good quality freshwater. The third layer is thick clay has a depth between 10 m to 30 m. The fourth layer is sand (water saturated) has a depth between 30 m to 50 m; this layer is the second aquifer. The quality of the groundwater within the second aquifer was identified to be very brackish water.

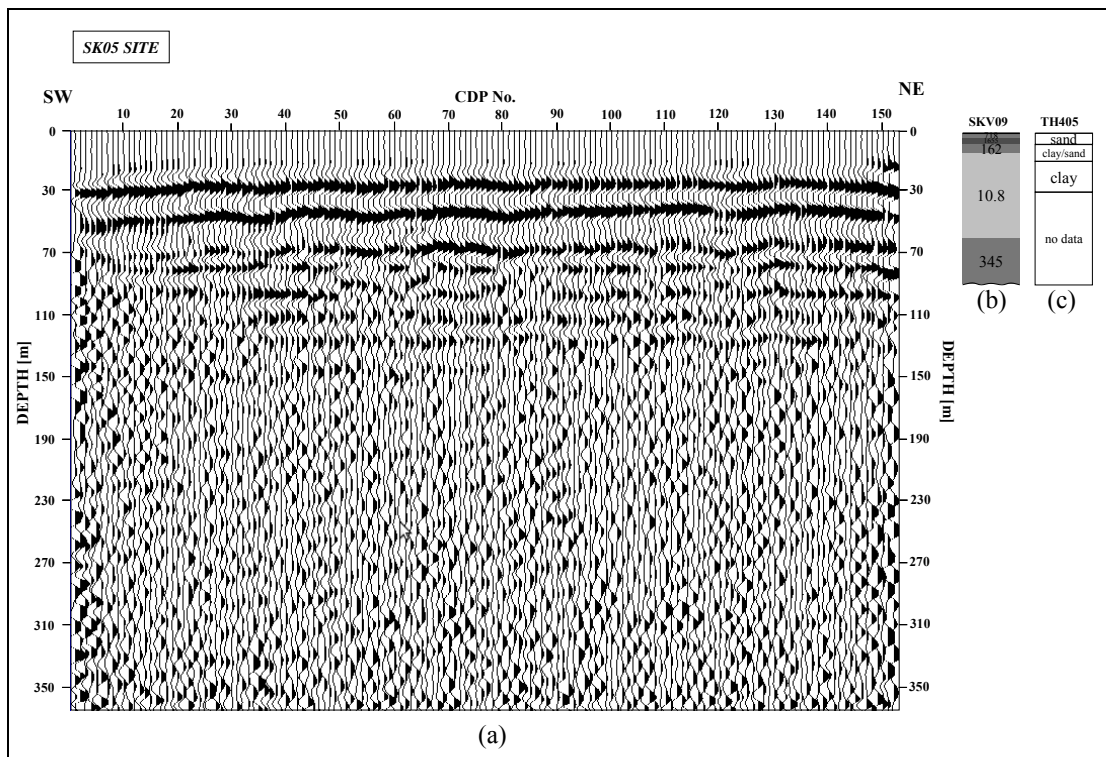


Figure 4.5 Correlation between (a) seismic reflection data (b) VES data and (c) borehole data of log of boring number TH405 of SK05 site.

SK06 site

The survey line in SK06 site was placed perpendicular to the coast near the Mermaid statue. The correlation between seismic refraction data (Figure 4.6a), and seismic reflection data (Figure 4.6b) can characterize the subsurface structure. The near surface layer is sand and has a depth less than 3 m. The second layer is sand and has a depth between 3 m to 10 m; this layer is the first aquifer. The third layer has a higher seismic P-wave velocity; this layer was interpreted to be metamorphic rock because hornfels was found in outcrops less than 100 m from the survey site.

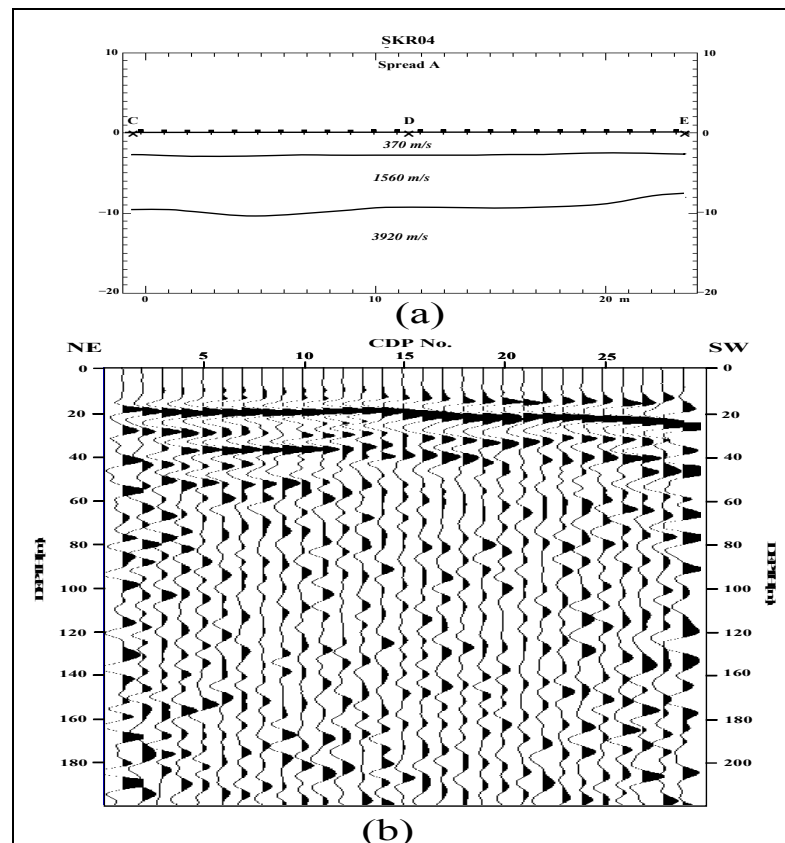


Figure 4.6 Correlation between (a) seismic refraction data (b) seismic reflection data of SK06 site.

4.3 Hydrogeological model of Bo Yang area

Three resistivity cross sections were derived from 12 VES stations. Figure 4.7 shows the resistivity cross section of the study area placed perpendicular to the coast along a southwest-northeast direction; the section shows four zones of resistivity. Near surface reveals the range of extension of a high resistivity layer (263 to 4,794 ohm-m) at a depth range from 0 to 4 m, which is interpreted to represent dry sand, beach sand. This interpretation is supported by lithological data from the well number H237. The second have the range of moderate resistivity layer (33 to 95 ohm-m) at a depth range from 4 to 13 m. Such resistivity values could be indicative of the presence of sandy layers with freshwater. This interpretation is supported by the seismic refraction result and the screen interval and lithological data from the well number H230. The third has the range of low resistivity layers (4 to 6 ohm-m) at a depth range from 13 to 40 m. These resistivity values could be indicative of the

presence of saline clay. This interpretation is supported by the lithological data from the log of boring number H230 and the chemical analysis of the groundwater samples of the borehole H1504 (DGR, 1970) was found to contain chloride concentrations at 1,400 mg/l.

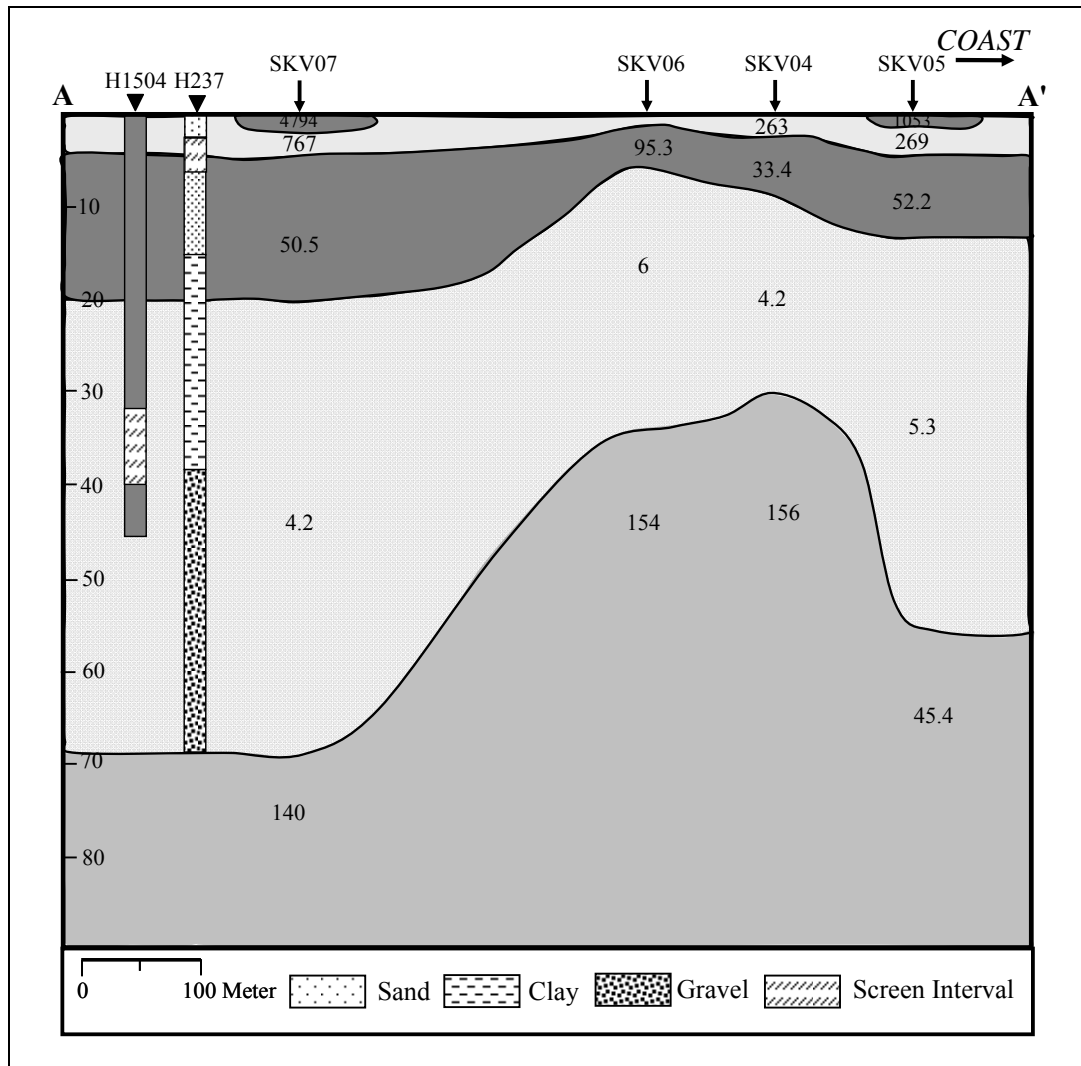


Figure 4.7 Resistivity cross section of the study area placed perpendicular to the coast along a southwest-northeast direction.

Figure 4.8 shows the resistivity cross section of the study area placed perpendicular to the coast along a southwest-northeast direction; the section shows four zones of resistivity. Near surface reveals the range of extension of a high resistivity layer (162 to 795 ohm-m) at a depth range from 0 to 4 m, which is

interpreted to represent dry sand, or beach sand. This interpretation is supported by lithological data from the well number TH405. The second has a range of moderate resistivity layers (21 to 50 ohm-m) at a depth range from 4 to 15 m. Such resistivity values could be indicative for the presence of sandy layers with freshwater. This interpretation is supported by the seismic refraction result and the screen interval of lithological data from the borehole number H49. The third has the range of low resistivity layers (4 to 11 ohm-m) at a depth range from 15 to 40 m, whose thickness increases toward the northeast. These resistivity values could be indicative of the presence of saline clay. This interpretation is supported by the lithological data from the well number TH405 and the chemical analysis of the groundwater samples of the log of boring number TH263 (DGR, 1970) was found to contain chloride concentrations at 2,400 mg/l.

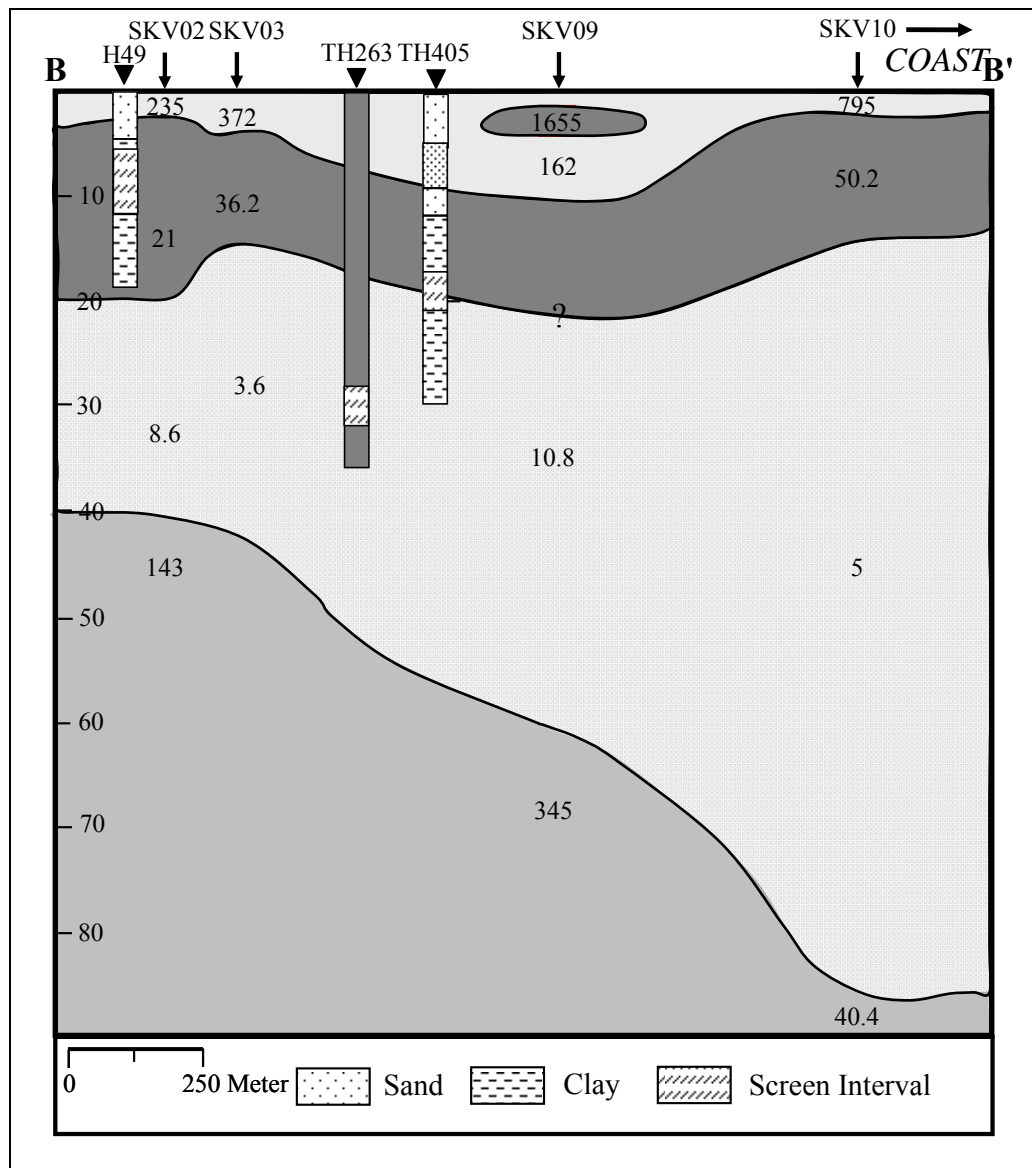


Figure 4.8 Resistivity cross section of the study area placed perpendicular to the coast along a southwest-northeast direction.

Figure 4.9 shows the resistivity cross section of the study area placed parallel to the coast along a southeast-northwest direction; the section shows four zones of resistivity. Near surface reveals the range of extension of a high resistivity layer (235 to 597 ohm-m) at a depth range from 0 to 2 m and very high resistivity layer (2,168 to 4,547 ohm-m) at the northwest end (SKV11, SKV12), which is interpreted to represent dry sand or beach sand. The second has a range of moderate resistivity layer (21 to 162 ohm-m) at a depth range from 2 to 10 m. Such resistivity

values could be indicative for the presence of sandy layers saturated with freshwater. The third has a range of low resistivity layers (4 to 11 ohm-m) and very low resistivity (1.8 to 2.5 ohm-m) at northwest end (SKV08, SKV12), whose thickness increases towards the northwest direction. These resistivity cross sections show saline water intrusion in deep layer at the northwest area of the profile and the thickness decreases towards the southeast.

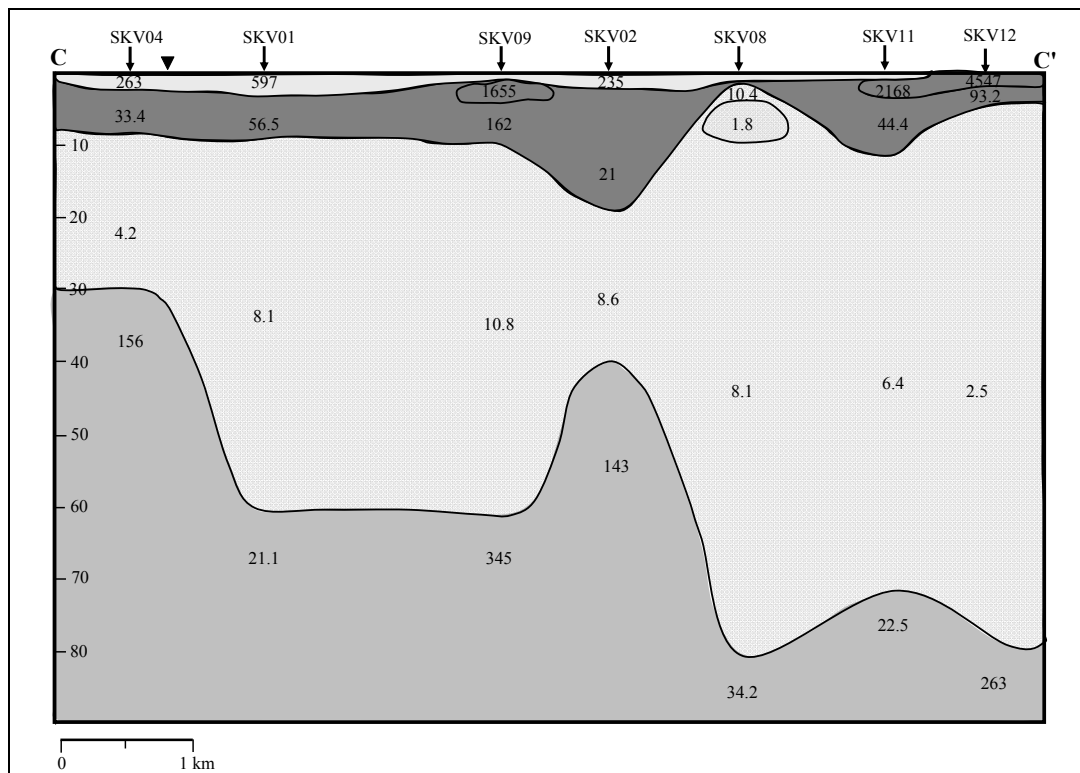


Figure 4.9 Resistivity cross section of the study area placed parallel to the coast along a southeast-northwest direction.

4.4 Conclusions

Saline water intrusion into aquifers of the coastal area in Bo Yang, Songkhla, has resulted in environmental problems. The objective of this study is the characterization of the coastal aquifer by using shallow seismic methods in order to characterize the subsurface structures and using VES to characterize aquifers and identify saline water intrusions in the fresh groundwater.

In this study area, the near surface first aquifer could not be mapped by the seismic reflection method because of channel limitations; therefore seismic

refraction method was used to characterize the first aquifer. The second and third aquifer was characterized by seismic reflection method.

The aquifer of Bo Yang district in Songkhla Province can be divided into three aquifers: (a) The first aquifer has a depth between 2–10 m. It is an unconfined aquifer (sand type), the very low velocity near surface layer indicates beach sand (dry, loose). The quality of groundwater within the first aquifer was identifying to be intermediate to good quality fresh water; (b) The second aquifer has a depth between 30–40 m. It is a confined aquifer (sand, clay type), the first and second aquifer separated by the thick clay layer, which shows the intrusion of saline water. The quality of groundwater within the second aquifer was identifying to be brackish water; (c) The third aquifer has a depth between 50–70 m. It is a confined aquifer (sand, clay type). The quality of the groundwater within the third aquifer was identified to be freshwater, brackish, and saline water.

BIBLIOGRAPHY

- Al-Amri, A.M. 1998. The application of geoelectrical vertical soundings in delineating the hydrostratigraphy of the southern Red Sea coastal area, Saudi Arabia. *Journal of King Abdulaziz University, Earth Sciences*. Vol 10: 73-90.
- Baker, G.S. 1999. *Processing near-surface seismic-reflection data: A primer*. Society of Exploration Geophysicists. United States of America.
- Baker, G.S., Schmeissner, C., Steeples, D.W. and Plumb, R.G. 1999. Seismic reflections from depths of less than two meters. *Journal of Applied Geophysics*. Vol 26. No. B2: 279-282.
- Bear, J., Cheng, A.H.-D., Sorek, S., Ouazar, D., and Herrera, I. 1999. *Seawater intrusion in coastal aquifers – concepts, methods and practices*. Dordrecht, The Netherlands, Kluwer Academic Publishers. 625 p.
- Boyd, M.T., 2003. *Introduction to geophysics exploration, USA*: Colorado School of Mines.
- Burger, H.R. 1992. *Exploration geophysics of the shallow subsurface*. Prentice-Hall Inc. New Jersey. 489 p.
- Choudhury, K., Saha, D. and Chakraborty, P. 2001. Geophysical study for saline water intrusion in a coastal alluvial terrain. *Journal of Applied Geophysics*. Vol 46: 189-200.
- Ela, Wendell P., *Introduction to Environmental Engineering and Science*, Prentice Hall, 3rd ed. 2007
- Henley, D.C., Hall, K., Bland, H., Gallant, E. and Margrave, G. 2007. “High-effort” Seismic acquisition: improving image detail, 2007 CSEG national convention.
- Kearey, P. and Brooks, M. 2002. *An introduction to geophysical exploration*. 3rd Edition. Blackwell Science.

- Krebes, E.S. 1989. Geophysical data processing: Geophysics 557. Course notes. Calgary University.
- Kutrubes, D., Zhang, J. and Hager. 2002. Conventional processing techniques and nonlinear refraction travelttime tomography for imaging bedrock at an Eastern Massachusetts Coastal Site. GeoTomo. LLC. Louisiville. CO 80027.
- Miller, P.T., McGeary, S. and Madsen, J.A. 1996. High resolution seismic reflection images of New Jersey coastal aquifers. Journal of Environmental and Engineering Geophysics. Vol 1: 55-66.
- Nowroozi, A.A., Horrocks, S.B. and Henderson, P. 1999. Saltwater intrusion into the freshwater aquifer in the eastern shore of Virginia: a reconnaissance electrical resistivity survey. Journal of Applied Geophysics. Vol 42: 1-22.
- Parasnis, D.S. 1997. Principles of applied geophysics. 5th Edition. Chapman & Hall. 429 p.
- Samsudin, A.R., Haryono, A., Hamzah, U. and Rafek, A.G. 2008. Salinity mapping of coastal groundwater aquifers using hydrogeochemical and geophysical methods: a case study from north Kelantan, Malaysia. Environmental Geology. Vol 55: 1734-1743.
- Sheriff, R.E. 1991. Encyclopedic dictionary of exploration geophysics. 3rd Edition. SEG Geophysical References Series 1. Tulsa. USA. 384 p.
- Sheriff, R.E. and Geldart, L.P. 1995. Exploration seismology. 2nd Edition. Cambridge University Press. New York. USA. 592 p.
- Shtivelman, V. 2001. Shallow water seismic surveys for site investigation in the Haifa Port Extension area, Israel. Journal of Applied Geophysics. Vol 46: 143-158.
- Shtivelman, V. and Goldman, M. 2000. Integration of shallow reflection seismics and time domain electromagnetics for detailed study of the coastal aquifer in the Nitzanim area of Israel. Journal of Applied Geophysics. Vol 44: 197-215.

- Sikandar, P., Bakhsh, A., Arshad, M. and Rana, T. 2010. The use of vertical electrical sounding resistivity method for the location of low salinity groundwater for irrigation in Chaj and Rachna Doabs. *Environmental Earth Sciences*. Vol 60: 1113-1129.
- Sjögren, B. 1984. *Shallow refraction seismic*. Chapman & Hall. London.
- Steeple, D. and Miller, R. 1990, Seismic reflection methods applied to engineering, environmental, and groundwater problems: in *Society of Exploration Geophysics Investigations in Geophysics*. Geotechnical and Environmental Geophysics. Vol 1: 1-30.
- Stone, G.D. 1994. *Designing seismic surveys in two and three dimensions*. Society of Exploration Geophysics. United States of America.
- Telford, W.M. Geldart, L.P., Sheriff, R.E. and Keys, D.A. 1990. *Applied geophysics*. 2nd Edition. Cambridge University Press. Cambridge. 770 p.
- Treadway, J.A., Steeples, D.W. and Miller, R.D. 1988. Shallow seismic study of a fault scarp near Borah Peak, Idaho. *Journal of Applied Geophysics*. Vol 93. No. B6: 6325-6337.
- Urish, D.W. and Frohlich, R.K. 1990. Surface electrical resistivity in coastal groundwater exploration. *Geoexploration*. Vol 26: 267-289.
- Yilmaz, O. 1987. *Seismic data processing*. Society of Exploration Geophysicists.
- Zohdy, A., Martin, P. and Bisdorf, R.A. 1993. A study of seawater intrusion using direct-current sounding in the southeastern part of the Oxnard plain, California. U.S. Geological Survey. 139 p.
- Zouhri, L., Carlier, E., Kabbour, B.B., Toto, E.A., Gorini, C. and Louche, B. 2008. Groundwater interaction in the coastal environment: hydrochemical, electrical and seismic approaches. *Bull. Eng. Geol. Environ.* Vol 67: 123-128.

APPENDIX

APPENDICES A
RESISTIVITY FIELD DATA

Survey no. SKV01		Location Wachiranukul School			Date 5/07/51			
Line no. 1		Operator Aeow			Time 17:30			
Electrode spacing in meters		TERRAMETER Reading in Ohms		K	Calculated Apparent Res. in Ohm-Meters			Comments
$C_1C_2/2$ (AB/2)	$P_1P_2/2$ (MN/2)	R_1	R_2		ρ_{a1}	ρ_{a2}	$\rho_{a(avg.)}$	
1.5	0.5	97.417		6.3	613.727			
2.0	0.5	46.762		11.8	551.792			
3.0	0.5	18.915		27.5	520.163			
4.5	0.5	6.179		62.8	388.035			
7.0	0.5	1.662		153.2	254.542			
7.0	2.0	8.067		35.3	284.751			
10.0	0.5	0.360		313.4	112.887			
10.0	2.0	1.542		75.4	116.259			
15.0	2.0	0.265		173.6	45.943			
20.0	2.0	0.080		311.0	24.853			
20.0	6.0	0.231		95.3	21.982			
30.0	6.0	0.052		226.2	11.852			
45.0	6.0	0.017		520.7	8.992			
45.0	10.0	0.033		302.4	9.894			
60.0	10.0	0.016		549.8	8.765			
60.0	20.0	0.039		251.3	9.679			
100.0	20.0	0.015		754.0	11.234			
100.0	30.0	0.023		476.5	10.826			

Survey no. SKV02		Location Mahavajiravudh School			Date 23/10/51			
Line no. 1		Operator AEOW			Time			
Electrode spacing in meters		TERRAMETER Reading in Ohms		K	Calculated Apparent Res. in Ohm-Meters			Comments
$C_1C_2/2$ (AB/2)	$P_1P_2/2$ (MN/2)	R_1	R_2		ρ_{a1}	ρ_{a2}	$\rho_{a(avg.)}$	
1.5	0.5	14.176		6.3	89.309			
2.0	0.5	7.976		11.8	94.113			
3.0	0.5	3.869		27.5	106.387			
4.5	0.5	1.417		62.8	88.994			
7.0	0.5	0.356		153.2	54.570			
7.0	2.0	1.640		35.3	57.903			
10.0	0.5	0.122		313.4	38.182			
10.0	2.0	0.545		75.4	41.101			
15.0	2.0	0.136		173.6	23.686			
20.0	2.0	0.068		311.0	21.121			
20.0	6.0	0.341		95.3	32.477			
30.0	6.0	0.157		226.2	35.482			
45.0	6.0	0.033		520.7	17.038			
45.0	10.0	0.057		302.4	17.371			
60.0	10.0	0.034		549.8	18.693			
60.0	20.0	0.097		251.3	24.365			
80.0	20.0	0.055		471.2	25.785			

Survey no. SKV03		Location Mahavajiravudh School			Date 23/10/51			
Line no. 2		Operator AEOW			Time			
Electrode spacing in meters		TERRAMETER Reading in Ohms		K	Calculated Apparent Res. in Ohm-Meters			Comments
$C_1C_2/2$ (AB/2)	$P_1P_2/2$ (MN/2)	R_1	R_2		ρ_{a1}	ρ_{a2}	$\rho_{a(avg.)}$	
1.0	0.5	37.066		2.4	88.958			
1.5	0.5	20.830		6.3	131.229			
2.0	0.5	13.445		11.8	158.651			
3.0	0.5	6.978		27.5	191.903			
4.5	0.5	3.477		62.8	218.381			
7.0	0.5	1.356		153.2	207.709			
7.0	2.0	5.345		35.3	188.668			
10.0	0.5	0.513		313.4	160.702			
10.0	2.0	1.979		75.4	149.217			
15.0	2.0	0.493		173.6	85.653			
20.0	2.0	0.188		311.0	58.596			
20.0	6.0	0.655		95.3	62.426			
30.0	6.0	0.127		226.2	28.680			
44.0	6.0	0.016		497.4	7.939			

Survey no. SKV04		Location Chalatat Road			Date 18/01/52			
Line no. 1		Operator AEOW			Time 14:00			
Electrode spacing in meters		TERRAMETER Reading in Ohms		K	Calculated Apparent Res. in Ohm-Meters			Comments
$C_1C_2/2$ (AB/2)	$P_1P_2/2$ (MN/2)	R_1	R_2		ρ_{a1}	ρ_{a2}	$\rho_{a(avg.)}$	
1.5	0.5	39.479	37.273	6.3	248.718	234.820		
2.0	0.5	20.009	19.824	11.8	236.106	233.923		
3.0	0.5	7.937	7.532	27.5	218.276	207.125		
4.5	0.5	3.934	3.691	62.8	247.074	231.782		
7.0	0.5	0.552	0.524	153.2	84.525	80.349		
7.0	2.0	2.802	2.721	35.3	98.896	96.051		
10.0	0.5	0.153	0.137	313.4	48.029	42.873		
10.0	2.0	0.626	0.641	75.4	47.233	48.353		
15.0	2.0	0.045	0.046	173.6	7.765	8.056		
20.0	2.0	0.034	0.036	311.0	10.709	11.169		
20.0	6.0	0.101	0.123	95.3	9.594	11.695		
30.0	6.0	0.025	0.120	226.2	5.748	27.124		
45.0	6.0	0.012	0.010	520.7	6.154	5.460		
45.0	10.0	0.017	0.016	302.4	5.131	4.866		
60.0	10.0	0.024	0.025	549.8	12.986	13.970		
60.0	20.0	0.040	0.050	251.3	9.951	12.544		
100.0	20.0	0.050	0.057	754.0	37.807	42.627		
100.0	30.0	0.059	0.058	476.5	28.269	27.789		
150.0	30.0	0.047	0.048	1131.0	53.591	54.389		
150.0	50.0	0.071	0.071	628.3	44.895	44.435		
200.0	50.0	0.102	0.102	1178.1	120.166	120.084		
200.0	50.0	0.058	0.058	1178.1	68.860	68.655		
250.0	50.0	0.044	0.044	1885.0	82.190	82.071		

Survey no. SKV05		Location Chalatat Road			Date 18/01/52			
Line no. 2		Operator AEOW			Time			
Electrode spacing in meters		TERRAMETER Reading in Ohms		K	Calculated Apparent Res. in Ohm-Meters			Comments
$C_1C_2/2$ (AB/2)	$P_1P_2/2$ (MN/2)	R_1	R_2		ρ_{a1}	ρ_{a2}	$\rho_{a(avg.)}$	
1.5	0.5	137.810		6.3	868.203			
2.0	0.5	66.668		11.8	786.682			
3.0	0.5	18.731		27.5	515.103			
4.5	0.5	5.480		62.8	344.125			
7.0	0.5	1.160		153.2	177.727			
7.0	2.0	5.559		35.3	196.215			
10.0	0.5	0.398		313.4	124.833			
10.0	2.0	1.556		75.4	117.300			
15.0	2.0	0.291		173.6	50.492			
20.0	2.0	0.110		311.0	34.260			
20.0	6.0	0.450		95.3	42.911			
30.0	6.0	0.071		226.2	16.163			
45.0	6.0	0.016		520.7	8.235			
45.0	10.0	0.021		302.4	6.281			
60.0	10.0	0.021		549.8	11.757			
60.0	20.0	0.021		251.3	5.373			
100.0	20.0	0.017		754.0	12.477			
100.0	30.0	0.016		476.5	7.472			
150.0	30.0	0.025		1131.0	28.479			
150.0	50.0	0.047		628.3	29.377			
200.0	50.0	0.008		1178.1	8.915			
250.0	30.0	0.006		3225.4	19.373			

Survey no. SKV06		Location Chalatat Road			Date 18/01/52			
Line no. 3		Operator AEOW			Time			
Electrode spacing in meters		TERRAMETER Reading in Ohms		K	Calculated Apparent Res. in Ohm-Meters			Comments
$C_1C_2/2$ (AB/2)	$P_1P_2/2$ (MN/2)	R_1	R_2		ρ_{a1}	ρ_{a2}	$\rho_{a(avg.)}$	
1.5	0.5	74.718		6.3	470.723			
2.0	0.5	35.151		11.8	414.782			
3.0	0.5	12.349		27.5	339.598			
4.5	0.5	2.364		62.8	148.459			
7.0	0.5	0.629		153.2	96.423			
7.0	2.0	3.997		35.3	141.094			
10.0	0.5	0.186		313.4	58.205			
10.0	2.0	1.033		75.4	77.851			
15.0	2.0	0.142		173.6	24.655			
20.0	2.0	0.046		311.0	14.454			
20.0	6.0	0.130		95.3	12.436			
30.0	6.0	0.029		226.2	6.574			
45.0	10.0	0.057		302.4	17.265			
60.0	10.0	0.030		549.8	16.551			
60.0	20.0	0.180		251.3	45.314			
100.0	20.0	0.122		754.0	92.033			
100.0	30.0	0.181		476.5	86.280			
150.0	30.0	0.163		1131.0	183.799			
150.0	50.0	0.177		628.3	111.014			
250.0	50.0	0.022		1885.0	40.831			
280.0	30.0	0.001		4057.9	5.923			

Survey no. SKV 07		Location Air Force Naval Base			Date 09/04/09			
Line no. 1		Operator AEW			Time			
Electrode spacing in meters		TERRAMETER Reading in Ohms		K	Calculated Apparent Res. in Ohm-Meters			Comments
C ₁ C ₂ /2 (AB/2)	P ₁ P ₂ /2 (MN/2)	R ₁	R ₂		ρ_{a1}	ρ_{a2}	$\rho_{a(avg.)}$	
1.5	0.5	423.140	423.100	6.3	2665.782	2665.530		
2.0	0.5	154.130	154.160	11.8	1818.734	1819.088		
3.0	0.5	37.071	37.067	27.5	1019.453	1019.343		
4.5	0.5	10.142	10.126	62.8	636.918	635.913		
7.0	0.5	2.055	2.051	153.2	314.826	314.213		
7.0	2.0	9.576	9.459	35.3	338.033	333.903		
10.0	0.5	0.516	0.507	313.4	161.692	158.872		
10.0	2.0	2.050	2.048	75.4	154.570	154.412		
15.0	2.0	0.369	0.369	173.6	64.110	64.081		
20.0	2.0	0.154	0.158	311.0	47.885	49.070		
20.0	6.0	0.441	0.439	95.3	42.005	41.805		
30.0	6.0	0.120	0.122	226.2	27.194	27.495		
45.0	10.0	0.014	0.010	302.4	4.332	2.978		
60.0	10.0	0.004	0.001	549.8	2.129	0.750		
60.0	20.0	0.028	0.026	251.3	7.088	6.620		
90.0	20.0	0.019	0.019	604.8	11.463	11.238		
90.0	30.0	0.019	0.027	377.0	7.221	10.034		
150.0	30.0	0.045	0.046	1131.0	50.335	51.813		
150.0	50.0	0.039	0.041	628.3	24.443	25.621		
225.0	50.0	0.041	0.040	1511.9	61.992	59.968		
225.0	30.0	0.017	0.021	2603.6	43.462	55.514		
300.0	50.0	0.027	0.028	2748.9	74.333	76.312		
350.0	50.0	0.006	0.006	3769.9	23.701	23.441		
350.0	50.0	0.011	0.008	3769.9	40.986	30.596		
500.0	50.0	0.013	0.012	7775.4	99.276	93.383		
600.0	50.0	0.009	0.009	11231.2	101.182	97.683		
700.0	50.0	0.002	0.001	15315.3	25.169	21.297		
800.0	60.0	0.003	0.004	16660.9	43.452	59.629		

Survey no. SKV08		Location Samilar Beach				Date 04/10/09		
Line no. 1		Operator AEW				Time 10:18		
Electrode spacing in meters		TERRAMETER Reading in Ohms		K	Calculated Apparent Res. in Ohm-Meters			Comments
$C_1C_2/2$ (AB/2)	$P_1P_2/2$ (MN/2)	R_1	R_2		ρ_{a1}	ρ_{a2}	$\rho_{a(avg.)}$	
1.5	0.5	82.385	82.478	6.3	519.026	519.611		
2.0	0.5	21.177	21.192	11.8	249.889	250.066		
3.0	0.5	3.288	3.156	27.5	90.420	86.790		
4.5	0.5	0.254	0.254	62.8	15.951	15.951		
7.0	0.5	0.040	0.034	153.2	6.082	5.163		
7.0	2.0	0.095	0.094	35.3	3.350	3.318		
10.0	0.5	0.010	0.021	313.4	3.197	6.519		
10.0	2.0	0.038	0.037	75.4	2.880	2.812		
15.0	2.0	0.022	0.022	173.6	3.871	3.871		
20.0	2.0	0.033	0.030	311.0	10.108	9.237		
20.0	6.0	0.153	0.152	95.3	14.581	14.486		
30.0	6.0	0.064	0.064	226.2	14.499	14.567		
45.0	6.0	0.008	0.009	520.7	4.270	4.790		
45.0	10.0	0.020	0.022	302.4	5.957	6.532		
60.0	10.0	0.018	0.020	549.8	9.896	11.051		
60.0	20.0	0.016	0.014	251.3	3.971	3.418		
150.0	30.0	0.004	0.006	1131.0	4.207	6.990		
150.0	50.0	0.027	0.037	628.3	16.901	23.473		
250.0	50.0	0.011	0.013	1885.0	19.793	23.563		
350.0	30.0	0.001	0.001	6367.0	8.468	8.659		
350.0	50.0	0.005	0.005	3769.9	17.719	17.492		

Survey no. SKV09		Location Tinsulanon Stadium			Date 04/10/09			
Line no. 2		Operator AEOW			Time 15:10			
Electrode spacing in meters		TERRAMETER Reading in Ohms		K	Calculated Apparent Res. in Ohm-Meters			Comments
$C_1C_2/2$ (AB/2)	$P_1P_2/2$ (MN/2)	R_1	R_2		ρ_{a1}	ρ_{a2}	$\rho_{a(avg.)}$	
1.5	0.5	156.670		6.3	987.021			
2.0	0.5	99.896		11.8	1178.773			
3.0	0.5	44.302		27.5	1218.305			
4.5	0.5	18.953		62.8	1190.248			
7.0	0.5	5.699		153.2	873.087			
7.0	2.0	32.819		35.3	1158.511			
10.0	0.5	1.490		313.4	466.966			
10.0	2.0	8.327		75.4	627.856			
15.0	2.0	1.131		173.6	196.342			
20.0	2.0	0.026		311.0	7.993			
20.0	6.0	1.109		95.3	105.688			
30.0	6.0	0.147		226.2	33.251			
45.0	6.0	0.030		520.7	15.621			
45.0	10.0	0.051		302.4	15.422			
60.0	20.0	0.024		251.3	6.031			
60.0	20.0	0.062		251.3	15.581			
90.0	20.0	0.022		604.8	13.306			
90.0	30.0	0.046		377.0	17.342			
120.0	30.0	0.023		706.9	16.259			
150.0	50.0	0.030		628.3	18.849			

Survey no. SKV10		Location Chalatat Beach			Date 22/10/52			
Line no. 1		Operator AEW			Time			
Electrode spacing in meters		TERRAMETER Reading in Ohms		K	Calculated Apparent Res. in Ohm-Meters			Comments
$C_1C_2/2$ (AB/2)	$P_1P_2/2$ (MN/2)	R_1	R_2		ρ_{a1}	ρ_{a2}	$\rho_{a(avg.)}$	
1.5	0.5	114.050	113.990	6.3	718.515	718.137		
2.0	0.5	61.744	61.765	11.8	728.579	728.827		
3.0	0.5	23.114	23.119	27.5	635.635	635.773		
4.5	0.5	6.628	6.629	62.8	416.238	416.301		
7.0	0.5	1.172	1.171	153.2	179.550	179.397		
7.0	2.0	5.992	5.993	35.3	211.518	211.553		
10.0	0.5	0.271	0.272	313.4	84.931	85.245		
10.0	2.0	1.225	1.227	75.4	92.365	92.516		
15.0	2.0	0.261	0.261	173.6	45.310	45.310		
20.0	2.0	0.100	0.100	311.0	31.231	31.100		
20.0	6.0	0.362	0.364	95.3	34.499	34.689		
30.0	6.0	0.078	0.078	226.2	17.644	17.644		
45.0	6.0	0.020	0.019	520.7	10.414	9.893		
45.0	10.0	0.042	0.040	302.4	12.701	12.096		
60.0	10.0	0.009	0.009	549.8	5.124	5.201		
60.0	20.0	0.027	0.028	251.3	6.785	7.036		
90.0	20.0	0.012	0.012	604.8	7.258	7.258		
90.0	30.0	0.017	0.017	377.0	6.409	6.409		
150.0	30.0	0.008	0.008	1131.0	9.431	9.331		
150.0	50.0	0.011	0.013	628.3	6.911	8.168		
225.0	50.0	0.001	0.002	1511.9	1.739	2.525		
225.0	30.0	0.002	0.003	2603.6	6.092	8.488		
350.0	50.0	0.006	0.006	3769.9	24.052	22.393		
450.0	50.0	0.007	0.007	6283.2	44.208	44.611		
500.0	50.0	0.004	0.004	7775.4	31.879	30.946		

Survey no. SKV11		Location Lam Son Onn				Date 22/10/52		
Line no. 2		Operator AEW				Time 14:00		
Electrode spacing in meters		TERRAMETER Reading in Ohms		K	Calculated Apparent Res. in Ohm-Meters			Comments
$C_1C_2/2$ AB/2	$P_1P_2/2$ (MN/2)	R ₁	R ₂		ρ_{a1}	ρ_{a2}	$\rho_{a(avg.)}$	
1.5	0.5	114.460	114.460	6.3	721.098	721.098		
2.0	0.5	78.837	78.896	11.8	930.277	930.973		
3.0	0.5	39.810	39.807	27.5	1094.775	1094.693		
4.5	0.5	16.316	16.315	62.8	1024.645	1024.582		
7.0	0.5	4.361	4.364	153.2	668.075	668.534		
7.0	2.0	17.265	17.249	35.3	609.455	608.890		
10.0	0.5	1.117	1.117	313.4	350.068	350.068		
10.0	2.0	4.417	4.417	75.4	333.042	333.042		
15.0	2.0	0.372	0.372	173.6	64.579	64.579		
20.0	2.0	0.062	0.062	311.0	19.282	19.282		
20.0	6.0	0.392	0.392	95.3	37.358	37.358		
30.0	6.0	0.017	0.017	226.2	3.845	3.845		
45.0	6.0	0.011	0.011	520.7	5.728	5.728		
45.0	10.0	0.022	0.022	302.4	6.653	6.653		
60.0	10.0	0.024	0.024	549.8	13.195	13.195		
60.0	20.0	0.033	0.033	251.3	8.293	8.293		
90.0	20.0	0.025	0.025	604.8	15.120	15.120		
90.0	30.0	0.023	0.023	377.0	8.671	8.671		
150.0	30.0	0.020	0.020	1131.0	22.620	22.620		
150.0	50.0	0.031	0.028	628.3	19.477	17.592		
225.0	50.0	0.007	0.007	1511.9	9.933	9.933		
225.0	30.0	0.004	0.004	2603.6	10.258	11.690		
350.0	50.0	0.000	0.000	3769.9	1.772	1.662		
500.0	50.0	0.002	0.002	7775.4	13.475	12.999		
594.0	50.0	0.002	0.002	11006.1	17.058	17.545		

Survey no. SKV12		Location Lam Son Onn			Date 28/02/53			
Line no. 1		Operator AEW			Time 11:00			
Electrode spacing in meters		TERRAMETER Reading in Ohms		K	Calculated Apparent Res. in Ohm-Meters			Comments
$C_1C_2/2$ AB/2	$P_1P_2/2$ (MN/2)	R ₁	R ₂		ρ_{a1}	ρ_{a2}	$\rho_{a(avg.)}$	
1.3	0.5	785.000	785.890	4.5	3532.500	3536.505		
1.6	0.5	568.040	567.800	7.3	4146.692	4144.940		
2.0	0.5	288.100	290.190	11.8	3399.580	3424.242		
2.5	0.5	144.930	146.850	18.8	2724.684	2760.780		
3.2	0.5	61.603	61.525	31.4	1934.334	1931.885		
4.0	0.5	25.795	25.842	49.5	1276.853	1279.179		
5.0	0.5	7.691	7.696	77.8	598.352	598.749		
6.5	0.5	1.648	1.775	131.9	217.318	234.083		
8.0	0.5	0.414	0.418	200.3	82.876	83.735		
10.0	2.0	0.453	0.447	75.4	34.161	33.736		
13.0	2.0	0.100	0.099	129.6	12.908	12.808		
16.0	2.0	0.014	0.013	197.9	2.696	2.624		
20.0	2.0	0.008	0.007	311.0	2.389	2.280		
25.0	2.0	0.010	0.012	487.7	4.707	5.665		
32.0	2.0	0.004	0.004	801.1	3.203	3.000		
32.0	5.0	0.007	0.009	313.8	2.251	2.684		
40.0	5.0	0.023	0.025	494.8	11.341	12.200		
50.0	5.0	0.001	0.001	777.5	1.151	1.031		
65.0	5.0	0.017	0.002	1319.5	22.826	2.288		
80.0	5.0	0.002	0.001	2002.8	3.005	2.717		
100.0	5.0	0.001	0.001	3133.7	3.911	3.892		
100.0	20.0	0.004	0.004	754.0	3.065	3.198		
130.0	20.0	0.005	0.004	1295.9	6.097	5.798		
160.0	20.0	0.001	0.001	1979.2	2.963	2.913		
200.0	20.0	0.003	0.004	3110.2	10.745	11.001		
250.0	20.0	0.001	0.001	4877.3	4.892	5.108		
320.0	20.0	0.001	0.001	8011.1	8.299	9.004		
320.0	50.0	0.004	0.004	3138.5	12.972	12.409		
405.0	50.0	0.008	0.008	5074.5	40.580	40.383		
500.0	50.0	0.003	0.002	7775.4	19.447	3536.505		

PUBLICATIONS

Proceedings of the 5th Siam Physics Congress, 2010

ที่ สฟท. ว.001/2553

19 กุมภาพันธ์ 2553

เรื่อง เชิญเสนอผลงาน

เรียน Jiraporn Srattakal

ตามที่สมาคมฟิสิกส์ไทย ร่วมกับมหาวิทยาลัยเกษตรศาสตร์ มหาวิทยาลัยรามคำแหง มหาวิทยาลัยศรีนครินทรวิโรฒ สถาบันวิจัยดาราศาสตร์แห่งชาติ (องค์การมหาชน) ศูนย์ความเป็นเลิศด้านฟิสิกส์ สถาบันเทคโนโลยีนิวเคลียร์แห่งชาติ และสถาบันวิจัยแสงซินโครตรอน (องค์การมหาชน) ดำเนินการจัดการประชุมเชิงวิชาการระดับชาติ Siam Physics Congress 2010 (SPC2010) ภายใต้แนวความคิด Physics for Creative Society ในช่วงระหว่างวันที่ 25-27 มีนาคม 2553 ณ โรงแรมริเวอร์แคว วิลเลจ อำเภอไทรโยค จังหวัดกาญจนบุรี โดยท่านได้ลงทะเบียนเพื่อเข้าร่วมเสนอผลงานในการประชุมนั้น ในการนี้ทางคณะกรรมการจัดการประชุมขอตอบรับการนำเสนอผลงานของท่านในหัวข้อเรื่อง *"High resolution seismic reflection and vertical electrical sounding for detailed characterization of a coastal aquifer"* ในรูปแบบการนำเสนอแบบ Oral โดยท่านสามารถดูรายละเอียดของกำหนดการประชุมได้ที่ <http://www.thps.org/spc2010> ทั้งนี้ ในการชำระเงินค่าลงทะเบียนสามารถดำเนินการได้ตั้งแต่วันที่เริ่มต้นไป โดยท่านสามารถตรวจสอบสถานะการชำระเงินค่าลงทะเบียนได้ที่เว็บไซต์ของการประชุม

สำหรับการจัดส่งผลงานฉบับเต็มเพื่อตีพิมพ์ลงใน SPC2010 Proceedings ได้กำหนดให้มีความยาวไม่เกิน 4 หน้ากระดาษ A4 ซึ่งท่านสามารถดาวน์โหลด Manuscript Template ได้ที่ <http://www.thps.org/spc2010/download.html> โดยขอให้ท่านจัดส่งต้นฉบับจำนวน 3 ฉบับ และไฟล์ในรูปแบบของ Microsoft Word บันทึกถกลง CD (เขียนชื่อที่หน้าแผ่นให้ชัดเจน) ณ ได้ลงทะเบียนภายในเวลา 12.00 น. ของวันที่ 26 มีนาคม 2553

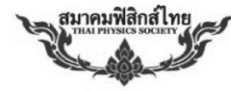
จึงเรียนมาเพื่อ โปรดทราบ

ขอแสดงความนับถือ



(ดร.ประเสริฐ สงศิริฤทธิกุล)

เลขานุการการประชุม SPC2010

สำนักงานเลขานุการ
สมาคมฟิสิกส์ไทย

ที่ตั้ง:

อาคารสุรพัฒน์ 3
ถนนมหาวิทยาลัย ตำบลสุรนารี
อำเภอเมือง จ.นครราชสีมา

ที่อยู่ไปรษณีย์:

ตู้ ป.ณ. 93
ป.ณ.จ. นครราชสีมา 30000

โทรศัพท์: 0-4421-7040

โทรสาร: 0-4421-7047

Secretariat Office
Thai Physics SocietyVisiting Address:
Suraphat 3 Building,
University Ave.,
Suranaree Subdistrict,
Muang, NakhonratchasimaPostal Address:
P.O. Box 93
Nakhonratchasima 30000
Thailand



High resolution seismic reflection and vertical electrical sounding for detailed characterization of the coastal aquifer

J. Srattakal, H. Dürrast*

Geophysics Group, Department of Physics, Faculty of Science, Prince of Songkla University, Hat Yai, Songkhla, Thailand.

In Southern Thailand with its extensive coastline villages and cities are often located near the shoreline, for example Songkhla municipality in Songkhla Province. In many areas the availability of fresh groundwater resource is limited due to the intrusion of saltwater into the coastal aquifers. Geophysical investigations comprising vertical electrical sounding (VES) and shallow seismic reflection methods have been employed in the coastal aquifers of Bo Yang district in Songkhla. The objective of the surveys was more detailed picture of the subsurface structures, lithologies and a detailed characterization of the coastal aquifer in the area, in particular, the subdivision of the aquifer into sub-aquifers and evaluation of groundwater quality within each sub-aquifer. The VES survey included eleven Schlumberger arrays to study and map the subsurface variation of resistivity in the area and identifying areas with saltwater intrusion. Resistivity values of less than 5 ohm-m were a clear indication of saltwater intrusion in many VES surveys. However, the resistivity profiles also showed an increase with depth that might relate to a fresh water aquifer below. The saltwater intrusion could be identified at least 500 m from the beach. The seismic reflection survey included six lines using the common depth point technique for data acquisition and geophone spacing of 1.5 m. Data processing is currently done to identify possible groundwater layers, especially coarse sand and gravel layers. Several hydrogeological observation wells and other borehole information were used for correlation with the geophysical data.

Keywords: coastal aquifer, Songkhla, high resolution seismic reflection, vertical electrical sounding

1. INTRODUCTION

Groundwater is one of the most important natural resources that sustain life on the earth. The global demand for fresh water will increase in the coming years. The high demand for freshwater, suggests clearly that, surface water can no longer meet the projected total demand. This growing demand is putting enormous pressure on water resources. Since many of the surface water sources have been degraded or depleted, due to exposure to pollution, increase in population, changes in climate and over-exploitation, much pressure is being exerted on the groundwater sources.

The situation near the coastline is often severe where a larger number of people live and the groundwater aquifers are threatened and/or contaminated by seawater intrusion. The groundwater contamination due to saltwater intrusion is usually caused by a violation of a sensitive hydrogeological balance that exists between freshwater and saltwater in coastal aquifers. This dynamic balance is often subverted by groundwater over-pumping and other human activities (e.g., land drainage) that lower groundwater levels and cause seawater movement into the coastal aquifers. It is obvious that the problem is important in all coastal aquifers.

Thailand has more than 3,200 km coastline, mainly in the Southern part along the Andaman Sea in the West and the Gulf of Thailand in the East. Major provincial cities are located near the shorelines; Songkhla is one of these cities. Therefore, Songkhla serves as an example for cities with similar problems regarding saltwater intrusion of coastal aquifers.

The study area itself is located in the Bo Yang District of Songkhla Province (Figure 1). The city is bordered by the Gulf of Thailand to the East and the Songkhla Lake in the West, and it is partly a delta with low lands that can be flooded both by river/runoff water during heavy rain and by sea water at high tide.

The main methods applied in the studies related to the saltwater intrusion in coastal aquifers are geophysical surface surveys, mainly electrical and electromagnetic methods, and also seismic methods. Each of the method has certain requirements, however in an urban area it can be challenging to meet these requirements. For example, vertical electrical sounding measurements need straight lines of several hundred meters with access to the ground. Seismic methods are sensitive with respect to noise, which in an urban area is coming almost throughout the whole day from traffic and transportation.

*Corresponding author. Tel: 074-288736
Fax: 074-212817; E-mail: helmut.j@psu.ac.th

J. Srattakal and H. Dürrast

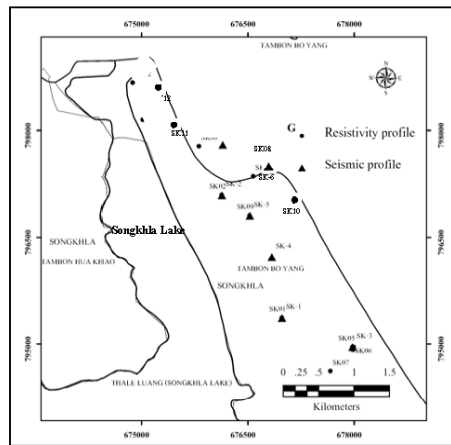


FIGURE 1. Map with the locations of the VES points and seismic profiles in Bo Yang District, Songkhla Province.

2. EXPERIMENT

Two geophysical methods have been applied for this study, vertical electrical sounding (VES) and shallow seismic reflection and refraction method.

2.1 Vertical electrical sounding

The vertical electrical sounding (VES) is based on measuring the potentials between one pair of electrodes transmitting a direct current between another pair of electrodes. Depth of current penetration is proportional to the spacing between the electrodes in homogeneous ground, and varying the electrode separation provides information about the stratification of the ground [1] (Koefoed 1979). VES method is very widely used for aquifers characterization because of the link that exists between the electrical resistivity of the subsurface, the rock water content and the water salinity.

The VES surveys were carried out in the study area with an ABEM SAS 1000 Terrameter for measuring the earth resistance and measuring by means of Schlumberger array. The maximum half current electrode spacing ($AB/2$) were up to 800 m. The resistivity survey was completed with 12 sounding stations. The selected half current electrode spacing values are: 1.5, 2, 3, 4.5, 7, 10, 15, 20, 30, 45, 60, 90, 150, 225, 350, 500, 600, 700 and 800 m. All data were plotted in the field to check the quality of data and to minimize mistakes.

IPI2Win, a software system which is designed for automated and interactive semi-automated interpreting of VES data, was the tool for data processing of VES data [2].

2.2 Seismic reflection

Seismic data were collected using in general the data acquisition parameters shown in Table 1. A sledgehammer striking a steel plate was used as a seismic source.

TABLE 1. Example of the acquisition parameters for seismic reflection surveys.

Recorder	12 channel E&G seismograph
Energy source	Sledgehammer; Offset 25 m
Receiver - single geophones	14 Hz (vertical)
Geophone spacing	1.5 m
Shot spacing	1.5 m (every station)
Shot location	Near 1st receiver
Coverage	6-fold
Record length	512 ms
Time sampling interval	250 μ s

Note: parameters can vary depending on site

Before any seismic acquisition was carried out the optimal offset was determined by changing the offset in small steps from one to 30 m or more.

WINSEIS Seismic Processing Software by the Kansas Geological Survey has been used for data processing of seismic reflection data. The following processing flow has been applied:

- format from SEG2 to KGS-SEG Y
- trace editing
- band-pass filtering-frequency domain (150-300 Hz)
- first arrival muting (direct wave and refraction)
- surgical muting (removal of ground roll)
- sort into CDP-gathers
- velocity analysis
- spectral analysis (frequency vs amplitude plots)
- NMO corrections
- stacking

However, the processing of the seismic data is still ongoing as the issue of noise reduction and signal to noise is still in process.

3. RESULTS AND DISCUSSIONS

VES method

As illustrated typical resistivity sounding curves of the area are depicted in Figure 2. No a priori information has been used at this stage. The initial model for each inversion was obtained by reducing to the possible minimum the number of layers in the recovered smooth model. Resistivity values vary from 2 to 2500 ohm-m on the inverse VES data. According to the above described hydro-geological setting of the area, the interpreted resistivity can be divided into four groups (see also Table 2, [3]):

- Very low resistivities (less than 5 ohm-m). These resistivities are typical for saline water saturated lithologies (both aquifers and aquicludes).
- Low resistivities (between 5 to 15 ohm-m). These resistivities are characterizing either brackish water saturated aquifers or aquicludes (mainly clay).
- Moderate resistivities (between 15 and 100 ohm-m). Typical for intermediate to good fresh water or fresh water saturated aquifers and some aquicludes.
- Higher resistivities (greater than 100 ohm-m). These resistivities are typical for very good quality fresh water or fresh water saturated aquifers.

J. Srattakal and H. Dürrast.

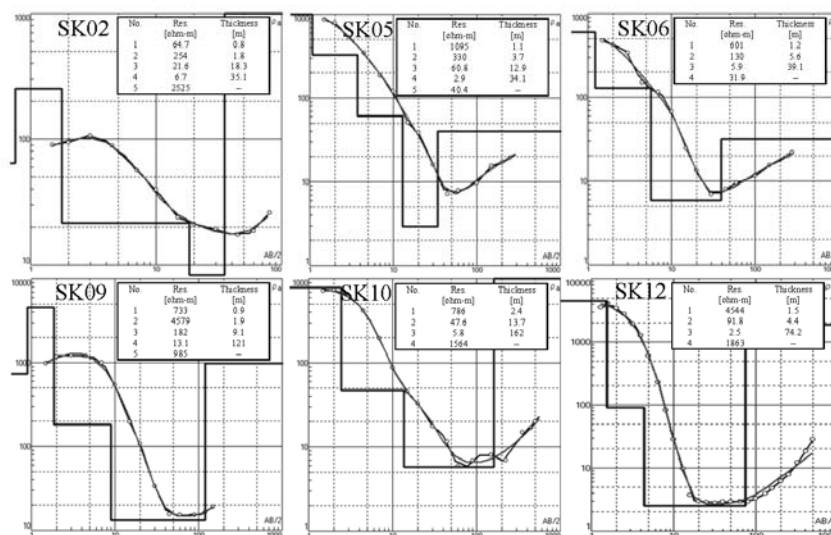


FIGURE 2. Examples of vertical electrical soundings. See Figure 1 for locations.

TABLE 2. Resistivity values of water and sediments. Modified after [3].

Resistivity, ohm-m	Sediments	Interpretation
0.5–2.0	Very porous sand, saturated clay	Seawater; very saline water
2.0–4.5	Porous sand, saturated clay	Saline water
4.5–10.0	Sandy saturated, sandy clay	Salty brackish water
10.0–15.0	Sandy clay, sandy gravel	Brackish water
15.0–30.0	Sand, gravel, some clay	Poor quality fresh water
30.0–70.0	Sand, gravel, minor clay	Intermediate quality fresh water
70.0–100.0	Sand, gravel, no clay	Good quality fresh water
> 100.0	Course sand, gravel, no clay	Very good quality fresh water

Generally, four geoelectrical zones can be selected. In the near surface, at depths of up to 4 m, it is characterized by high resistivities (> 100 ohm-m) [3]. The second zone extends between 4 and 10 m, and it is characterized by moderate resistivities (15–100 ohm-m). Figure 3 gives an overview of the first 16 m from the borehole cutting description. The third zone extends between 10 and 60 m, and it is characterized by low resistivities (5–15 ohm-m). The fourth zone deeper than 60 m, and it is characterized by the moderate resistivities, with resistivities from 15 to 100 ohm-m.

Due to its low resistivity values the third layer zone can be interpreted as the zone with seawater intrusion. The resistivity values can go below 5 ohm-m suggesting in parts of the zone seawater without any mixing with freshwater (brackish water). Further, the data show that below the saltwater layer the resistivity values increase significantly above the brackish value, either related to lithology and/or

the occurrence of a freshwater aquifer. Local authorities hinted to three main aquifer system in this area, with the salty aquifer in-between a confined aquifer on top and a freshwater aquifer below. However, further data analysis and interpretation has to confirm that.

PROJECT: COASTAL AQUIFER. LOCATION: Mahavijayapada Stn. LOG OF BORING NO: H49			
TOTAL DEPTH: 16.77 m		EASTING: 0676265	
REFERENCE BY: DOR		NORTHING: 0797011	
DEPTH (m)	GRAPHIC LOG	TYPE	DESCRIPTION
0–5	[Symbol]	Sand	plaz yellowish brown, medium to very coarse, angular to sub-rounded, poorly sorted, composed of quartz of various colors, with chert fragments
5–10	[Symbol]	Clay	dark yellowish brown, very sandy, partially limonitic, compacted, non-plastic, with some shells fragments
10–15	[Symbol]	Sand	same as at 0–5 m, but color changed to dark yellowish brow
15–16.77	[Symbol]	Clay	dark yellowish brown to dark olive gray, shaly, limonitic, compacted silastic
Bottom of hole at 16.77 m.			

FIGURE 3. Geological profile from cutting analysis showing the general geology of the upper part, mainly alternating clay and sand layers. Data from the Department of Groundwater Resources, Songkhla.

It has to be pointed out that in order to confirm the existence of a higher resistivity layer beneath the saltwater layer a minimum AB/2 of 150–250 in most cases was necessary. Better data were achieved with an AB/2 value of 800 m, but the urban area setting made this approach often impossible. Electromagnetic methods might be here of use, but they are not available for this study.

Seismic reflection method

The stacked reflection section (Figure 4) covers the layers deposited from 50–300 m (50–160 ms). A seismic time section for the reflection line is presented in Figure 4 and 5. The horizontal axis on the sections shows CDP numbers, while the vertical axis is two-way travel time in milliseconds. Two different seismic environments can be seen. The first environment is placed at two-way travel time of 50–160 ms, where the strong reflections appear. The reflections are continuous. Strong reflections also point to strong vertical changes of lithology. The reflections appear at the time of 50 ms in the beginning of the profile. The second seismic environment extends below the marker reflection at 160 ms, is characterized by a very weak discontinuity.

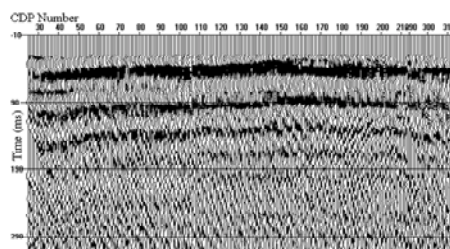


FIGURE 4. Stacked seismic reflection section.

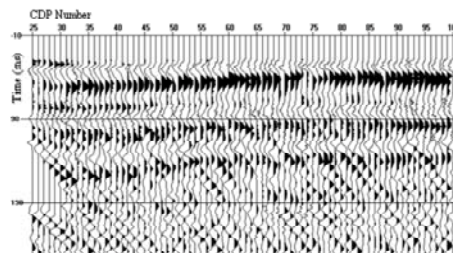


FIGURE 5. Part of the stacked seismic reflection section.

The processing of the seismic data is still ongoing as so the interpretation. One of the main questions to be addressed here will be the possible nature of the reflector. In the target depth section two possibilities exist, first the lithological boundary between clay and sand layers, or second gravel layers inside sand layers or in contact to clay layers.

4. CONCLUSIONS

The geophysics surveys carried out in the Bo Yang area provided important information necessary for a detailed study of the aquifer in the area. The seismic sections obtained along the reflection lines display a sequence of reflected events down to times of about 160 ms (about 50–240 m depth). The VES survey results are clearly shows sea water intrusion. Until so far and with several data still needed to be processed and interpreted, the integrated geophysical surveys employing vertical electrical sounding and shallow seismic reflection method already have delineated the various subsurface geological formations, the aquifer and the saline/brackish ground water zones.

ACKNOWLEDGMENTS

The authors would like to thank the Graduate School of Prince of Songkla University for the scholarship to carry out this study. Thanks to the IPPS of Uppsala University, Sweden, for the research equipment and interpretation software. The authors also express their gratitude to the graduate geophysics students at Prince of Songkla University who helped during the fieldwork.

1. Koefoed, O., Resistivity soundings measurements, In: Geosounding principles, vol. 1, Elsevier, New York, 1979
2. PI2Win User's Guide, version 2.1, Geoscan-M Ltd, Moscow State University, Moscow, 2001
3. Zohdy, A, Martin, P. and Bisdorf, R. A study of seawater intrusion using Direct-Current Soundings in the southeastern part of the Oxnard plain, California, U.S. Geological Survey, Open-File Report, 93-524, 139 p, 1993

VITAE

Name Miss Jiraporn Srattakal

Student ID 5010220027

Education

Degree	Name of Institution	Year of Graduation
B.Sc. (Physics)	Prince of Songkla University	2006

List of Publications

- Srattakal, J. and Dürrast, H. 2010. High resolution seismic reflection and vertical electrical sounding for detailed characterization of the coastal aquifer. In: Proceeding of the 5th Siam Physics Congress (SPC2010), Thai Journal of Physics Series 6: Thai Physics Society, 25–27 March 2010, Kanchanaburi, Thailand. 159–162
- Dürrast, H. and Srattakal, J. 2010. Σ mB as a tool for rapid magnitude determination of tsunamogenic earthquakes. In: Proceeding of the 5th Siam Physics Congress (SPC2010), Thai Journal of Physics Series 6: Thai Physics Society, 25–27 March 2010, Kanchanaburi, Thailand. 170–173.